Mathematical Modeling and Sensitivity Analysis of Lumped-Parameter Model of the Human Cardiovascular System

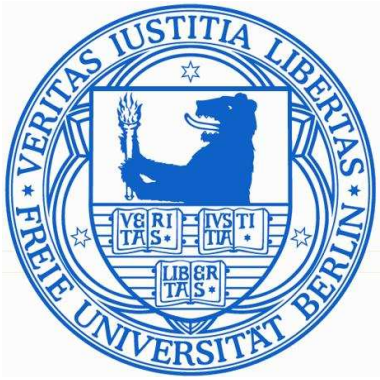

zur Erlangung des

Doktorgrades der Naturwissenschaften (Dr. rer. nat.)
im Fachbereich Mathematik und Informatik
der Freien Universität Berlin

vorgelegt von
Raheem Gul
aus Abbottabad, K.P.K, Pakistan

January 2016

Erstgutachter: Prof. Dr. Christof Schütte

Zweitgutachter: Prof. Dr. Stefan Bernhard

Disputation am: 27. 01. 2016

Abstract

In this thesis, a lumped-parameter model of the systemic circulation is developed and sensitivity analysis (local and global) is applied to quantify the impact of input parameters on output variables. The thesis is divided into two major parts, (1) cardiovascular (CV) modeling and (2) sensitivity analysis. In the CV modeling part, the major arteries of the systemic circulation are modeled explaining the elastic and the visco-elastic vessel walls behavior. In the sensitivity analysis part of the thesis, two local sensitivity analysis (LSA) and three variance-based global sensitivity analysis (GSA) methods are applied on a full and partial cardiovascular system (CVS).

LSA is applied on a linear elastic model of arm arteries (with and without anastomosis). While GSA is applied on MACSim (Major Arterial Cardiovascular Simulator), visco-elastic model of the CVS and carotid bifurcation. The main aim of this research work is to provide a general framework of parameter estimation using sensitivity analysis. However, the objectives of this thesis are summarized as:

- Formulate a reliable and clinically relevant model of the systemic circulation using the lumped-parameter approach (linear elastic and visco-elastic).
- Identify and rank the most important CV parameters, which contribute most on the output uncertainty. Furthermore, these sensitive parameter can be accurately estimated from measurements.
- Find the optimal measurement locations and optimal time regions in pressure and flow waves, which are very helpful in the parameter estimation.
- Find a GSA method for multi-compartment lumped-parameter model of the CVS on the basis of computational cost, simplicity and straightforward implementation.
- Discuss and explain the combine effect of *vasodilation* and *vasoconstriction* in linear elastic model of MACSim (Major Arterial Cardiovascular Simulator) by considering the sensitivity of the boundary resistance.
- Study different levels of *stenosis* and *aneurysm* in visco-elastic model of the CVS. The study could benefit medical students and doctors to understand the dependence of hemodynamic variables on CV model parameters.

Deutsche Kurzzusammenfassung

Die grundlegenden physikalischen Eigenschaften des Herz-Kreislaufsystems lassen sich durch dimensionsreduzierte parametrisierte Multi-Kompartiment-Modelle mit Hilfe von computergestützten Rechenverfahren effizient beschreiben. Einblicke in das Verhalten des Herz-Kreislaufsystems bietet dabei vor allem die Veränderung von Modellparametern.

In dieser Dissertation werden die systemischen Hauptarterien des menschlichen Kreislaufsystems in 122 Kompartimente (Knoten oder Segmente) unterteilt. Die Zustandsvariablen (Druck und Fluss) eines jeden Segments werden durch 3-elektrische (RCL) bzw. 4-strukturelle Parameter ($Eldh$) beschrieben. In computergestützten Herz-Kreislaufmodellen stellen die Parameter die Hauptquelle der Unsicherheit dar, weil diese sich direkt auf die Unsicherheit der Zustandsvariablen und damit auf die Verlässlichkeit des Modells auswirken. Bei der Erstellung von patienten-spezifischen Herz-Kreislaufmodellen die sich zur Untersuchung von Herz-Kreislauferkrankungen eignen, werden die Parameter aus patienten-spezifischen Messdaten geschätzt. In Multi-Kompartiment Herz-Kreislaufmodellen gibt es eine Vielzahl von elektrischen und strukturellen Parametern, eine genaue Schätzung aller Parameter aus gegebenen Messdaten ist deshalb nur bedingt möglich. Ein möglicher Ausweg aus dieser Situation ergibt sich durch die Quantifizierung der einflussreichsten Modellparameter bezüglich der Zustandsvariablen ergänzt durch optimale Messstellen und Zeiträume, um aus den patienten-spezifischen Daten die einflussreichsten Parameter zu schätzen.

In dieser Arbeit wurden die Modellparameter mit Hilfe der Sensitivitätsanalyse bezüglich ihrer Wichtigkeit geordnet, sowie optimale Messstellen und Zeiträume in den Druck- und Flusswellenformen identifiziert. Hierfür wurde die lokale Sensitivitätsanalyse auf die Armarterien und die globale Sensitivitätsanalyse auf eine Karotis Bifurkation und den gesamten Herz-Kreislauf angewendet. Die Ergebnisse zeigen eine starke Ortsabhängigkeit der Sensitivität bezüglich Druck und Fluss, d.h. in jedem Ort des arteriellen Netzwerks ergab sich eine unterschiedliche Ordnung der einflussreichsten Parameter. Grundsätzlich erwiesen sich der Durchmesser, die Länge des Gefäßes und der Widerstand des Blutflusses, speziell an den Gefäßenden als einflussreiche Parameter des Herz-Kreislaufsystems. Weiterhin bietet die vorliegende Arbeit eine Orientierung für Experimentatoren, welche Messgrößen (Druck und Fluss), an welchen Orten (optimale Messstellen) und zu welchen Zeiten bei der Schätzung von einflussreichen Parametern berücksichtigt werden sollten. Die optimalen Druck-/Flussmessungen, die zur Schätzung von einflussreichen Parametern verwendet werden sollten, hängen stark vom Ort im Netzwerk ab, wohingegen sich die optimalen Zeiträume im Druck- und Flussverlauf bezüglich der einzelnen Parameter gleichen, d.h. in der frühen Systole, End Systole und frühen Diastole.

Dedication

To my beloved *parents* and *siblings*, specially to my wife *Rahima Rahman* and my sweet daughter *Hadia Gul*.

Declaration

I hereby declare that this thesis is my own work and effort and that it has not been submitted anywhere for any award. Where other sources of information have been used, they have been acknowledged.

Raheem Gul
Berlin, 2016.

Acknowledgements

To begin with the name of Almighty **Allah**, the most merciful, Who inculcated in me the strength and spirit to complete such a mandatory task of this dissertation. First of all, I would like to thank my thesis supervisor **Prof. Dr. Christof Schütte** for his enormous help, invaluable suggestions and guidance, without which the completion of this doctoral thesis would not have been possible.

I wish to acknowledge the tutelage, valuable instructions, remarks and constructive criticism from my sincere, kind and cooperative co-supervisor **Prof. Dr. Stefan Bernhard** for his generous encouragement throughout my research work. I most vigorously and sincerely wish to thank **Rudolf Huttary** for his kind cooperation and remarkable suggestions throughout this research work.
I gratefully acknowledge financial support awarded by Higher Education Commission of Pakistan. I am also thankful to German Academic Service Exchange (DAAD) for their support and coordination to facilitate my research and stay in Berlin.

I am thankful to all faculty members, teaching and non-teaching staff, especially to **Dorothé Auth** for her kindness and assistance in office matters.
Last, but not least, I deeply thankful to my beloved parents, brothers and sisters who prayed for my edification, endeavored and betterment, especially to Rahima Rahman and Hadia Gul, who have been very helpful and due to their cooperative behavior my research work present in this dissertation become possible.

Raheem Gul
Berlin, 2016.

List of Publications

1. R. Gul and S. Bernhard. Local sensitivity analysis of cardiovascular system parameters. International Journal of Scientific and Engineering Research (IJSER), 4 (7). pp. 2648-2661. ISSN 2229-5518 (2013).

2. R. Gul, Ch. Schütte, S. Bernhard. Mathematical modeling and sensitivity analysis of arterial anastomosis in arm arteries. ZIB-Report (15-22), ISSN 1438-0064 (2015)

3. R. Gul and S. Bernhard. Mathematical modeling and sensitivity analysis of arterial anastomosis in arm arteries. Applied Mathematical Modeling (submitted) (2015).

4. R. Gul and S. Bernhard. Parametric uncertainty and global sensitivity analysis in a model of the carotid bifurcation: Identification and ranking of most sensitive model parameters. Mathematical Biosciences (submitted) (2015).

CONTENTS

LIST OF FIGURES

LIST OF TABLES

CHAPTER 1

Introduction

1.1 The cardiovascular system

Blood flow through the cardiovascular system (CVS) plays a crucial role in transporting and distributing the nutrients, oxygen and water to the body and removing the metabolic by-products (CO_2, water) away from the body tissues. It is also responsible to regulate the body temperature as well as adjust oxygen and nutrients supply in various physiological situations (homeostasis) [1]. Therefore, the importance of circulatory system is very obvious and malfunction of the system can cause various fatal diseases.

The circulatory system consists of the three major components, **heart**, **blood** and **vessels**. The blood is pumped out from the heart to the peripheral vessels (arteries, capillaries, veins). Arteries take the oxygenated blood away from the left ventricle to the organs. Nutrients, water and oxygen are exchanged in the capillaries, known as exchange system. The de-oxygenated blood is collected in the veins and sent back to the heart (right ventricle). From the right ventricle the blood is pumped out into the lungs, where, de-oxygenated blood gets oxygen and releases CO_2 to the air sacks of the lungs. Finally, the fresh blood (oxygenated) returns to the left ventricle.

1.1.1 Types of blood circulation

Blood circulation can be divided into three parts:

1. **The systemic circulation** is a network of the vessels that carry oxygenated blood away from the left ventricle to the body and de-oxygenated blood back to the right ventricle.

2. **The pulmonary circulation** are the vessels that carry de-oxygenated blood from the right ventricle to the lungs and oxygenated blood from the lungs to the left ventricle.

3. **The coronary circulation** are the vessels that supply blood to the cardiac tissues.

A graphical representation explaining the types of circulation is given in figure (1.1, left).

1.1.2 Structure of an artery

In general, the arteries are composed of three layers, *tunica intima* (inner layer), *tunica media* (middle layer) and *tunica externa* (outer layer). Moreover, the *lumen* is the inside space of an artery, where the blood flows. The three layers of an artery can be seen in figure (1.1, right).

1.1.3 Classification of arteries

On the basis of structures and functions, arteries are classified into three categories:

Elastic arteries
Elastic arteries have large diameter ranging from $1cm$ to $2.5cm$. Due to the large (*lumen*) area, these arteries are also known as low-resistance vessels. Elastic arteries have a large number of collagen and elastin filaments in the *tunica media*, which help in storing the blood during systole and to maintain a relatively constant pressure in arteries. The aorta, common carotid, subclavian, pulmonary and common iliac arteries fall in the category of the elastic arteries.

Muscular arteries
In the circulatory system, the basic function of muscular arteries is to distribute blood to the different organs of the body. Their diameter is in between $1cm$ and $0.2mm$. They have high amount of smooth muscle fibers in the *tunica media*, which help to regulate the blood flow.

Arterioles
The arterioles have a small lumen diameter ranging from 10 μm to 0.2 mm and play an important role in maintaining and regulating the peripheral blood pressure.

In physiological terms, the behavior of the vessel walls is visco-elastic. The elastic property provides the "energy storing mechanism", like a compressed spring or electrical capacitor, to store the blood during the systole. The viscous property dissipates the energy transmitted to the vessel walls during systole. In diastole, the stored blood is pushed to the downstream of the arterial tree, as a result, a smooth pulsatile blood flow occurs in the circulatory system [2] , see figure (1.2).

1.2 History of cardiovascular modeling

In 13^{th} century, Ibn Al-Nafis (1213-1288) was the first physician who described correctly the pulmonary circulation [6]. Before the work of Ibn Al-Nafis, the common theory of blood circulation was that the food is converted into blood in the liver and then work as a fuel. Later on in 1628, William Harvey (1578-1657) demonstrated experimentally that the blood is pumped from the heart and circulate in the body. He published "An anatomical study of motion of the heart and of the blood of animals". This was the first publication in the Western world, claiming that the heart is responsible for the blood circulation.

In 1738, Daniel Bernoulli (1700-1782) investigated the laws governing the blood pressure. He also published his well-known Bernoulli's equation, which relates the blood pressure to the blood velocity. The first pulse wave propagation model for in-viscid fluid was introduced by Leonhart Euler (1707-1783) in 1775 [7]. After L. Euler, Thomas Young (1773-1829) presented a mathematical model describing the wave-like nature of blood flow, that was not recognized in the Euler's model.

In 1838, Jean Lonard Marie Poiseuille (1797-1869) and in 1839, Gotthilf Heinrich Ludwig Hagen (1797-1884), independently derived a physical law that explained

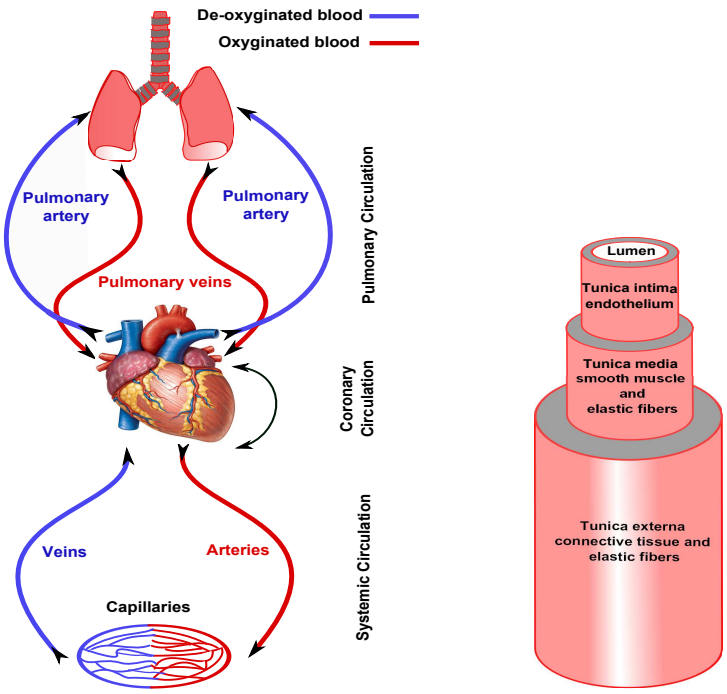

Figure 1.1: Types of the blood circulation (left) and the structure of an artery (right).

the relationship between the pressure drop and blood flow under steady flow conditions. Later on, The physical law, known as Hagen-Poiseuille law was published by Poiseuille in 1840 and 1846. In the field of cardiac physiology, several important contributions were made by Otto Frank (1865-1944). Out of those, "Windkessel effect" and "Frank-Starling law of the heart" are significant. In 1890, O. Frank published "Fundamental form of arterial pulse", which was first ever most theory of "Windkessel effect" in the field of blood circulation.

In 1955, John R. Womersley (1907-1958) derived the exact solution of viscous fluid in a circular tube under a periodic pressure gradient [17]. In case of a complex vascular network, the exact 3D-solution of fluid flow problems are not easy to obtain. However, Noordagraaf [23], Westerhof [22] and Avolio [14] used the concept given by O. Frank (Windkessel theory) and constructed the electrical analog model of the major arteries in the systemic circulation. In their study, the major arteries of the systemic circulation were divided into finite number of arterial segments (nodes or compartments). Each segment was represented by an electrical circuit, composed of a resistor, inductor and capacitor.

Due to complex geometrical structure, 3D simulations of the blood flow in the arterial network are beyond the capability of current computing facilities. In this context, multiscale modeling is an important concept in which desired vascular structures are modeled with 3D and lower dimensions (1D, OD) are used to provide boundary conditions to built a patient-specific CV model [8–12].

From the last few decades, lumped-parameter models of cardiovascular system have gained attention to study various normal and pathological conditions [15]. Lumped-parameter models are simple, computationally less expensive and explain the physics of the real-world problems well enough.

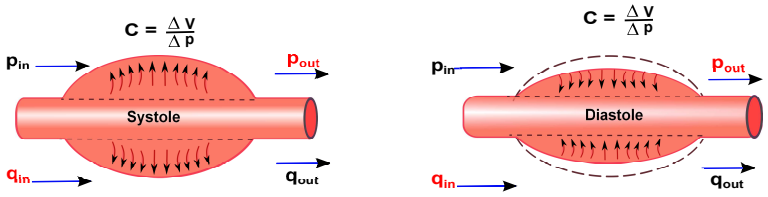

Figure 1.2: Blood flow through a compliant vessel during systole (left) and diastole (right).

1.3 Lumped-parameter model of the CVS

Although 3D modeling of fluid flow in the cardiovascular system gives detailed simulations, the complex model derivations and implementations make it computationally expensive. As mentioned before, the current computing facilities do not allow a 3D simulations of whole cardiovascular system. However, it is possible to derive more simple and less computationally expensive models using 1D and 0D modeling approaches [20, 28]. Lumped-parameter models of CVS have received increasing attention in the last few decades. In order to understand the relationship between the pressure and flow, many researchers have used 0D models to mimic blood flow and pressure in the human circulatory system [13, 14, 21–23, 25–27]. Importantly, the lumped-parameter models describe the physics of the problem in a simple way and changing the model parameters give insight to the behavior of the whole (partial) CVS .

Lumped-parameter models can be divided into two subgroups, namely mono-compartment models and multi-compartment models.

1.3.1 Mono-compartment models

In a mono-compartment models, the whole vessel network is represented with a single electric circuit, composed of resistance, inductance and compliance (RLC). The first two-element (RC in parallel) mono-compartment model was introduced by Otto Frank in 1899. The model explained aortic pressure decay in the diastolic phase, but cannot capture the high frequency components of pressure reflections in the vessel network. Later on, Westerhof [16] and Burattini [13] developed more sophisticated three-element Windkessel model (RCR) for the CVS. Westerhof et al. also added blood inertia in the three-element Windkessel model and proposed a four-element Windkessel element. The major limitation of mono-compartment model is that it cannot describe the pressure and flow-rate changes in specific or desired locations of the arterial network. Therefore, multi-compartment lumped-parameter models are suitable to study and analyze the overall behavior of the cardiovascular system.

1.3.2 Multi-compartment models

In multi-compartment approach, the arterial network is divided into multiple segments or compartments. Each compartment is represented by an electrical circuit consisting of RLC. The values of R, L and C are calculated from the blood vessel properties (Young's modulus, diameter, length of the vessel, wall-thickness, viscosity of the fluid, etc) [14, 22, 23]. In order to construct a full vessel network, the electrical compartments are connected together using appropriate in-output and bifurcation conditions. The bifurcation conditions are derived from the laws of conservation of mass and momentum. Before constructing a detailed vessel network, it is important to know and consider the characteristics of the vessel segments i.e.

their mechanical behavior, in-output boundary conditions, etc. Detailed derivations of different vessel compartments, explaining the appropriate vessel descriptions are given in [11, 21].

Although multi-compartment lumped-parameter models give a detailed and accurate description of the CVS, but in practice, it is very difficult to estimate plenty of model parameters from measurements to built a patient-specific model. In principal, it is not possible to estimate all model parameters from measurements, as the estimation of more parameters need more measurements. However, estimation is possible, if we identify optimal measurement locations in the CVS for important parameters. In this regard, sensitivity analysis can be used in finding important parameters as well as optimal measurements locations during the estimation process.

1.4 Cardiovascular diseases

Cardiovascular diseases (CVDs) are the number one cause of death worldwide. According to World Health Organization (WHO), 17.5 million people died in 2012 due to CVDs, representing 31% of all global deaths. Out of these deaths, 7.4 million were due to coronary heart disease and 6.7 million were due to stroke [3]. Among many cardiovascular risk factors (high cholesterol, diabetes, inactivity, excessive use of alcohol, etc), hypertension (high blood pressure) is the single biggest risk factor of CVD and widely used for diagnosis the heart attack and stroke. The World Heart Federation stated that, at least 950 million people world wide are suffering from high blood pressure and number is increasing day by day [4]. Another study published by WHF estimated that in 2025, 1.56 billion people will have high blood pressure [5].

1.4.1 Arteriosclerosis

Arteriosclerosis is one of the major cause of high blood pressure. Arteriosclerosis is the hardening and thickening of the vessel walls in which the elasticity of the blood vessels decreases and as a result, the blood pressure increases. These vessels abnormalities can occur due to the calcification of the vessel walls *(Monkeberg's arteriosclerosis)*, growing age (*medial arteriosclerosis*) and the fatty deposits on the inner most layers of the arteries (*atherosclerosis*). In atherosclerosis, the severe wall thickening (*stenosis*) narrow the blood vessels and limits the blood flow beyond the stenosis. The obstruction of blood flow causes failure of the organs and structures or ischemia; a restriction in blood supply to organs or structures tissues.

1.4.2 Aneurysm

An aneurysm is the abnormal widening or ballooning of the blood vessels due to a weak thin vessel wall. Aneurysms commonly occur in the abdomen (abdominal aortic aneurysms, AAA) or the brain (cerebral aneurysms, CA). An AAA is known as silent killer, because in most of the cases there are no symptoms of abnormal vessel enlargement. A ruptured aneurysm can cause life-threatening blood loss, which leads to death.

In this thesis, artificial stenosis and aneurysm are created by changing model parameters (blood flow resistance or diameter) and the impact of vessel abnormalities on pressure and flow of cardiovascular system are studied through sensitivity analysis.

1.5 Uncertainty analysis

Computational cardiovascular models are very useful in the understanding of physiological and pathological processes as well as to study and analyze the behavior of the whole (partial) circulatory system. Cardiovascular models also play a vital role in designing and constructing patient-specific models using clinically obtained measurements.

From the derivation of physical laws of hemodynamics to the computer simulations of the computational cardiovascular models, there exist several sources of uncertainty which make the model unreliable and less predictive. Uncertainty must be reduced to achieve a reliable and predictive cardiovascular model that allow the investigations of the cardiovascular diseases.

1.5.1 Sources of uncertainty

Mainly, the sources of uncertainty are model parameters, in-output boundary conditions, spatio-temporal variabilities of parameters, structure and numerical uncertainty. The structural uncertainty comes from the lack of knowledge while deriving mathematical models from physical laws and numerical uncertainty comes from numerical errors.

1.5.2 Propagation of uncertainty

Propagation of uncertainty is the quantification of uncertainty in the model outputs (pressure and flow) caused by uncertain input parameters (electrical and structural). Uncertainty in model parameters is propagated through Monte Carlo sampling with a known probability distribution (pdf), Latin hypercube sampling, log-normal distribution and normal distribution. The ultimate goal of uncertainty propagation is to evaluate the low-order moments (mean and variance), to represent the model output variability in a compact way.

1.5.3 Parameter calibration, inverse uncertainty quantification

A mathematical model is basically a simplification of real-world system (physical system) and in case of complex cardiovascular system, a real behavior of hemodynamics cannot be produced even if we have a most detailed model. However, if the model has no significant disagreement with the real system, then, the discrepancy between model outputs and the measurements of the real system can be reduced by estimating the important (key) model parameters (parameter calibration). In this context, the model parameters which contribute most on output uncertainty can be estimated accurately from the measurements. In this way, the structural uncertainty can be converted into parametric uncertainty, which shows the importance of the model parameters in building a reliable and predictive cardiovascular model.

1.6 Sensitivity analysis

Lumped parameter model of the CVS consists of plenty parameters. For reliable, predictive and patient-specific CV models, the uncertainty in the model outputs should be reduced by estimating the important CV parameters. A patient-specific model could be achieved by estimating the model parameters using clinically obtained investigations (measurements). An important step in the parameter estimation process is to find a subset of important parameters and fix less important

parameters on their nominal values (factor fixing). This is because, only the important model parameters can be estimated accurately from the given measurements. Sensitivity analysis is the study of how the uncertainty in the output of a mathematical model or system (numerical or otherwise) can be apportioned to different sources of uncertainty in its inputs [45].

1.6.1 Local sensitivity analysis (LSA)

In LSA, a parameter value is perturbed around its nominal value once at a time, keeping all other parameters fixed at their nominal values [18, 44]. The procedure is repeated for all parameters one by one to study the effect of individual perturbations on the output variables. Although, LSA is common, simple, easy to implement and computationally less expensive, it does not explore the effect of entire parameter spaces on output variables as well as the interactions between the parameters [19].

1.6.2 Global sensitivity analysis (GSA)

The drawbacks associated with LSA can be perceived using GSA. The GSA quantifies the interactions effects among the parameters and also explores the impact of entire feasible parameter spaces on output variables [45–49]. The only drawback of GSA is, its computational cost.

In this work, two local sensitivity analysis (LSA) (one factor at a time, relative norms sensitivity) and three variance-based global sensitivity analysis (GSA) methods (Sobol, FAST, sparse grid) are applied on different arterial structures.

1.7 Motivation and aims of the thesis

The basic aim of this work is to formulate a whole (partial) cardiovascular model of the systemic circulation and perform sensitivity analysis (local and global) to quantify the impact of input parameters on output variables. The ultimate goal of research is to provide a framework for parameter estimation on the basis of sensitivity analysis, to build a patient-specific CV model. The key objectives of the thesis are summarized as follows:

- Formulate a reliable and clinically relevant model of the systemic circulation using lumped parameter approach (linear elastic and visco-elastic).
- Apply sensitivity analysis (local and global) on different arterial structures (carotid bifurcation and arm arteries with and without anastomosis), to analyze and study the behaviors of the arterial structures in normal and pathological situations.
- Find a suitable method for global sensitivity analysis on the basis of simplicity, straightforward implementation and less computational cost.
- Identify and rank the most important cardiovascular parameters, that contribute most on output uncertainty.
- Finding less important parameters, that can be fixed on their nominal values.
- Perform sensitivity analysis for MACSim (Major Arterial Cardiovascular Simulator), to guide experimentalists what to measure and where to measure to estimate the important CV parameters.
- Apply sensitivity analysis with respect to boundary resistance for MACSim to study the impact of *vasodilation* and *vasoconstriction* on pressure and flow in the arterial network.

- Explain the impact of stenosis and aneurysm on pressure and flow in the various parts of the systemic circulation. The analysis could help the medical doctors to detect the CVDs (stenosis and aneurysm) in early stages.
- Discuss and explain the network location and temporal dependent sensitivities, which are useful in finding optimal measurement locations in different arterial structures and optimal time regions in pressure and flow waves to estimate the model parameters.

1.8 Thesis outline

In chapter 2, a detailed derivation of lumped parameter models (linear elastic and linear visco-elastic) of systemic circulation is given. Chapter 3 explains, the effect of electrical and structural parameters on pressure and flow in the linear elastic model of the arm artery (with and without anastomosis). In chapter 4, three variance-based GSA methods are briefly discussed and applied on a linear visco-elastic model of the carotid bifurcation. Moreover, we discuss the ranking of important electrical and structural parameters, factor fixing, locations and time-dependent sensitivities. In Chapter 5, the method of Sobol is applied on the linear elastic model of MACSim to find the impact of diameter and boundary resistance on output variables. We also discuss different levels of stenosis and aneurysm and their impact on other locations of visco-elastic CVS. Finally, in chapter 6, the conclusion of the research work and future directions are discussed.

CHAPTER 2

Lumped-Parameters Model of the CVS

2.1 Introduction

Cardiovascular diseases are one of the major problems in todays medicine and the number of patients increases worldwide. To find the most efficient treatment, prior knowledge about function and malfunction of the cardiovascular system is required. To identify the CV diseases in early stage, suitable methods need to be developed. Mathematical modeling is a powerful tool for prediction and investigation of cardiovascular diseases. Over the last few decades many researchers have attempted to model the partial or full cardiovascular system [29–32]. The basic objective of these models is a better understanding of the cardiovascular system in an inexpensive and non-invasive way. Fortunately, there are large number of CV models (3D,1D,0D) available in the literature. The selection of appropriate model dimensionality, from 0D to 3D can be chosen according to the given scenarios, objectives and applications [33].

There are four major difficulties associated with the CV modeling:

- Formulation of models for a large and complex vessel network.
- Computational cost for solving high dimensional CV models (3D,2D).
- The inaccuracy and unreliability in the model outputs, caused by input factors (model parameters, initial and boundary conditions, etc).
- Selection or estimation of the key parameters to built a patient-specific CV model.

It has been investigated, that the lumped-parameter models, drawing an analogy between electrical circuits and fluid flow, are simple, computationally inexpensive and effective methods to model the human cardiovascular system. In lumped-parameter models, the continuous variation of hemodynamic state variables is represented by a finite number of variables, defined at specific vascular segments. Although, the model has low spatial resolution, it is still useful to asses the overall performance of the whole cardiovascular system or subsystems, like the carotid bifurcation, the arm arteries, arterial anastomosis or femoral arteries etc.

For reliable model predictions, the output uncertainty in such models needs to be reduced. The output uncertainty could be minimized by estimating those model parameters, which contribute most on output uncertainty. The identification of the important model parameters can be done by sensitivity analysis, which further can

Mechanical system	**Electrical system**	**Hydraulic system**
Stress (σ)	Voltage $(\mathcal{V})$	Pressure (p)
Time derivative of strain $(\frac{d\epsilon}{dt})$	Current $(\mathcal{I})$	Flow rate (q)
Viscosity (η)	Resistance $(\mathcal{R})$	Blood viscosity (R)
Mass $(\mathfrak{m})$	Inductance $(\mathcal{L})$	Blood inertia (L)
Elastic modulus (E)	Compliance $(\mathcal{C})$	Wall compliance (C)

Table 2.1: Analogies between mechanical, electrical and hydraulic systems.

be estimated using clinically obtained measurements. In forthcoming chapters (3, 4, 5), a detailed explanation on the identification and ranking of important parameters and factor fixing is given.

In this chapter, the mathematical formulation of the lumped-parameter models (linear elastic and visco-elastic) is derived by decomposing the CVS into single arterial segments with prescribed in-output boundary conditions. In the next step, the detailed arterial network of the systemic circulation is derived using appropriate bifurcation conditions, that result from the laws of conservation of mass and momentum.

2.2 Lumped-parameter model of a vessel segment

Lumped parameters models can be derived from the 3D Navier-Stokes equations of incompressible and Newtonian fluid in a straight rigid cylindrical tube. By integrating over the cross section after considering the simplified assumptions and by further integrating over space, we get system of coupled ODEs, describing the variation in time for average pressure and flow rate [11,20]. The lumped parameters models are also known as 0D models as they do not consider variations in space.

2.2.1 Electrical analogy

In lumped-parameter approach, a vessel segment is represented by an electrical circuit, which is the combination of a resistor, inductor and capacitor. There exist an analogy between the flow in a tube and flow of a current in an electric circuit. The electrical potential or voltage $(\mathcal{V})$ corresponds to the driving pressure difference (Δp) in the vessel segment, current $(\mathcal{I})$ is analogous to the blood flow (q), resistor is represented as viscous flow resistance , capacitance is analogous to the compliance of the vessel (C), inductor is replaced by blood inertia (L) and impedance corresponds to terminal (boundary) resistance (R_b). See table (2.1) and figure (2.2) for complete description.

2.2.2 Formulation of an elastic segment

Pressure and flow equations at non-terminal segments:
Let us consider a single compliant vascular segment with diameter (d), vessel length (l) and wall-thickness (h). The equivalent electrical circuit representation ($\mathbb{L}$ - inverted) of compliant vessel segment is given in figure (2.1, B). Let $(p_{in},\ q_{in})$ and $(p_{out},\ q_{out})$ are the pressure and flow rate at the inlet and outlet of the vascular segment respectively. If p_{in} and q_{out} are the prescribed boundary conditions, then after applying Kirchhoff current and voltage laws, we get system of two differential

equations:

$$\dot{q}_{in} = \frac{p_{in}}{L} - \frac{p_{out}}{L} - \frac{R\ q_{in}}{L} \qquad \text{(Flow equation)} \tag{2.1}$$

$$\dot{p}_{out} = \frac{q_{in}}{C} - \frac{q_{out}}{C} \qquad \text{(Pressure equation)} \tag{2.2}$$

Where, q_{in} and p_{out} are the state variables, R is the viscous flow resistance, L is the blood inertia and C represents the vessel compliance. In figure (2.1), variables in the red color represent the state variables.

Pressure and flow at terminal segments:
As mentioned in section 1.3, in multi-compartment modeling the arterial network is divided into a finite number of vessel segments. Including more and more vessel segments makes the model complicated and computationally expensive. Finally, it is not practically feasible to model tens of billions of capillaries. In order to close the arterial network and accommodate the cumulative effects of capillaries beyond the terminal segments, the cascade connection of two linear elastic, $\mathbb{L}$ and $\mathbb{L}$ -inverted electrical circuits (T-element) is used, see figure (2.1, A). Applying Kirchhoff laws, the following linear first order system of ordinary differential equations are obtained,

$$\begin{aligned}
\dot{q}_{in} &= \frac{2\ p_{in}}{L} - \frac{2\ p}{L} - \frac{2\ R\ q_{in}}{L} && \text{(Flow equation)} \\
\dot{p} &= \frac{q_{in}}{C} - \frac{q_{out}}{C} && \text{(Pressure equation)} \\
\dot{q}_{out} &= \frac{2\ p}{L} - \frac{2\ p_{out}}{L} - \frac{2\ R_b\ q_{out}}{L} && \text{(Flow equation)}
\end{aligned} \tag{2.3}$$

Where, p_{in} and p_{out} are the prescribed boundary conditions and q_{in}, p and q_{out} are the state variables. At the terminal segment p_{in} is the pressure obtained from the previous segment and p_{out} is 15 $mmHg$, the mean venous pressure is used to calculate the boundary outflow, q_{out}. For more detail of in-output boundary conditions, see section 2.3.1.

Viscous flow resistance (R):
Resistance to the blood flow mainly depends on the three factors, (i) diameter of the vessel (d), (ii) length of the vessel (l) and (iii) blood viscosity (ν (0.004 $Pa\ s$)). Out of these, the diameter is the most important parameter. This is because the diameter of the vessel changes during systole and diastole and even small changes in the diameter lead to the large change in the resistance.

The value of R can be calculated from the Poiseuille's equation, which describes the relation between pressure drop, Δp and the steady blood flow, q through a uniform and stiff blood vessel,

$$q = \frac{\Delta p\ \pi\ (\frac{d}{2})^4}{8\ \nu\ l} = \frac{\Delta p}{R} \qquad \text{where,} \tag{2.4}$$

$$R = \frac{8\ \nu\ l}{\pi\ (\frac{d}{2})^4} \tag{2.5}$$

Eqn. (2.4) is also known as Ohm's law of hydrodynamics. Generally, R is obtained from the Poiseuille's law, but in practice it can be measured from Ohm's law of hydrodynamics.

Vessel compliance (C):
The ability of a vessel wall to expand and contract with changes in pressure is known as vessel compliance (C). The inverse of C is volume elasticity i.e. $E_v = \frac{1}{C}$.

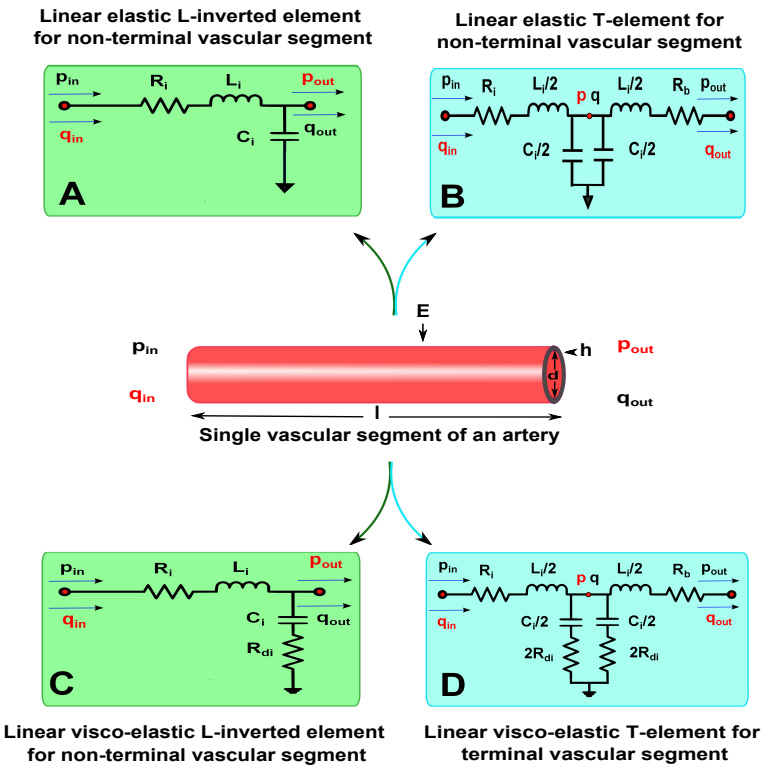

Figure 2.1: Single segment of a compliant vessel and its linear elastic (A,B) and visco-elastic (C,D) circuit representations.

In other words, the pressure-volume relationship is quantified in two ways, in terms of compliance, C and elasticity, E_v (bulk modulus). Compliance is calculated using the following equation, where, ΔV is the change in blood volume, and Δp is the change in pressure,

$$C = \frac{\Delta V}{\Delta p} \tag{2.6}$$

Vessel compliance, C can also be obtained from blood vessel properties,

$$C = \frac{2\ \pi\ (\frac{d}{2})^3\ l}{E\ h} \tag{2.7}$$

Blood inertia:
Blood inertia, L plays a role in accelerating and decelerating the blood with every heart beat. L relates pressure drop, Δp to the rate of change of flow $\frac{dq}{dt}$. Mathematically it can be written as,

$$\Delta p = L\frac{dq}{dt} \tag{2.8}$$

The numerical value of L can also be obtained using the blood vessel properties. Starting from the Newton's law of motion relating, force ($\mathcal{F}$), mass ($\mathfrak{m}$) and acceleration ($\mathfrak{a} = \frac{dv}{dt}$) as,

$$\mathcal{F} = \mathfrak{m}\ \mathfrak{a} = \mathfrak{m}\ \frac{dv}{dt} \tag{2.9}$$

In case of a vessel of length l,

$$\begin{aligned} \mathcal{F} &= \Delta p\ A, \qquad \text{and} \\ \mathfrak{m} &= \rho\ V. \end{aligned}$$

Where, A is the luminal cross-section area of the vessel, ρ ($1050\ kg/m^3$) is the blood density and V is the volume of blood in a compliant vessel. From the definition of volumetric flow rate,

$$\begin{aligned} q &= v\ A, \qquad \text{taking derivative} \\ \dot{q} &= \frac{dv}{dt}\ A \\ \frac{dv}{dt} &= \frac{\dot{q}}{A} \end{aligned} \tag{2.10}$$

Substituting the values of $\mathcal{F}$, $\mathfrak{m}$ and $\frac{dv}{dt}$ in eqn. (2.9), we have,

$$\begin{aligned} \Delta p\ A &= \rho\ V\ \frac{\dot{q}}{A} \\ \Delta p &= \frac{\rho\ l}{A}\ \dot{q}, \qquad \text{where} \\ L &= \frac{\rho\ l}{\pi\ (\frac{d}{2})^2} \end{aligned} \tag{2.11}$$

2.2.3 Formulation of a visco-elastic segment

For the derivation of electrical circuits describing the visco-elastic nature of the vessel walls (figure 2.1, C, D), the same in-output boundary conditions described in section 2.2.2 are used.

Pressure and flow equations at non-terminal segments:

$$\dot{q}_{in} = \frac{p_{in}}{L} - \frac{p_{out}}{L} - \frac{Rq_{in}}{L} \qquad \text{(Flow equation)} \tag{2.12}$$

Before the deriving the pressure equation, it is important to know the mechanical behavior of the vessel wall, which is not purely *elastic*, it exhibits *viscoelastic* nature in the cardiovascular system. The dual nature of vessel walls can be represented by Voigt model [13, 56, 57]. The mechanical representation of Voigt model consists of a spring and a dash pot in parallel, where, the spring and the dash pot represents elastic and viscous behavior of the material respectively, see figure (2.2). Mathematically, the stress-strain relationship and their time-dependencies can be written as,

$$\sigma = \underbrace{E\epsilon}_{\text{Elastic component}} + \underbrace{\eta\frac{d\epsilon}{dt}}_{\text{Viscous component}} \tag{2.13}$$

Where, σ is the stress, E is the elastic modulus, ϵ denotes strain, η is the viscosity of the material and $\frac{d\epsilon}{dt}$ is the time derivative of the strain.

The electrical analog of the Voigt model can be obtained by considering resistance ($\mathcal{R}$) and capacitance ($\mathcal{C}$) in series. Applying Kirchoff's current and voltage laws we get,

$$\mathcal{V} = \underbrace{\frac{1}{\mathcal{C}}\mathcal{Q}}_{\text{Elastic component}} + \underbrace{\mathcal{R}\frac{d\mathcal{Q}}{dt}}_{\text{Viscous component}} \tag{2.14}$$

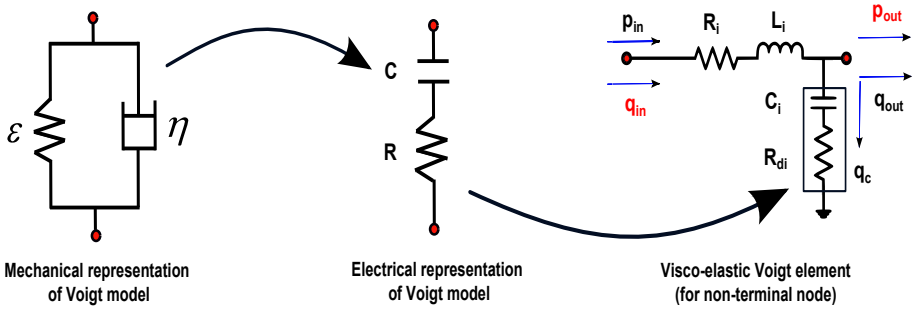

Figure 2.2: Mechanical and its equivalent electrical representation of the Voigt model.

Where, $\mathcal{V}$ is the voltage, $\mathcal{C}$ is the capacitance, $\mathcal{Q}$ denotes charge, $\mathcal{R}$ is the resistance and $\frac{d\mathcal{Q}}{dt} = \mathcal{I}$ is the current.

In case of arterial vessels the stress-strain or voltage-charge relationship can be simplified in terms of pressure-volume relationship. The corresponding equation which explains the visco-elastic nature of vessels wall will be,

$$p = \underbrace{\frac{1}{C} Q_c}_{\text{Elastic component}} + \underbrace{R_d\, q}_{\text{Viscous component}} \tag{2.15}$$

Where, p is the pressure (p_{out} in our case), C is the compliance of the vessel, Q_c denotes blood volume, R_d is the viscous part of the vessel and $\frac{dQ_c}{dt} = q_c$ is the blood flow through the vessel.

By letting $p_{out} = p$ and taking the derivative of eqn. (2.15) we get,

$$\dot{p}_{out} = \frac{q_c}{C} + R_d\, \dot{q}_c \tag{2.16}$$

Where,

$$q_c = q_{in} - q_{out}, \quad \text{and} \tag{2.17}$$

$$\dot{q}_c = \dot{q}_{in} - 0 \tag{2.18}$$

By substituting eqns. (2.12), (2.17) and (2.18) into eqn. (2.16), we get the final equation for the pressure,

$$\dot{p}_{out} = \frac{R_d}{L} p_{in} + \Big(\frac{1}{C} - \frac{R_d R}{L}\Big) q_{in} - \frac{q_{out}}{C} - \frac{R_d}{L} p_{out} \tag{2.19}$$

Pressure and flow at terminal segments:

$$\begin{aligned}
\dot{q}_{in} &= -\frac{2R}{L} q_{in} - \frac{2}{L} p + \frac{2}{L} p_{in} && \text{(Flow equation)} \\
\dot{p} &= \Big(\frac{1}{C} - \frac{2RR_d}{L}\Big) q_{in} - \frac{4R_d}{L} p + \Big(\frac{2R_b R_d}{L} - \frac{1}{C}\Big) q_{out} \\
&+ \frac{2R_d}{L} p_{in} + \frac{2R_d}{L} p_{out} && \text{(Pressure equation)} \\
\dot{q}_{out} &= \frac{2}{L} p - \frac{2R_b}{L} q_{out} - \frac{2}{L} p_{out} && \text{(Flow equation)}
\end{aligned} \tag{2.20}$$

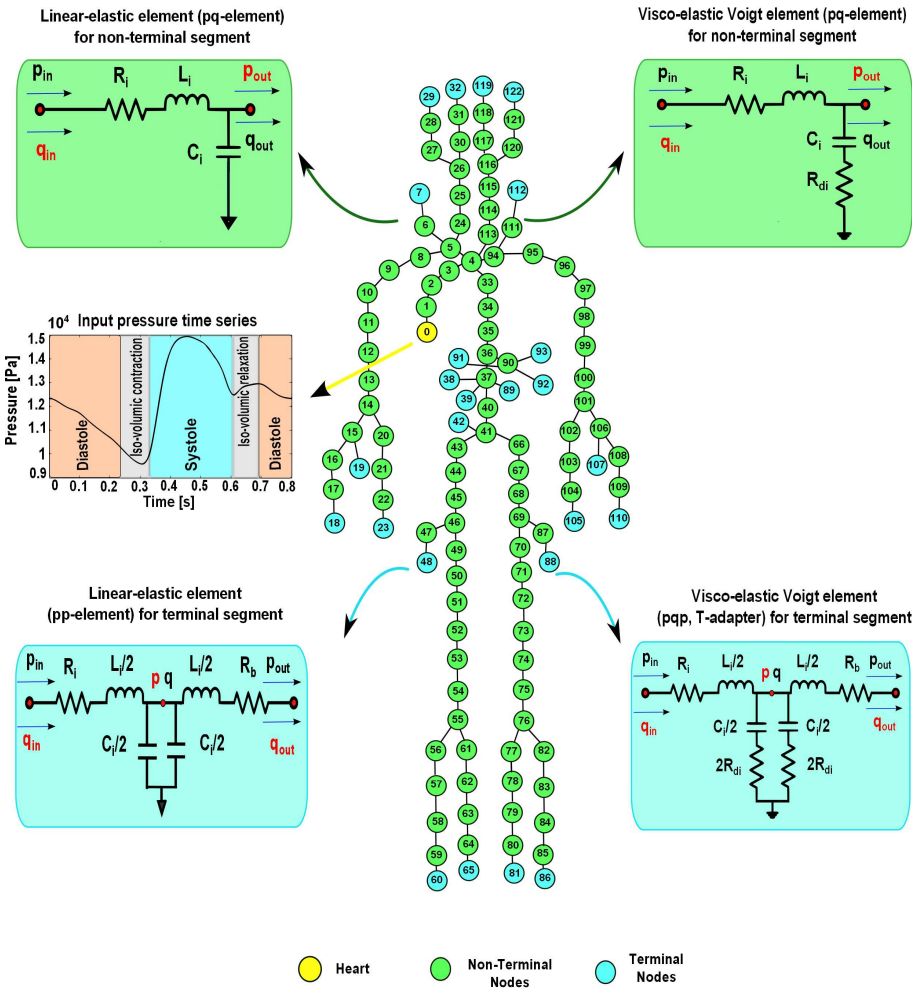

Figure 2.3: Simplified model geometry of the systemic circulation with input pressure time series, linear elastic and linear visco-elastic circuit elements for non-terminal and terminal segments in the arterial network.

2.3 Network structure and model equations

To generate the arterial model of the whole systemic circulation, we used domain decomposition (DD) method [34], in which the major arterial network is decomposed into a number of vascular segments (nodes), where the parameters are approximately constant. Each non-terminal and terminal segment in a network structure is represented by its non-terminal and terminal electrical circuit (linear elastic and visco-elastic) respectively. In total, the CV model under consideration contains $N_s = 122$ segments, including $N_t = 25$ terminal segments (●) and remaining $N_{nt} = 96$ non-terminal segments (●). The node 0 (●) is used for input pressure time series, see figure (2.3).

At each non-terminal segment of the model, a system of two first order differential equations is obtained, representing first equation for flow (q) and second for pressure (p). On the other hand, at the terminal segment, we have two flow and one pressure equations. During analysis, the extra one flow solution is dropped, as both are identical. We end up with a system of $2 \times N_s + N_t$ differential equations.

Decomposition into vascular segments, however, requires relations between the

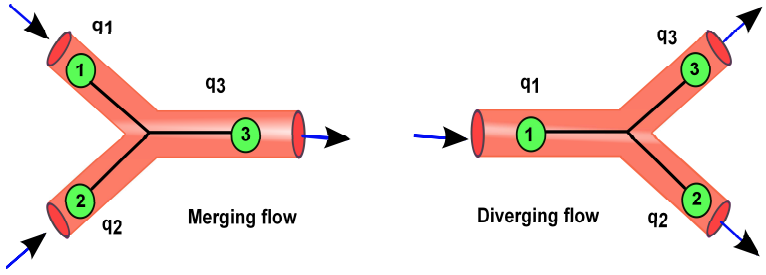

Figure 2.4: Model geometry for merging and diverging flows at junctions.

arterial segments to reconstruct the network structure of the arterial tree. Therefore, we define bifurcation conditions for the mother and daughter vessels as follows:

$$q_1 = q_2 + q_3, \quad \text{(diverging)} \tag{2.21}$$
$$q_3 = q_1 + q_2, \quad \text{(merging)} \tag{2.22}$$
$$p_1 = p_2 = p_3 \tag{2.23}$$

These conditions are derived from conservation of mass and momentum, i.e. pressure is constant and flow has to be conserved at the bifurcation (see figure 2.4). For more details see [28].

2.3.1 In-output boundary conditions

The total length of blood vessels in human cardiovascular system is approximately 60,000 miles [11]. Practically, it is impossible to model tens of billions small arteries and capillaries in the circulatory system. A more practical solution is to lump together all nodes downstream from the terminal segments. The capillaries are considered as resistance vessels, so that a terminal resistance (R_b) is used to represent the cumulative effect of microcirculation beyond the terminal segments. Moreover, in the terminal segments, a constant pressure boundary condition, p_{out} is applied (Dirichlet boundary condition). The value of p_{out} is taken $15mmHg$ (2000 Pa), the mean venous pressure to calculate the boundary outflow, q_{out} (eqns. 2.3, 2.20). Also, p_{in} is used as an input boundary condition at segment 0, with a cardiac cycle time is 0.8 sec (75 beat/min), see figure (2.3).

2.3.2 Diverging and merging flows at junctions

Blood flow at junctions plays an important role in normal and pathological conditions of the cardiovascular system. In this section, we briefly discuss pressure and flow at junctions for both diverging (at bifurcations) and merging blood flows. In the arterial system, merging flow conditions appear in the context of anastomosis.

2.3.2.1 Diverging blood flow

Diverging flows occur at the bifurcation of the vessels, see figure (2.4, right) . According to the conservation of mass, the flow at node 1 is, $q_1 = q_2 + q_3$ and the total pressure is constant at the bifurcation, i.e. the output pressure at node 1 is the input pressure for both nodes 2 and 3.

2.3.2.2 Merging blood flow

To model the merging flows at junctions has a great importance to understand the effect of anastomosis and bypass in the cardiovascular system, see figure (2.4,

left). These type of flows also occur in vascular grafting and arteriovenous fistula (AVF). According to the conservation of mass, the flow at node 3 is, $q_3 = q_1 + q_2$ and according to the law of conservation of momentum, the total pressure remains continuous at node 3.

2.3.3 Formulation of the linear elastic CV model

With all essential information at hand, now we are able to derive a full cardiovascular model for both elastic and visco-elastic vessel wall behaviors (see figure 2.3).

Pressure and flow equations for linear elastic model:

Flow equations:

$$\dot{q}_i = \frac{p_{i-1} - p_i - R_i q_i}{L_i} \qquad \text{for } i \neq \begin{cases} 8, 19, 20, 24, 30, 33, 39, 43, 49, \\ 61, 66, 82, 87, 89, 90, 92, 93, 94, \\ 106, 108, 111, 113, 120 \end{cases}$$

$$\begin{aligned}
\dot{q}_8 &= \frac{p_5 - p_8 - R_8 q_8}{L_8}, & \dot{q}_{19} &= \frac{p_{15} - p_{19} - R_{19} q_{19}}{L_{19}} \\
\dot{q}_{20} &= \frac{p_{14} - p_{20} - R_{20} q_{20}}{L_{20}}, & \dot{q}_{24} &= \frac{p_5 - p_{24} - R_{24} q_{24}}{L_{24}} \\
\dot{q}_{30} &= \frac{p_{26} - p_{30} - R_{30} q_{30}}{L_{30}}, & \dot{q}_{33} &= \frac{p_4 - p_{33} - R_{33} q_{33}}{L_{33}} \\
\dot{q}_{39} &= \frac{p_{37} - p_{39} - R_{39} q_{39}}{L_{39}}, & \dot{q}_{43} &= \frac{p_{41} - p_{43} - R_{43} q_{43}}{L_{43}} \\
\dot{q}_{49} &= \frac{p_{46} - p_{49} - R_{49} q_{49}}{L_{49}}, & \dot{q}_{61} &= \frac{p_{55} - p_{61} - R_{61} q_{61}}{L_{61}} \\
\dot{q}_{66} &= \frac{p_{41} - p_{66} - R_{66} q_{66}}{L_{66}}, & \dot{q}_{82} &= \frac{p_{76} - p_{82} - R_{82} q_{82}}{L_{82}} \\
\dot{q}_{87} &= \frac{p_{69} - p_{87} - R_{87} q_{87}}{L_{87}}, & \dot{q}_{89} &= \frac{p_{37} - p_{89} - R_{89} q_{89}}{L_{89}} \\
\dot{q}_{90} &= \frac{p_{36} - p_{90} - R_{90} q_{90}}{L_{90}}, & \dot{q}_{92} &= \frac{p_{90} - p_{92} - R_{92} q_{92}}{L_{92}} \\
\dot{q}_{93} &= \frac{p_{90} - p_{93} - R_{93} q_{93}}{L_{93}}, & \dot{q}_{94} &= \frac{p_4 - p_{94} - R_{94} q_{94}}{L_{94}} \\
\dot{q}_{106} &= \frac{p_{101} - p_{106} - R_{106} q_{106}}{L_{106}}, & \dot{q}_{108} &= \frac{p_{106} - p_{108} - R_{108} q_{108}}{L_{108}} \\
\dot{q}_{111} &= \frac{p_{94} - p_{111} - R_{111} q_{111}}{L_{111}}, & \dot{q}_{113} &= \frac{p_4 - p_{113} - R_{113} q_{113}}{L_{113}} \\
\dot{q}_{120} &= \frac{p_{116} - p_{120} - R_{120} q_{120}}{L_{120}}
\end{aligned} \tag{2.24}$$

Pressure equations:
At non-furcation nodes:

$$\dot{p}_i = \frac{q_i - q_{i+1}}{C_i} \tag{2.25}$$

At furcations:

$$\begin{aligned}
\dot{p}_4 &= \frac{q_4 - q_5 - q_{33} - q_{94} - q_{113}}{C_4}, \quad \dot{p}_5 = \frac{q_5 - q_6 - q_8 - q_{24}}{C_5} \\
\dot{p}_{14} &= \frac{q_{14} - q_{15} - q_{20}}{C_{14}}, \qquad \dot{p}_{15} = \frac{q_{15} - q_{16} - q_{19}}{C_{15}} \\
\dot{p}_{36} &= \frac{q_{36} - q_{37} - q_{90}}{C_{36}}, \qquad \dot{p}_{37} = \frac{q_{37} - q_{38} - q_{39} - q_{40} - q_{89}}{C_{37}} \\
\dot{p}_{41} &= \frac{q_{41} - q_{42} - q_{43} - q_{66}}{C_{41}}, \qquad \dot{p}_{46} = \frac{q_{46} - q_{47} - q_{49}}{C_{46}} \\
\dot{p}_{55} &= \frac{q_{55} - q_{56} - q_{61}}{C_{55}}, \qquad \dot{p}_{69} = \frac{q_{69} - q_{70} - q_{87}}{C_{69}} \\
\dot{p}_{76} &= \frac{q_{76} - q_{77} - q_{82}}{C_{76}}, \qquad \dot{p}_{94} = \frac{q_{94} - q_{95} - q_{111}}{C_{94}} \\
\dot{p}_{101} &= \frac{q_{101} - q_{102} - q_{106}}{C_{101}}, \qquad \dot{p}_{106} = \frac{q_{106} - q_{107} - q_{108}}{C_{106}} \\
\dot{p}_{116} &= \frac{q_{116} - q_{117} - q_{120}}{C_{116}}
\end{aligned} \tag{2.26}$$

At terminal nodes:

$$\begin{aligned}
\dot{q}_{in} &= \frac{2\ p_{in}}{L} - \frac{2\ p}{L} - \frac{2\ R\ q_{in}}{L} \\
\dot{p} &= \frac{q_{in}}{C} - \frac{q_{out}}{C} \\
\dot{q}_{out} &= \frac{2\ p}{L} - \frac{2\ p_{out}}{L} - \frac{2\ R_b\ q_{out}}{L}, \\
\text{for } i &= \begin{cases} 7, 18, 19, 23, 29, 32, 38, 39, 42, \\ 48, 60, 65, 81, 86, 88, 89, 91, 92, \\ 93, 105, 107, 110, 112, 119, 122 \end{cases}
\end{aligned} \tag{2.27}$$

2.3.4 Formulation of the visco-elastic CV model

Pressure and flow equations for non-terminal nodes:

Flow equations:
Flow equations for linear- and visco-elastic models are identical (see section 2.3.3).

Pressure equations:
At non-furcation nodes:

$$\dot{p}_i = \frac{R_{d_i} p_{i-1}}{L_i} + \Big(\frac{1}{C_i} - \frac{R_{d_i} R_i}{L_i}\Big) q_{i-1} - \frac{q_i}{C_i} - \frac{R_{d_i} p_i}{L_i} \tag{2.28}$$

At furcations:

$$
\begin{aligned}
\dot{p}_4 &= \frac{R_{d_4}p_3}{L_4} + \Big(\frac{1}{C_4} - \frac{R_{d_4}R_4}{L_4}\Big)q_3 - \frac{q_5+q_{33}+q_{94}+q_{113}}{C_4} - \frac{R_{d_4}p_4}{L_4} \\
\dot{p}_5 &= \frac{R_{d_5}p_4}{L_5} + \Big(\frac{1}{C_5} - \frac{R_{d_5}R_5}{L_5}\Big)q_4 - \frac{q_6+q_8+q_{24}}{C_5} - \frac{R_{d_5}p_5}{L_5} \\
\dot{p}_{14} &= \frac{R_{d_{14}}p_{13}}{L_{14}} + \Big(\frac{1}{C_{14}} - \frac{R_{d_{14}}R_{14}}{L_{14}}\Big)q_{13} - \frac{q_{15}+q_{20}}{C_{14}} - \frac{R_{d_{14}}p_{14}}{L_{14}} \\
\dot{p}_{15} &= \frac{R_{d_{15}}p_{14}}{L_{15}} + \Big(\frac{1}{C_{15}} - \frac{R_{d_{15}}R_{15}}{L_{15}}\Big)q_{14} - \frac{q_{16}+q_{19}}{C_{15}} - \frac{R_{d_{15}}p_{15}}{L_{15}} \\
\dot{p}_{36} &= \frac{R_{d_{36}}p_{35}}{L_{36}} + \Big(\frac{1}{C_{36}} - \frac{R_{d_{36}}R_{36}}{L_{36}}\Big)q_{35} - \frac{q_{37}+q_{90}}{C_{36}} - \frac{R_{d_{36}}p_{36}}{L_{36}} \\
\dot{p}_{37} &= \frac{R_{d_{37}}p_{36}}{L_{37}} + \Big(\frac{1}{C_{37}} - \frac{R_{d_{37}}R_{37}}{L_{37}}\Big)q_{36} - \frac{q_{38}+q_{39}+q_{40}+q_{89}}{C_{37}} - \frac{R_{d_{37}}p_{37}}{L_{37}} \\
\dot{p}_{41} &= \frac{R_{d_{41}}p_{40}}{L_{41}} + \Big(\frac{1}{C_{41}} - \frac{R_{d_{41}}R_{41}}{L_{41}}\Big)q_{40} - \frac{q_{42}+q_{43}+q_{66}}{C_{41}} - \frac{R_{d_{41}}p_{41}}{L_{41}} \\
\dot{p}_{46} &= \frac{R_{d_{46}}p_{45}}{L_{46}} + \Big(\frac{1}{C_{46}} - \frac{R_{d_{46}}R_{46}}{L_{46}}\Big)q_{45} - \frac{q_{47}+q_{49}}{C_{46}} - \frac{R_{d_{46}}p_{46}}{L_{46}} \\
\dot{p}_{55} &= \frac{R_{d_{55}}p_{54}}{L_{55}} + \Big(\frac{1}{C_{55}} - \frac{R_{d_{55}}R_{55}}{L_{55}}\Big)q_{54} - \frac{q_{56}+q_{61}}{C_{55}} - \frac{R_{d_{55}}p_{55}}{L_{55}} \\
\dot{p}_{69} &= \frac{R_{d_{69}}p_{68}}{L_{69}} + \Big(\frac{1}{C_{69}} - \frac{R_{d_{69}}R_{69}}{L_{69}}\Big)q_{68} - \frac{q_{70}+q_{87}}{C_{69}} - \frac{R_{d_{69}}p_{69}}{L_{69}} \\
\dot{p}_{76} &= \frac{R_{d_{76}}p_{75}}{L_{76}} + \Big(\frac{1}{C_{76}} - \frac{R_{d_{76}}R_{76}}{L_{76}}\Big)q_{75} - \frac{q_{77}+q_{82}}{C_{76}} - \frac{R_{d_{76}}p_{76}}{L_{76}} \\
\dot{p}_{94} &= \frac{R_{d_{94}}p_{93}}{L_{94}} + \Big(\frac{1}{C_{94}} - \frac{R_{d_{94}}R_{94}}{L_{94}}\Big)q_4 - \frac{q_{95}+q_{111}}{C_{94}} - \frac{R_{d_{94}}p_{94}}{L_{94}} \\
\dot{p}_{101} &= \frac{R_{d_{101}}p_{100}}{L_{101}} + \Big(\frac{1}{C_{101}} - \frac{R_{d_{101}}R_{101}}{L_{101}}\Big)q_{100} - \frac{q_{102}+q_{106}}{C_{101}} - \frac{R_{d_{101}}p_{101}}{L_{101}} \\
\dot{p}_{106} &= \frac{R_{d_{106}}p_{105}}{L_{106}} + \Big(\frac{1}{C_{106}} - \frac{R_{d_{106}}R_{106}}{L_{106}}\Big)q_{101} - \frac{q_{107}+q_{108}}{C_{106}} - \frac{R_{d_{106}}p_{106}}{L_{106}} \\
\dot{p}_{116} &= \frac{R_{d_{116}}p_{115}}{L_{116}} + \Big(\frac{1}{C_{116}} - \frac{R_{d_{116}}R_{116}}{L_{116}}\Big)q_{115} - \frac{q_{117}+q_{120}}{C_{116}} - \frac{R_{d_{116}}p_{116}}{L_{116}}
\end{aligned}
\tag{2.29}
$$

Pressure and flow equations for terminal nodes:

$$
\begin{aligned}
\dot{q}_i &= \frac{2p_{i-1}}{L_i} - \frac{2p_i}{L_i} - \frac{2R_iq_i}{L_i} \\
\dot{p}_i &= \frac{4R_{d_i}p_i}{L_i} + \Big(\frac{2R_{d_i}R_b}{L_i} - \frac{1}{C_i}\Big)q_{out} + \Big(\frac{1}{C_i} - \frac{2R_{d_i}R_i}{L_i}\Big) \\
&+ \frac{2R_{d_i}p_{out}}{L_i} + \frac{2R_{d_i}p_{i-1}}{L_i} \\
\dot{q}_{out} &= \frac{2p_i}{L_i} - \frac{2p_{out}}{L_i} - \frac{2R_bq_{out}}{L_i}, \\
\text{for } i &= \begin{cases} 7,18,19,23,29,32,38,39,42, \\ 48,60,65,81,86,88,89,91,92, \\ 93,105,107,110,112,119,122 \end{cases}
\end{aligned}
\tag{2.30}
$$

2.3.5 Arterial geometry and physiological data

The geometry of arterial network and parameter values were taken from [23]. At each artery segment there are 3-electrical (R_i, C_i, L_i) and 4-structural parameters

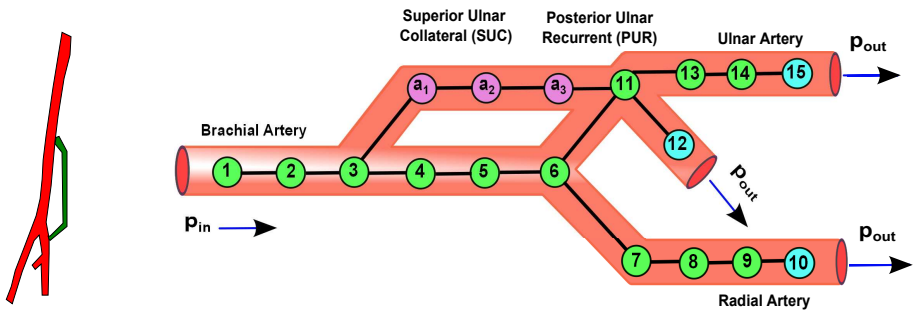

Figure 2.5: Simplified anatomy of the arm arteries (left) and model geometry of brachial, superior ulnar collateral anastomosis with posterior ulnar recurrent (SUC-PUR), ulnar and radial arteries (right). The number of segments is $N_s = 15$ (without anastomosis) and $N_{as} = 18$ (with anastomosis), both with $N_t = 3$ terminal nodes.

(E_i, l_i, d_i, h_i). The values of electrical parameters can be obtained from structural parameters, using the relationships given in eqns. (2.5), (2.7) and (2.11). The nominal parameter values are given in appendix A.6. For arterial anastomosis the value of parameters are taken from [24] and given in appendix A.5.

2.4 Important cardiovascular structures under consideration

Two important cardiovascular structures, arm arteries (with and without anastomosis) and carotid bifurcation are extensively studied using sensitivity analysis, see figures (2.5) and (2.6). In chapter 3, a linear elastic model of the arm arteries is considered for local sensitivity analysis, while in chapter 4, a linear visco-elastic model of carotid bifurcation is taken for global sensitivity analysis. For better readability, the segments are renumbered in arm artery and carotid bifurcation. The geometry of the arm artery is taken from the figure (2.3) and segments from 9-23 are renumbered as 1-15. On the other hand, the geometry of the carotid bifurcation is taken from MACSim (see figure 2.7) and nodes number 90-95 are renumbered as 1-6. The derivation of both structures can be obtained from sections 2.3.3 and 2.3.4, however, the additional anastomosis equations are given below:

2.4.1 Model equations with anastomosis

From the network structure of the arm artery with SUC-PUR anastomosis, it is evident, that the flow will split at nodes 3 and 6 and will merge at node 11. Further, the inlet pressure at node 11 is the same as in nodes 6 and a_3, see figure (2.5). The additional equations for three nodes of SUC-PUR anastomosis are,

Anastomosis flow equations:

$$\begin{aligned} \dot{q}_{a_1} &= \frac{p_3 - p_{a_1} - R_{a_1} q_{a_1}}{L_{a_1}} \quad \dot{q}_{a_2} = \frac{p_{a_1} - p_{a_2} - R_{a_2} q_{a_2}}{L_{a_2}} \\ \dot{q}_{a_3} &= \frac{p_{a_2} - p_6 - R_{a_3} q_{a_3}}{L_{a_3}} \end{aligned} \tag{2.31}$$

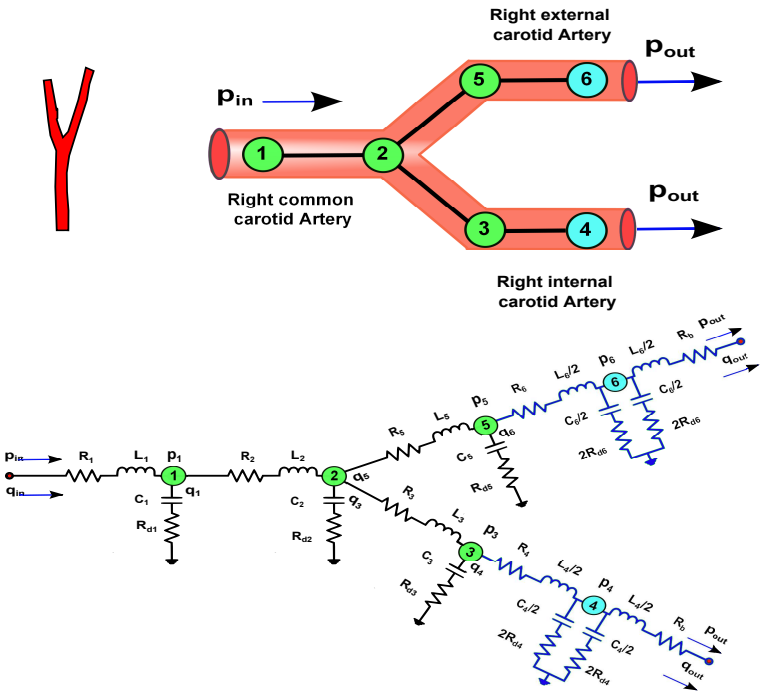

Figure 2.6: Simplified anatomy (top, left) and model geometry of RCC, RIC and REC arteries with number of nodes $N_s = 6$ and terminal nodes $N_t = 2$ (top, right). Each non-terminal and terminal node of carotid bifurcation is modeled by its corresponding non-terminal and terminal electric circuit (bottom).

Anastomosis pressure equations:

$$\begin{aligned} \dot{p}_3 &= \frac{q_3 - q_4 - q_{a_1}}{C_3}, \quad \dot{p}_{a_1} = \frac{q_{a_1} - q_{a_2}}{C_{a_1}}, \quad \dot{p}_{a_2} = \frac{q_{a_2} - q_{a_3}}{C_{a_2}} \\ \dot{p}_{a_3} &= \frac{q_{a_3} + q_6 - q_{11}}{C_6 + C_{a_3}} \end{aligned} \tag{2.32}$$

According to the conservation of momentum the pressure at nodes 6 and a_3 is identical.

2.5 MACSim (Major Arterial Cardiovascular Simulator)

MACSim is a physical flow simulator developed for research and teaching purposes, e.g. early detection of stenoses and aneurysms and their impact on the pressure and flow waves at different locations of the circulatory system [75]. The model consists of an artificial 1:1 replica of linear-elastic model of human circulatory system, where, the major arteries are divided into 96 nodes, including one heart node (), 62 non-terminal () and remaining 33 terminal nodes () (see figure 2.3). Each non-terminal and terminal node is represented by its corresponding non-terminal and terminal linear-elastic Windkessel element. The model equations for MACSim can easily be derived using section 2.3.3. Foe further details, see Chapter 5.

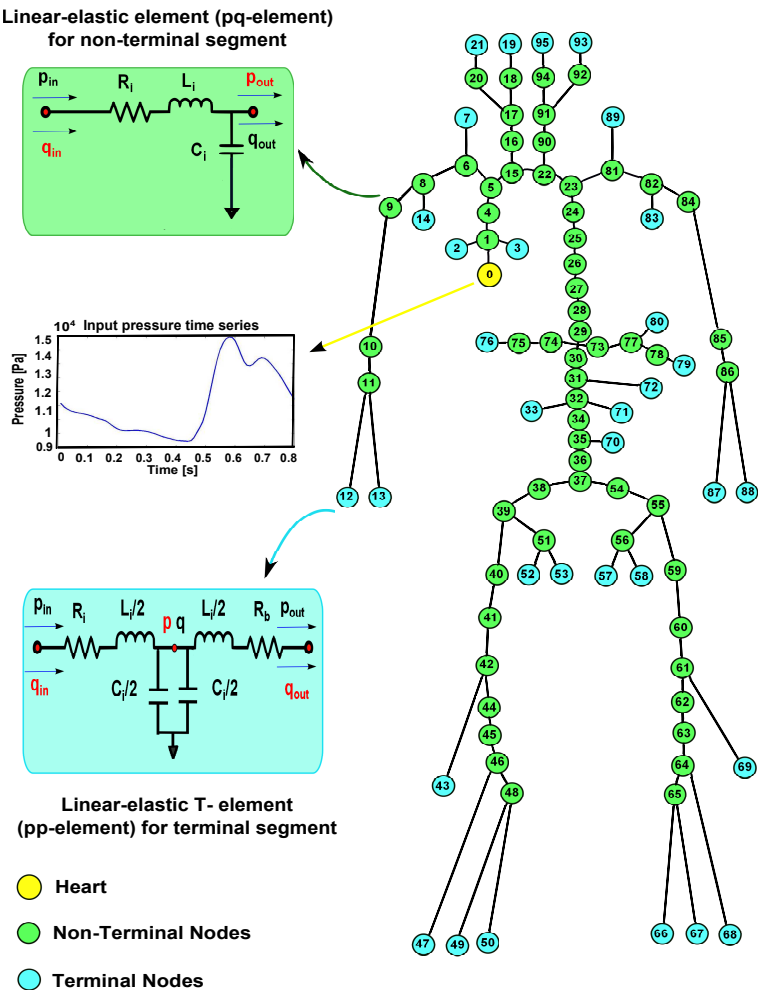

Figure 2.7: MACSim model geometry of systemic circulation with input pressure time series and linear elastic circuit elements for non-terminal and terminal segments.

2.6 State representation of the model

The state representation is a compact way to model a physical system as a set of input, output and state variables related by first order differential equations [43]. In this representation, there is a system of two equations: an equation for determining state x_t of the system (state equation), and another equation to describe the output y_t of the system (observation equation). The matrix form can be written as

$$\dot{x}_t = Ax_t + Bu_t, \tag{2.33}$$

$$y_t = Cx_t + Du_t. \tag{2.34}$$

Here, x_t, is the state vector of the system, u_t the input vector and y_t, the observation vector. The dynamics of the system is described by the state dynamics matrix, $A \in M(n \times n)$. The input matrix, $B \in M(n \times i)$ specifies the time dependency on boundary conditions (BC) applied at in- and outflow locations and the observation matrix, $C \in M(m \times n)$ defines the observation locations within the state-space system, i.e. the nodal location in the network. Here, m denotes the number of observations. Finally, the input to observation matrix, $D \in M(m \times i)$ models

the influence of the input vectors and accounts for the observation of the BC. Besides its computational advantage, the state-space form allows the integration of experimental measurements (observations) into the model building process. This step is essential for the adjacent model parameter estimation from experimental measurements, that are planned in a future study. The state vector, x_t, contains the flow and pressure functions at all network locations, whereas, the output vector, y_t contains the flow and pressure at observed nodes i. The state representation matrices, A, B, C and D of linear elastic, linear visco-elastic vessel segments and carotid bifurcation are given in appendices A.1, A.2 and A.3 respectively.

2.6.1 Numerical solvers

As the model under consideration is LTI-MIMO (linear time invariant-multiple inputs and multiple outputs) system, the MATLAB built in solvers '*lsim*' and '*ode45*' were used to solve the model equations, (2.33) and (2.34). The MATLAB solver, *lsim* is very useful in GSA to get a reasonable measure of sensitivity analysis with affordable computational cost. The simulations in this thesis are carried out on a personal computer with an Intel Core 2 Duo (2.10 GHz) processor and 3 GB memory. The overall computational cost of LSA and GSA methods applied on partial or complete CV system is given in appendix A.9.

CHAPTER 3

Local Sensitivity Analysis of Arterial Anastomosis

3.1 Introduction

With growing interest in the prediction and diagnosis of cardiovascular diseases, different mathematical models have been developed and applied. Lumped-parameter models (electrical analogy to fluid flow) have shown to be an effective approach in modeling the human cardiovascular system [20–23, 25–28, 43]. A mathematical model is a simplified version of the real-world problem. The reliability of the CV models in medical decision making depends upon the accuracy of the model outputs. Model outputs mainly rely on input factors i.e. parameters and their feasible regions, in- and output boundary conditions, model structure and spatio-temporal variabilities. In practice, the values of all input factors are not precisely known, which further introduce uncertainty in the outputs due to the imprecision in input factors.

In order to make cardiovascular models more predictive, to explain the most important features of the real process, the output uncertainty can be reduced through sensitivity analysis. In sensitivity analysis, the uncertainty in the outputs of a mathematical model or system can be apportioned to different sources of uncertainty in its inputs [36, 48–52]. Sensitivity analysis is a powerful approach to find influential and therefore important cardiovascular system (CVS) parameters [35–38]. In order to reduce the output uncertainty, important parameters can further be estimated using clinically obtained measurements.

The simplest and efficient form of the sensitivity analysis is to vary one model parameter at a time by a given amount and examine the impact on output results. The analysis could be repeated for all model parameters independently at different times. The method is known as local sensitivity analysis (LSA) or one-factor-at-a-time (OFAT) [18, 19, 44].

Before performing the sensitivity analysis, it is important to know the input and output quantities of interest (QoI) in a CV model. In this work, LSA is applied on a linear elastic model of the arm artery (with and without anastomosis). The output quantities of interest are the pressure and the flow at all nodes of the arm artery, whereas, electrical and the structural parameters are considered as input quantities of interest.

3.1.1 Scope of the current work

In this study, we are interested how structural changes, like for example anastomosis influence local sensitivities. Anastomoses are the interconnection between vessels, which provide a collateral circulation and also act as a second rout of blood flow when main vessels are blocked by plaque, atherosclerosis or stenosis, to minimize the damages at tissue level.

In the context of anastomosis, another important concept is valve-less flow. William Harvey published a report explaining "impedance defined flow", which explained a mechanism for valve-less flow [39]. Later on, Weber [40] stated that the heart is not able to pump blood alone, but there are other forces which help in circulation. There are several structural aspects in the cardiovascular system, which control the blood flow or simply create valve-less flow like, viscous and inertial effects and also elastic properties of two vessels [41]. Details of the valve-less flow mechanism are given in [42] and will not be discussed here in detail. Further, we will not discuss turbulent effects that appear in merging flows at the end-to-side anastomosis, which mainly depend upon the angle and flow rate of the merging vessels.

In this work, a lumped-parameter model of anastomosis around the elbow joint (SUC-PUR) is presented. The luminal diameter or equivalently the flow resistance is an important parameter, the study concentrates on the sensitivity of the pressure and flow with respect to the viscous flow resistance and the boundary resistance.

Keeping in mind the geometry of the arm arteries (with and without anastomosis) with in- and output quantities of interest, the aims of study are summarized as,

1. Identify the most influential CV parameters on the hemodynamic state variables, pressure and flow.
2. Finding optimal measurement locations and optimal time regions in the flow and pressure waves w.r.t. each CV parameters. The information can further be used in setting the optimal measurement locations of state variables to estimate the most influential CV parameters.
3. Discuss and explain the clinically relevant cardiovascular parameters in the arterial anastomosis.

With this work, we also intend to validate different methodologies of local sensitivity analysis, using a simple example problem of the arm artery to show the principle agreement with Ohm's law of hydrodynamics. However, the method could be used to analyze more complex CV networks.

3.2 Methods of local sensitivity analysis

For the purpose of evaluating the relative effect of CV parameters on the model output at a single point, the normalized partial derivative provides a useful sensitivity index. Normalized sensitivity coefficients are obtained by multiplying the partial derivative with the ratio of nominal point estimates as,

$$S_{ij} = \frac{\partial y_i}{\partial \theta_j} \times \frac{\theta_j}{y_i}, \tag{3.1}$$

where y_i is the i-th model output and θ_j is the j-th model parameter.

Another way to calculate sensitivity coefficients (S_{ij}), is the *direct differential method* (DDM), which solves the system of differential equations for sensitivity coefficients (for complete derivation, see Appendix $\mathbb{A}$)

$$\dot{S} = f_\theta + J \times S. \tag{3.2}$$

The sensitivity coefficients matrix, S can be obtained by solving the model equations (with and without anastomosis) simultaneously with the system (eqn. 3.2) using an appropriate differential equation solver. Although the model under consideration is linear and can be solved analytically, the solution of eqn. (3.2) is problematic. Another drawback associated with DDM is, that the Jacobian needs to be defined, which is time consuming for large-scale problems [44].

These shortcomings and the focus on more complex systems, persuade us to apply the finite difference approach to calculate the sensitivity coefficients, because the method is simple easy to implement.

3.2.1 Sensitivity by finite difference method

In local sensitivity analysis, parameters are varied segment wise by some portion around a fixed value (nominal value) and the effects of individual perturbations on the observations are studied [44]. Mathematically, the normalized sensitivity coefficients can be obtained using a first order *finite difference* method as,

$$\begin{aligned} S_{ij} = \frac{\partial y_i}{\partial \theta_j} \times \frac{\theta_j}{y_i} &= \lim_{\Delta\theta \to 0} \frac{y_i(\theta_j + \Delta\theta_j) - y_i(\theta_j)}{\Delta\theta_j} \times \frac{\theta_j}{y_i}, \\ &\simeq \frac{y_i(\theta_j + \Delta\theta_j) - y_i(\theta_j)}{\Delta\theta_j} \times \frac{\theta_j}{y_i}, \end{aligned} \tag{3.3}$$

where $\Delta\theta_j = 0.001 \times \theta_j$ is the change in the model parameters. Eqn. (3.3) produces a set of two sensitivity time series, $S_{ij}(t)$ (one for pressure and one for flow) per parameter and per network node.

3.2.2 Sensitivities by using norms

Another method to quantify percentage changes in the state variables due to a change in model parameters is to introduce a norm. To obtain a measure that validates the sensitivities, the mean Euclidean distances of the observations are computed with different parameter sets, θ_1 and θ_2. Here θ_1 is the nominal parameter set and θ_2 is a parameter set with 0.1% change in θ_1.

$$\|\theta_1, \theta_2\| := \underset{t \in T}{mean} \frac{\| \ y_i(\theta_2, t) - y_i(\theta_1, t) \ \|_2}{\|y_i(\theta_1, t)\|_2} \times 100 \qquad i = 1, 2, 3...2 \times N_s.$$

3.3 Simulation setup

In this Chapter, two-LSA methods are applied on a linear elastic lumped-parameter model of the arm arteries (with and without anastomosis). For the arm artery without anastomosis the total number of segments (nodes), $N_s = 15$. At each node 3-electrical and 4-structural parameters are considered for sensitivity analysis. For the arm artery anastomosis the number of segments (nodes), $N_s = 18$ and sensitivity analysis was carried out with respect to R and R_b. The network equations are solved by MATLAB built in solver, *lsim* and *ode45*. Initially the model was run for three heart beats, so that a steady state condition was reached. Then the results from last heart beat were used for sensitivity analysis.

For each electrical and structural parameter, there are two sensitivity time series at each node, one for the pressure and one for the flow. In total, there are $2 \times N_s \times K$ sensitivity time series obtained. Where, K is the total number of parameters. The time series obtained are large in number, so the mean of absolute sensitivities (MAS) for each parameter is computed to analyze the sensitivity of the whole network. Each cell in figures (3.2), (3.4) and (3.6) represents the mean absolute value of the time series, $S_{ij}(t)$. In these figures, the results of sensitivity analysis can be

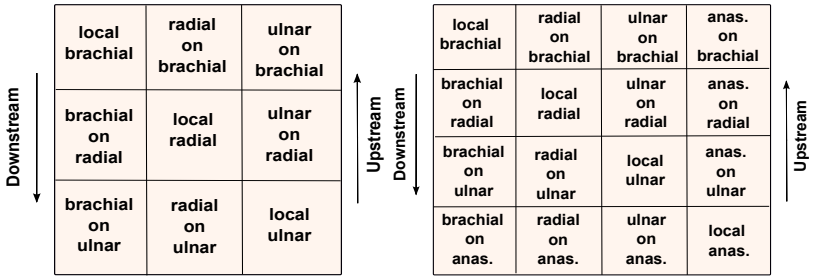

Figure 3.1: Sensitivity pattern in arm arteries with anastomosis (right) and without anastomosis (left), obtained by changing the values of structural and electrical cardiovascular parameters.

interpreted with the help of figure (3.1). Where, the matrix diagonal displays the sensitivities within the segments of variation itself and the off diagonals are related to the sensitivities of upstream and downstream segments

3.4 Results and discussion

The results of LSA are divided into two parts as,

1. Sensitivity analysis with respect to structural parameters, $Eldh$ (without anastomosis).

2. Sensitivity analysis with respect to electrical parameters, $RCLR_b$ (with and without anastomosis).

In this context, network location and time-dependent sensitivities are discussed. Also, the sensitivity results of structural parameters in the arm artery (without anastomosis) are compared to the 2-norm of the distance vector of the state variables of two time series.

3.4.1 Sensitivity analysis with respect to (E,l,d,h)

In this section, sensitivity with respect to E, l, d and h is studied for state variables in the arm artery (without anastomosis). Moreover, location and time-dependent sensitivities are also discussed. The sensitivity results of structural parameters in the arm artery (without anastomosis) are finally compared to the 2-norm of the distance vector of the state variables of two time series.

3.4.1.1 Sensitivity analysis in the arm artery (without anastomosis)

In the arm artery (without anastomosis), there are 60-structural parameters (E, l, d, h), influencing all state variables. From figure (3.2, A_1), it is evident that E has a small impact on the flow in the brachial artery, while no sensitivity was found for the pressure. The sensitivity results of pressure and flow w.r.t E and h are identical, as they appear linearly in the model equation (eqn. (2.7)). Flow is sensitive w.r.t. l and d at the location itself in the brachial artery and has strong upstream sensitivity within the brachial artery. Strong upstream and downstream sensitivity was observed at node 11 (ulnar artery) (figure (3.2, A_2, A_4)). Pressure is also sensitive w.r.t. l and d at node 11 and has strong sensitivity within the ulnar artery, see figure (3.2, A_3, A_5).

The sensitivity results reveal, that d and l are the key parameters in the arm artery, especially, in the brachial artery. More importantly, the sensitivity of the

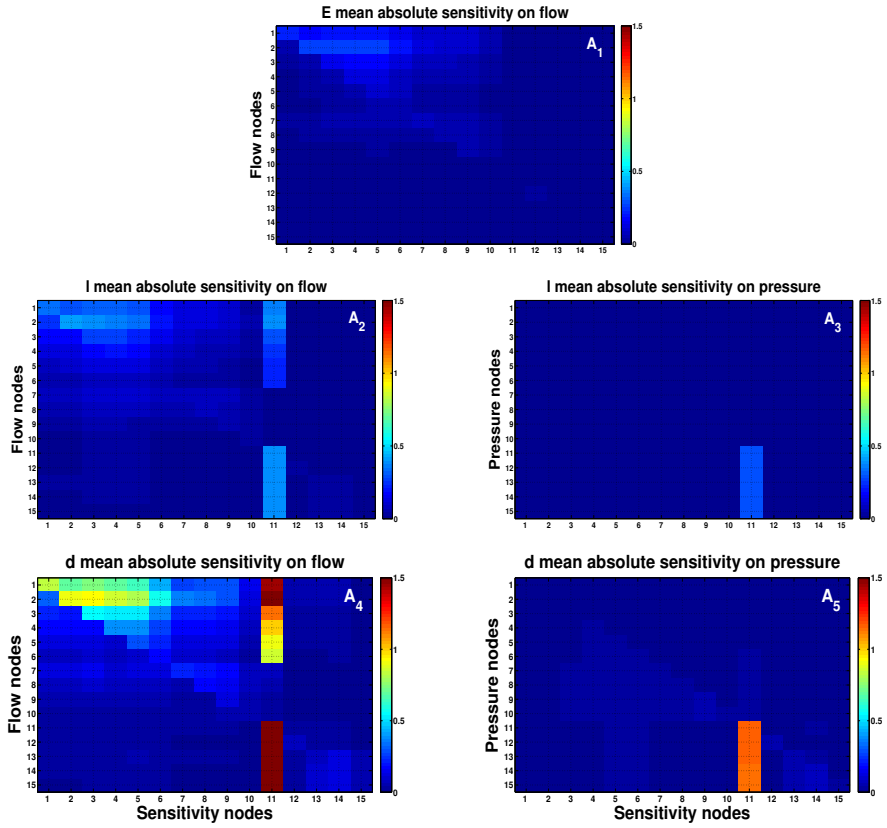

Figure 3.2: Sensitivity of the pressure and flow with respect to E, l, d and h. The results reveal that l and d are the most important, while E and h are less important CV parameters.

pressure and flow with respect to d and l is location-dependent.

Network location and time-dependent sensitivities:
Network location and time-dependent sensitivities play an important role in finding optimal measurement locations in the arm artery and optimal time regions of the state variables with respect to each parameter. The results of the time-dependent sensitivity analysis contain several aspects that are important, especially, in the estimation of cardiovascular parameters from pressure and flow measurements. It is well known, the parameters that have a strong influence on the pressure and flow can be estimated with high accuracy, while less influential parameters cannot be estimated at all. Thus, the identification of optimal measurement locations and sensitive regions with the cardiac cycle could benefit parameter estimation. For example, during the parameter estimation if only sensitive regions of the flow and pressure waves are used in complement with optimal measurement locations, then a better estimation of parameters is expected.

For flow, the optimal measurement locations of key parameters $(l_1, ...l_6)$ and $(d_1, ...d_6)$ are in the brachial artery. Also, the optimal measurement locations of d_{11} are in the brachail and the ulnar artery.

The time-dependent sensitivity of parameters was found in common time regions i.e. at early systole, peak systole, end systole and end diastole. In figure (3.3), time-dependent sensitivities of d_3 and d_7 are plotted against the pressure and flow waves in the arm artery. For the flow, the optimal time regions are only in the end systole

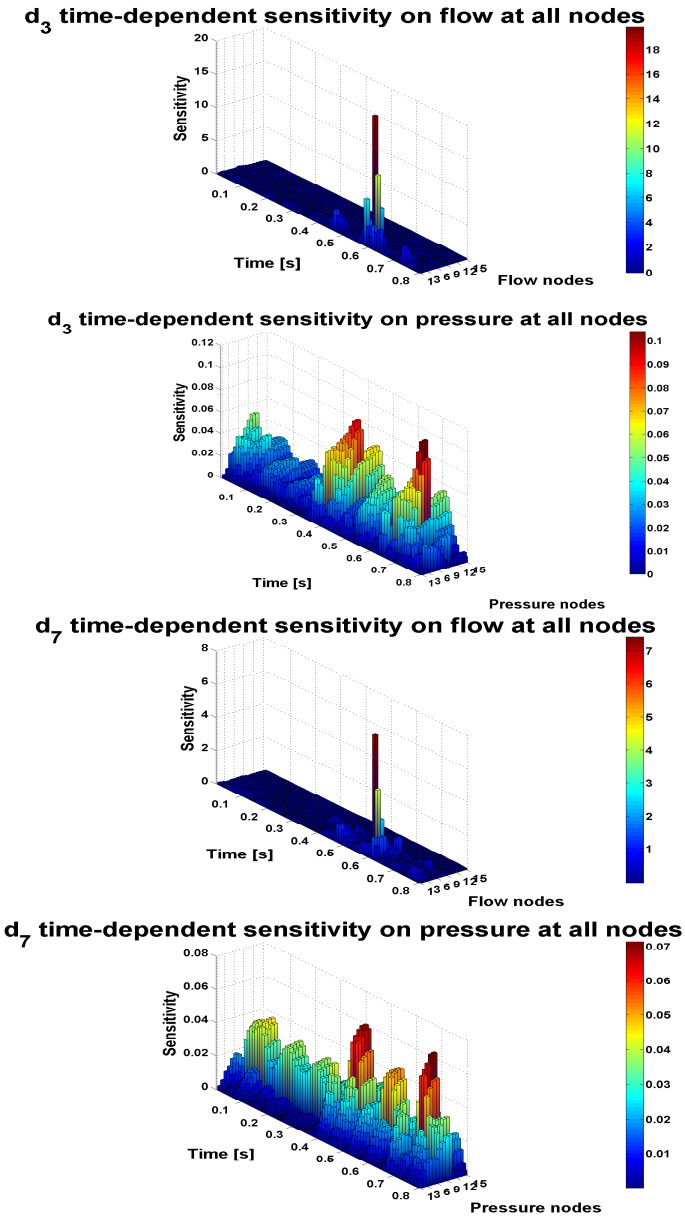

Figure 3.3: Time-dependent sensitivity of the pressure and flow with respect to d_3 and d_7 in the arm artery.

and early diastole, while for the pressure, the optimal time regions are early systole, end systole and early diastole.

3.4.1.2 Results comparison with sensitivity by norms

In order to validate the sensitivity results, a comparison is made between the sensitivity results of structural parameters (without anastomosis) with those obtained by using norms. As mentioned in section **??**, for structural parameters the total number of sensitivity time series obtained is $2 \times N_s \times K = 2 \times 15 \times 60 = 1800$. Therefore, it is not possible to present complete sensitivity results. In this work, sensitivity of pressure and flow w.r.t. structural parameters is shown at node 7 (ra-

dial artery). It was found that the diameter and length of vessel are most influential parameters, while E and h were found less influential parameters. Moreover, the norm computed for the wall thickness and elastic modulus has identical values (see table 3.1 and table 3.2).

3.4.2 Sensitivity analysis with respect to (R_i, C_i, L_i, R_b)

This section describes the sensitivity of the state variables with respect to R, C and L in the arm artery (without anastomosis). Also, the impact of flow control parameters, R and R_b under different conditions is discussed in the arm artery anastomosis.

3.4.2.1 Sensitivity analysis in the arm artery (without anastomosis)

The sensitivity of the flow with respect to the viscous flow resistance, R indicates a small impact within brachial, radial and ulnar arteries. A strong sensitivity was found at node 12 with significant upstream effect on the brachial artery (see figure 3.4, C_1). Pressure is sensitive at the location itself and has significant downstream sensitivity within brachial, radial and ulnar arteries. While, negligible effect was found from radial to ulnar and from ulnar, radial to brachial arteries, see figure (3.4, C_2).

The results indicate, that the flow is sensitive with respect to the compliance, C and the blood inertia, L at the location itself within the brachial artery. Also, strong upstream sensitivity was observed from each node of the brachial artery. Pressure is also sensitive in the brachial artery and has significant downstream sensitivity on radial and ulnar arteries, see figure (3.4, C_3, C_4, C_5, C_6).

Network location and time-dependent sensitivities:
The optimal network locations for the flow and pressure measurements to estimate $\{C_1, ...C_6\}$ and $\{L_1, ...L_6\}$ are in the brachial artery, see figure (3.4, C_3, C_5). Also, these parameter values can be accessed from the flow and pressure measurements at radial and ulnar arteries (see figure (3.4, C_4, C_6)). In figure (3.5), time-dependent sensitivity of the flow and pressure is plotted with respect to d_3 and d_7. For the flow, the optimal time regions are only during the end systole and early diastole, while for the pressure, the optimal time regions are early systole, end systole and early diastole.

	N_1	N_2	N_3	N_4	N_5	N_6	N_7	N_8	N_9	N_{10}	N_{11}	N_{12}	N_{13}	N_{14}	N_{15}
	q_1	q_2	q_3	q_4	q_5	q_6	q_7	q_8	q_9	q_{10}	q_{11}	q_{12}	q_{13}	q_{14}	q_{15}
E	0.015	0.019	0.014	0.019	0.016	0.019	0.024	0.018	0.027	0.013	0.004	0.005	0.005	0.003	0.002
l	0.029	0.028	0.021	0.029	0.027	0.037	0.050	0.049	0.052	0.025	0.007	0.008	0.008	0.006	0.003
d	**0.064**	**0.062**	**0.047**	**0.060**	**0.063**	**0.061**	**0.103**	**0.068**	**0.073**	**0.033**	**0.015**	**0.014**	**0.020**	**0.014**	**0.007**
h	0.015	0.019	0.014	0.019	0.016	0.019	0.024	0.018	0.027	0.013	0.004	0.005	0.005	0.003	0.002

Table 3.1: Sensitivity of E, l, d and h at node 7 of the arm artery (see figure (2.5), without anastomosis) and their corresponding percentage change in flow at each node. In agreement to sensitivity computations the norm is large for change in d.

	N_1	N_2	N_3	N_4	N_5	N_6	N_7	N_8	N_9	N_{10}	N_{11}	N_{12}	N_{13}	N_{14}	N_{15}
	p_1	p_2	p_3	p_4	p_5	p_6	p_7	p_8	p_9	p_{10}	p_{11}	p_{12}	p_{13}	p_{14}	p_{15}
E	0.001	0.001	0.001	0.002	0.002	0.002	0.004	0.003	0.004	0.004	0.001	0.001	0.001	0.001	0.001
l	0.002	0.003	0.003	0.004	0.004	0.003	0.007	0.006	0.009	0.009	0.002	0.002	0.002	0.002	0.002
d	**0.004**	**0.005**	**0.007**	**0.006**	**0.008**	**0.008**	**0.009**	**0.008**	**0.011**	**0.012**	**0.004**	**0.005**	**0.005**	**0.005**	**0.005**
h	0.001	0.001	0.002	0.002	0.002	0.002	0.004	0.003	0.004	0.004	0.001	0.001	0.001	0.001	0.001

Table 3.2: Sensitivity of E, l, d and h at node 7 of the arm artery (see figure (2.5), without anastomosis) and their corresponding percentage change in pressure at each node. In agreement to sensitivity computations the norm is large for change in d.

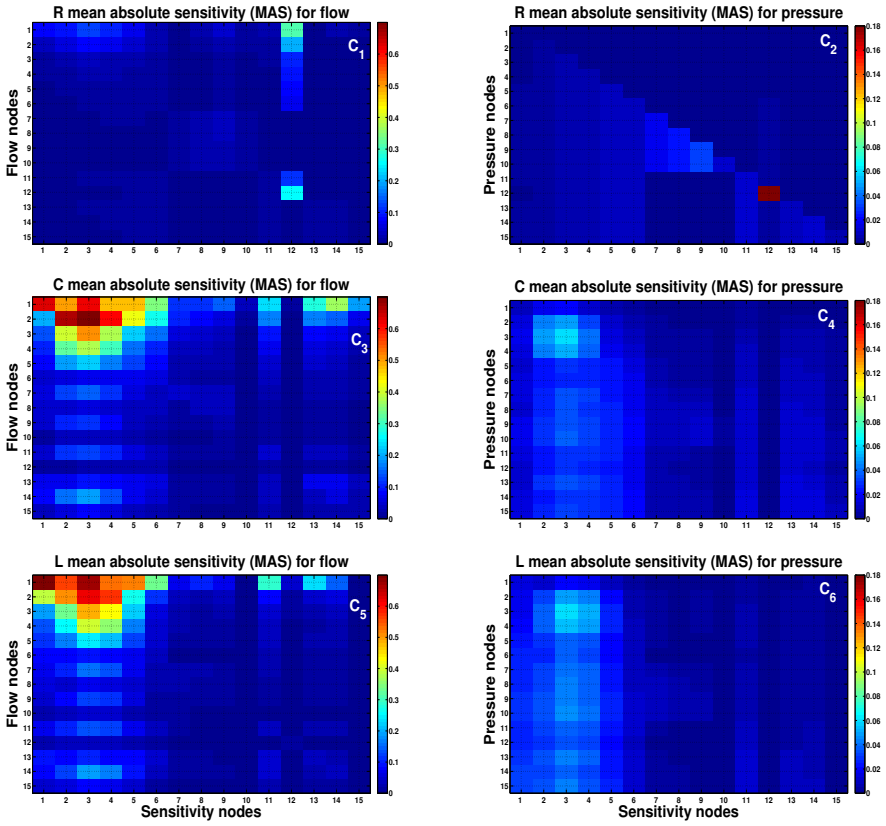

Figure 3.4: Effects of viscous flow resistance R (top), vessel compliance C (middle) and blood inertia L (bottom) on pressure and flow in the arm arteries. Changes in the vessel compliance, C and blood inertia, L in the brachial artery have strong local effects on the flow and have significant downstream effects on radial and ulnar arteries.

3.4.2.2 Sensitivity analysis in the arm artery (with anastomosis)

Blood flow in the SUC-PUR anastomosis (collateral circulation) depends on the size and mainly on the diameter of the anastomosis i.e. smaller diameters reduce the flow in the anastomosis and vice versa. In this study, we focus on the end-to-side anastomosis and show the sensitivity of the anastomosis structure on the pressure and flow by changing the flow resistance, R and the boundary resistance, R_b. Moreover, four different sensitivity scenarios of the arterial anastomosis are discussed, which are explain below.

(a) Effect of R when, $\{RCL\}_a \simeq \{RCL\}_b$:
In order to study the influence of flow resistance through the arterial anastomosis, identical values of RCL are taken for both anastomosis and its parallel brachial artery, i.e. $\{RCL\}_a \simeq \{RCL\}_b$. Here $\{RCL\}_a$ are parameter values of anastomosis nodes (a_1, a_2 and a_3) and $\{RCL\}_b$ are parameter values of brachial nodes which appear in parallel to anastomosis nodes (4, 5 and 6). The equality sign means that corresponding anastomosis nodes have identical parameter values, segment wise as its counterpart brachial nodes.

As it is mentioned earlier, the diameter or equivalently the blood resistance plays an important role in pressure and flow distribution in the cardiovascular system, so we limit our study to changes in the blood resistance in the arterial anastomosis.

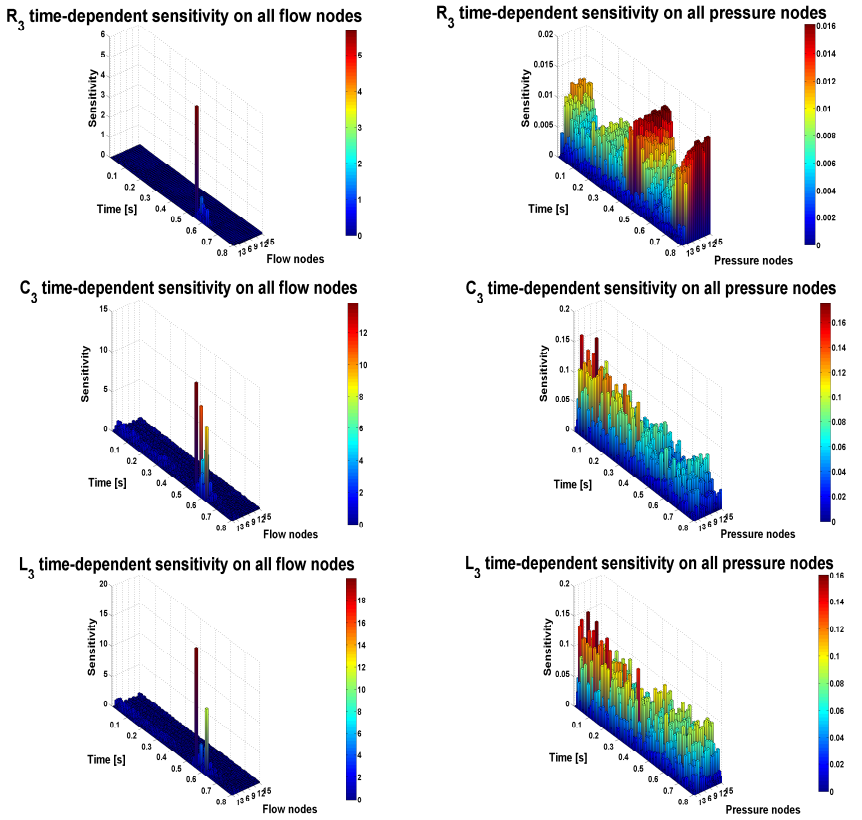

Figure 3.5: Time-dependent sensitivity of the pressure and flow with respect to R_3, C_3 and L_3 in the arm artery.

Flow has small sensitivity with respect to R at nodes 1,2, and 3. More importantly, changing R in the anastomosis or its counter part brachial artery has identical local and upstream/downstream influence on each other (see figure 3.6, E_1). Pressure is sensitive for R at the first three nodes and has small downstream sensitivity on all following nodes. Also, pressure is sensitive within radial and ulnar arteries, see figure (3.6, E_2).

(b) Effect of R in ideal case:
A physiological network with an arterial anastomosis is taken, based on parameter values given in appendix A.5. Flow is sensitive w.r.t. R at the first three nodes and has small downstream influence on the brachial artery, particularly, a strong sensitivity is observed on the anastomosis. Flow is also sensitive within the anastomosis. (see figure 3.6, E_3). Pressure is sensitive at the location itself and has significant downstream sensitivity on the following nodes, see figure (3.6, E_4).

(c) Effect of R in ideal case with large R_b:
When a body has no physical activity then the boundary resistance (R_b) has a large value (here, $R_b = 30 \times R_b$). By increasing R_b, flow will reduce and pressure increase near the terminals. A strong sensitivity is observed with respect to R in the brachial artery with strong downstream sensitivities on the radial, ulnar and anastomosis, particularly, at node 8, 13 and a_3 (see figure 3.6, E_5). Pressure has small sensitivity in the brachial artery with negligible downstream impact on all following nodes (see figure 3.6, E_6).

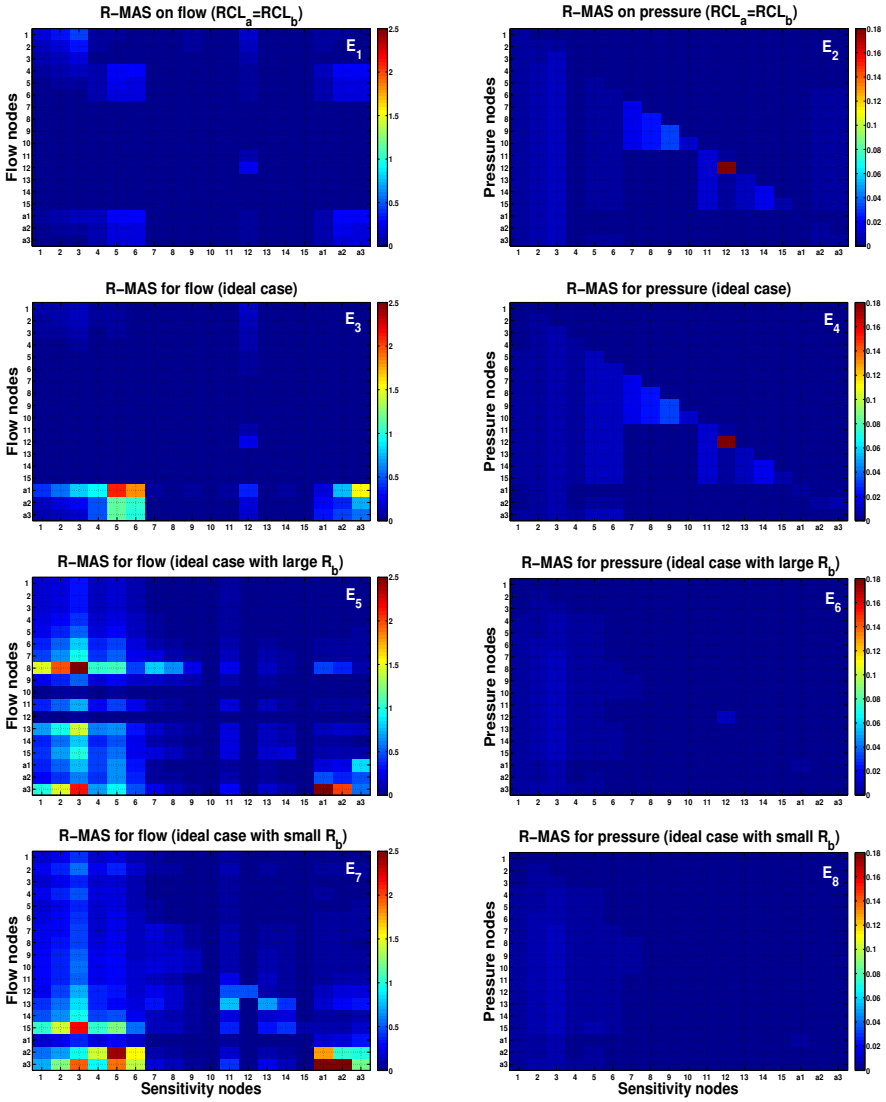

Figure 3.6: Effects of viscous flow resistance, R and boundary resistance, R_b on the pressure and flow at different locations of the arterial anastomosis. From the results, it is seen that, the flow has small sensitivity w.r.t. R in the brachial artery and has strong downstream influence, mainly on the anastomosis.

(d) Effect of R in ideal case with small R_b:
Physical activities lead to a reduction in the boundary resistance, R_b (in our study, $R_b = \frac{R_b}{30}$), which increases the blood flow and decreases mean cardiovascular pressure. As a result, the cardiac output will increase. These are the temporary changes which appear only when we do some physical exercise.

Another artificial reason for low terminal resistance is the implantation of arteriovenous fistula (AVF), which is an abnormal connection between a peripheral artery and a vein. Again flow is sensitive for R in the brachial artery and has significant downstream effect on all following nodes, particularly at nodes 15, a_2 and a_3. Also, pressure has small sensitivity in the brachial artery with negligible downstream influence on all nodes. For the flow, a variation in R within the anastomosis has small upstream sensitivity on the brachial artery, while for the pressure there are small

upstream effects on ulnar, radial and brachial arteries (see figure 3.6, E_7, E_8).

3.5 Conclusion

The methods applied in this study, are seen as a first step towards cardiovascular system identification from cardiovascular measurements. In this work, we have applied local sensitivity analysis on a linear elastic lumped-parameter model of the arm arteries with and without anastomosis. The results indicate a strong dependence of the pressure and flow state variables onto a variation in vessel diameter. Concerning to the elastic properties and the thickness of the arterial wall, a much lower sensitivity was found.

Alternatively, flow is sensitive w.r.t. C and L in the brachial artery and has shown significant downstream effects on all following nodes. On the other hand, pressure is also sensitive w.r.t. C and L in the brachial artery and has significant downstream effects on radial and ulnar arteries.

The method allows to determine network location and time-dependent sensitivities, which are helpful in finding optimal measurement locations and optimal time regions in the cardiac cycle (e.g. early systole, end systole and end diastole). These information can further be used for estimation of key CV parameters. For example, if only sensitive regions of the flow and pressure waves are taken with the complement of optimal measurement locations, then a better estimation of key parameters is expected. The results of time-dependent sensitivity revealed, that most of sensitivity was found in common time regions i.e. early systole, end systole, early diastole and end diastole.

In the arm artery anastomosis, flow has small sensitivity w.r.t. R in the brachial artery and has strong impact on the anastomosis. Changing R_b has strong effects on the flow near the terminal and within the anastomosis. To quantify the results and to compare the variation in state variables according to parameter changes, the concept of norms was used. We found a good agreement to the sensitivity results of structural parameter in the arm artery (without anastomosis) with those obtained using norms.

The methods applied, give satisfactory results if the cardiovascular parameters are independent. In the real scenarios however, they are often interdependent like e.g. the observation of a high correlation between the extension of the elastic walls and the tangential tension caused by transmural pressure. To study these type of effects in a more general way, global sensitivity analysis has to be applied, which deals with variations in many parameters at a time.

CHAPTER 4

Global Sensitivity Analysis of Carotid Bifurcation

4.1 Introduction

In order to overcome the limitations of LSA, global sensitivity analysis (GSA) is used in this Chapter [47–49, 51, 53–55]. GSA performs analysis over the entire feasible region of input parameters and quantifies the impact of parameters and their interactions on output variables. From the last few decades, variance-based GSA methods gained increasing attention among the practitioners. The history of variance-based GSA methods has started with a Fourier implementation in the seventies [51]. Later on, Sobol [48], Homma and Saltelli [49] put great contributions to calculate main and total effect of input parameters on output variables. The main effect or first-order index represents the contribution of each input parameter on output uncertainty. While, the total effect of a parameter represents the first-order effect plus higher-order effects due to interactions with other parameters. Variance-based methods are useful for non-linear and non-monotonic systems, the only difficulty related to these methods is their computational cost. The general scheme for performing variance-based GSA is summarized as:

- First, define input and output quantities of interest (QoI).
- Assign probability density function (pdf) to each input parameter.
- Generate the random numbers within the feasible regions of parameters from a known pdf and evaluate the model outputs deterministically.
- Quantify the impact of input parameters on output variables.

A simplified scheme of conducting GSA can be seen in figure (4.1).

In this Chapter, special emphasis was given to three variance-based GSA methods (Sobol, FAST, sparse grid), applied on a lumped-parameter model of the carotid bifurcation. However, the results (only electrical) obtained from GSA are also compared with LSA (sensitivity using norms). The motivations behind using three GSA methods are:

i To validate and verify the results obtained from one another.

ii Quantify the interactions effect between the parameters, as model is linear but non-linear in parameters.

iii Finding a suitable GSA methodology on the basis of computational cost, simplicity and straightforward implementation.

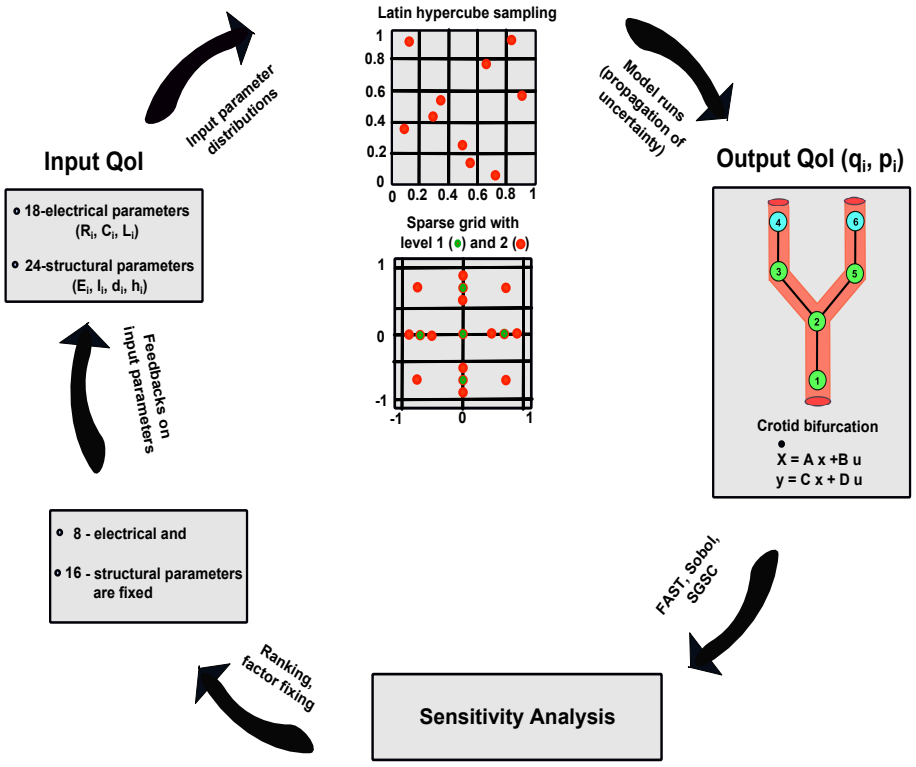

Figure 4.1: A simplified scheme for performing global sensitivity analysis (GSA).

The objectives of current research work are summarized as follow:

1. Quantify cause and effect relationships between input parameters (electrical and structural) and output variables (pressure and flow).
2. Identify and rank the key parameters, that contribute most on output uncertainty.
3. Discuss and explain the network location and temporal-dependent sensitivities, which are useful in finding optimal locations in carotid bifurcation and optimal time regions in pressure and flow waves to estimate model parameters.
4. Finding least important parameters, that can be fixed on their nominal values (factor fixing, model reduction and simplification).

The Chapter is organized as follows: In section 4.2, three variance-based GSA methods are briefly discussed. A detailed working algorithm using Sobol method is presented to calculate sensitivity indices in the carotid bifurcation. Moreover, the convergence of sensitivity indices is also discussed. Simulations setup are explained in section 4.3. Results of prescribed GSA methods are discussed/compared in section 4.4. Finally, conclusions are given in section 4.6.

4.2 Methods of global sensitivity analysis

In this section, three different variance-based GSA methods are briefly discussed. In variance-based GSA, the total output variance, $V(Y)$ of a model is apportioned into its parameters. Influential parameters contribute most on output uncertainty as compared to the less influential parameters. The variance-based GSA is a model

free method and is useful to investigate the interaction effects of parameters on state variables. These methods provide the *main effect* (S_i) and *total effect* (S_{T_i}) of each parameter on state variables.

4.2.1 Sobol variance decomposition method

Let us define a model of the form $Y = f(X) = f(x_1, x_2, ..., x_K)$, where X is the vector of K uncertain parameters, which are independently generated within a unit hypercube i.e. $x_i \in [0,1]^K$ for $i = 1, 2, 3...K$. Compared to the other GSA methods, the Sobol's method is one of the most commonly used variance decomposition method, because its ease of implementation. The method is primarily based on the decomposition of output Y into summands of elementary functions in terms of increasing dimensionality [45, 46, 48, 49],

$$f(x_1, x_2, ..., x_K) = f_0 + \sum_{i}^{K} f_i(x_i) + \sum_{i<j}^{K} f_{ij}(x_i, x_j) + ... + f_{1,2,..,K}(x_1, x_2, ..., x_K). \quad (4.1)$$

In eqn. (4.1), f is integrable and f_0 is a constant function, defined as,

$$f_0 = \int_{\Omega^K} f(X)\ dX. \quad (4.2)$$

where, Ω^K is a K-dimensional space of parameters. The total unconditional variance can be obtained by,

$$V = \int_{\Omega^K} f^2(X)\ dX - f_0^2. \quad (4.3)$$

From eqn. (4.3), the total unconditional variance can be decomposed in a similar manner like in eqn. (4.1) as,

$$V(Y) = V = \sum_{i}^{K} V_i(x_i) + \sum_{i<j}^{K} V_{ij}(x_i, x_j) + ... + V_{1,2,..,K}(x_1, x_2, ..., x_K) \quad (4.4)$$

Where,

$$\begin{aligned} V_i &= V_{x_i}(E_{x\sim i}(Y|x_i)) \\ V_{ij} &= V_{x_i x_j}(E_{x\sim ij}(Y|(x_i, x_j))) - V_{x_i}(E_{x\sim i}(Y|x_i)) - V_{x_j}(E_{x\sim j}(Y|x_j)) \\ &... \end{aligned}$$

Here, V is the variance operator, E describes the mathematical expectation and $x_{\sim i}$ denotes all parameters except x_i. The *main effect* or first-order sensitivity index, S_i for the i-th parameter is then obtained by,

$$S_i = \frac{V_i}{V}. \quad (4.5)$$

Another popular variance based measure is the total effect [49]

$$\begin{aligned} S_{T_i} &= \frac{E_{x\sim i}(V_{x_i}(Y|x_{\sim i}))}{V} \\ &= 1 - \frac{V_{x_{\sim i}}(E_{x_i}(Y|x_{\sim i}))}{V} \end{aligned} \quad (4.6)$$

In general, the *main effect* is used to identify most important parameters and the total effect is taken into account for factor fixing. The *total effect*, S_{T_i} of the i-th parameter means first-order effect plus higher-order effect due to interactions of the i-th parameter. In this study, the interaction effect between parameters are negligible ($< 2\%$), we used the *main effect* for factor fixing and ranking of important parameters (for more details, see section 4.4).

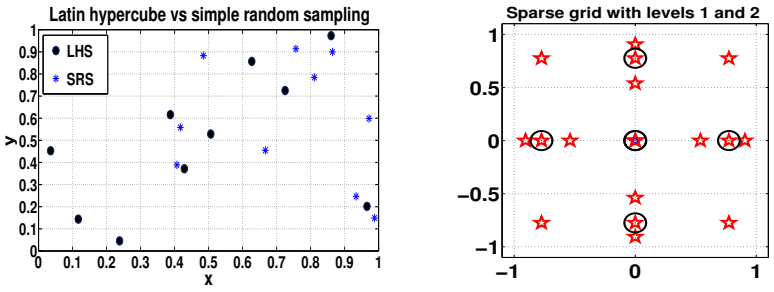

Figure 4.2: Random numbers, generated from Latin hypercube sampling and uniform distribution (left) and two dimensional (K=2) sparse grid, based on Gauss-Hermite collocation points with level of interpolation equal to 1 (5 collocation points (◯)) and equal to 2 (17 collocation points (★)) (right). In Latin hypercube sampling the parameter spaces are evenly covered, while in simple random sampling, no random numbers fall in columns (0,0.4) and (0.5,0.6).

4.2.1.1 Input parameter distributions

The dynamic behavior of the cardiovascular system depends on input parameter distributions. For more accurate quantification of uncertainty and sensitivity analysis, the parameter distributions should be estimated from medical data [58]. In practice, experimental data is not easy to obtain. Due to limited data availability, the parameters are randomized within $\pm 10\%$ range of their nominal values. To cover the entire range of parameter spaces with reasonable computational cost, Latin hypercube sampling (LHS) was used. Moreover, LHS is capable of reducing the number of runs necessary to stabilize the Monte Carlo simulations. A comparison between LHS and Monte Carlo sampling (MCS) is given in figure (4.2, left).

4.2.1.2 Estimation of sensitivity indices from Monte Carlo method

We present a detailed working algorithm to compute the *main effect*, S_i using the Monte Carlo method, we follow the steps, given in [45].

1. Generate two independent sampling matrices, $\mathcal{A}(N, K)$ and $\mathcal{B}(N, K)$ by using LHS. Where, N is the total number of simulations and K is the number of parameters.

2. Define matrix $\mathcal{C}_i$, which is matrix $\mathcal{A}$ except the i-th column of matrix $\mathcal{B}$.

3. Compute and save model runs for all parameter spaces using matrices $\mathcal{A}, \mathcal{B}$ and $\mathcal{C}_i$ i.e. $Y_{\mathcal{A}}(t, TS, N) = f(\mathcal{A})$, $Y_{\mathcal{B}}(t, TS, N) = f(\mathcal{B})$ and $Y_{\mathcal{C}_i}(t, TS, N, K) = f(\mathcal{C}_i)$, where, t are the time points for one heart beat with period $t_p = 0.8s$. TS, represents the state variables (pressure and flow time series at six locations of carotid bifurcation, $N_{TS} = 12$) and N is the total number of model runs ($N = 10000$).

4. Compute the time dependent main sensitivity index, $S_{\text{main}_{\text{time}}}$ and total sensitivity index, $S_{\text{total}_{\text{time}}}$ of each parameter at each time-point of the pressure

and flow waves, using the estimator offered by Jansen [59, 60].

$$S_{\text{main}_{\text{time}}} = 1 - \frac{1}{2N \times V_{\text{main}_{\text{time}}}} \sum_{n=1}^{N} (Y_{\mathcal{B}}^{(n)} - Y_{\mathcal{C}_i}^{(n)})^2, \qquad \text{where} \quad (4.7)$$

$$V_{\text{main}_{\text{time}}} = \frac{1}{N} \sum_{n=1}^{N} (Y_{\mathcal{B}}^{(n)})^2 - E_{\text{main}_{\text{time}}}^2, \qquad \text{and}$$

$$E_{\text{main}_{\text{time}}} = \Big(\frac{1}{N} \sum_{n=1}^{N} Y_{\mathcal{B}}^{(n)} \Big)^2.$$

Jansen's formula for $S_{\text{total}_{\text{time}}}$ proceeds as,

$$S_{\text{total}_{\text{time}}} = \frac{1}{2N \times V_{\text{total}_{\text{time}}}} \sum_{n=1}^{N} (Y_{\mathcal{A}}^{(n)} - Y_{\mathcal{C}_i}^{(n)})^2, \qquad \text{where} \quad (4.8)$$

$$V_{\text{total}_{\text{time}}} = \frac{1}{N} \sum_{n=1}^{N} (Y_{\mathcal{B}}^{(n)})^2 - E_{\text{total}_{\text{time}}}^2, \qquad \text{and}$$

$$E_{\text{total}_{\text{time}}} = \Big(\frac{1}{N} \sum_{n=1}^{N} Y_{\mathcal{B}}^{(n)} \Big)^2.$$

The total variances ($V_{(.)}$) and the expectations ($E_{(.)}$) are also calculated at each time-point of pressure and flow waves with respect to each parameter.

5. Finally, the *main effect*, S_i and the *total effect*, S_{T_i} of each parameter on the state variables are calculated as,

$$S_i = \frac{1}{N_{TS}} \frac{1}{N_t} \sum_{j=1}^{N_{TS}} \sum_{t=0}^{N_t} S_{\text{main}_{\text{time}}}(t, j, i), \quad (4.9)$$

$$S_{T_i} = \frac{1}{N_{TS}} \frac{1}{N_t} \sum_{j=1}^{N_{TS}} \sum_{t=0}^{N_t} S_{\text{total}_{\text{time}}}(t, j, i) \qquad i = 1, ..., K \quad (4.10)$$

In eqns. (4.9) and (4.10), $N_{TS} = 12$ is the number of output variables (pressure and flow time series at all locations) and $N_t = 80$ is the number of time-points [62].

4.2.1.3 Convergence analysis of sensitivity indices

To calculate the sensitivity indices of each parameter, $N(K + 2)$ Monte Carlo simulations are executed. As it is mentioned earlier, the only drawback associated with variance-based global sensitivity analysis is its computational cost. A general question arises, how many simulations are required to achieve the convergence of sensitivity indices (S_i)? There exist several methods in the literature, which monitor and check convergence of sensitivity indices. The central limit theorem (CLT) and bootstrap method are the most popular and convenient to check the convergence [61, 63, 64].

In this work, the bootstrap technique is used to find a 95% confidence interval (CI) of each parameter for each state variable, that lies within ±5% uncertainty as compared to the mean value of all Monte Carlo simulations. The implementation of the bootstrap method is very straightforward. The time dependent main sensitivity indices are calculated for $N = [250,\ 500,\ 1000,\ 1500,\ 2000,\ 2500,\ 3000,\ 3600,\ 5000, 10000]$. After each N-model run the bootstrap technique ($\mathfrak{B} = 1000$) is applied to find a 95% CI. As the total number of simulations increases, the standard

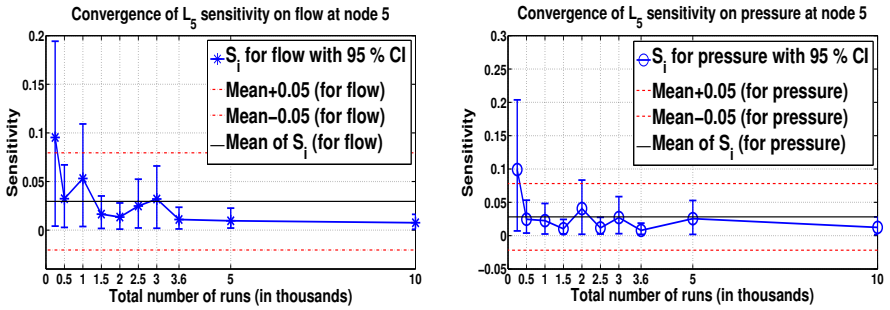

Figure 4.3: Estimation of S_i as a function of model runs per parameter to achieve 95% confidence interval (CI). The results show the convergence of S_i of blood inertia (L_5) on pressure and flow at node 5.

No. of runs	L_5 sensitivity on flow at node 5			L_5 sensitivity on pressure at node 5		
	S_i	SD	CI	S_i	SD	CI
250	0.095	0.0020	[0.091, 0.099]	0.099	0.0031	[0.092, 0.104]
500	0.032	0.0014	[0.029, 0.034]	0.024	0.0020	[0.020, 0.028]
1000	0.053	0.0017	[0.049, 0.056]	0.022	0.0015	[0.020, 0.025]
1500	0.016	0.0011	[0.014, 0.018]	0.01	0.0016	[0.007, 0.014]
2000	0.013	0.0005	[0.012, 0.014]	0.04	0.0011	[0.038, 0.042]
2500	0.024	0.0012	[0.022, 0.027]	0.011	0.0016	[0.009, 0.015]
3000	0.032	0.0010	[0.030, 0.034]	0.027	0.0019	[0.024, 0.031]
3600	0.01	0.0007	[0.009, 0.012]	0.007	0.0012	[0.005, 0.010]
5000	0.009	0.0013	[0.007, 0.013]	0.025	0.0009	[0.023, 0.027]
10000	0.007	0.0004	[0.006, 0.008]	0.012	0.0011	[0.010, 0.015]

Table 4.1: Numerical values of convergence analysis given in figure (4.3). It is evident that by increasing the number of simulations the standard deviation decreases and sensitivity index of each parameter approaches to the mean values of all Monte Carlo simulations.

deviation (SD) decreases, as a result, the sensitivity index for each parameter converges to the mean value of all Monte Carlo simulations (see table 4.1). Figure (4.3) shows, the convergence of L_5 sensitivity index for both pressure and flow at node 5. The minimum number of simulations for each parameter to achieve a uncertainty in main sensitivity index lies within $\pm 5\%$ uncertainty as compared to the mean value of all Monte Carlo simulations, is around 3000.

4.2.2 Fourier Amplitude Sensitivity Test (FAST)

The FAST method was originally presented by Cukier, R. I. et. al. in 1973 [51]. The method calculates only the *main effect* of the model parameters. Later on, Saltelle et al. proposed the extension to the FAST method, which calculates both *main effect* and *total effect* like the method of Sobol [46]. The only difference lies in the procedure of calculating the sensitivity indices. The key idea of the FAST method is to transform $K-$dimensional integrals (eqns. 4.2, 4.3) into a one-dimensional integrals as,

$$X_i(s) = G_i(sin(\omega_i s)) = \frac{1}{2} + \frac{1}{\pi} sin^{-1}(sin(\omega_i s)) \tag{4.11}$$

where, ω_i is a set of linearly independent integer frequencies assigned to each uncertain parameter and $s \in (-\infty, +\infty)$. According to the Ergotic theorem [65] eqn.

(4.2) and eqn. (4.3) can be computed as,

$$\begin{aligned} E &= \frac{1}{2\pi}\int_{-\pi}^{\pi} f(s)\,ds \\ &= \frac{1}{2\pi}\int_{-\pi}^{\pi} f[(G_1\omega_1 s),(G_2\omega_2 s),...,(G_K\omega_K s)]ds \end{aligned} \tag{4.12}$$

and variance will be,

$$\begin{aligned} V &= \frac{1}{2\pi}\int_{-\pi}^{\pi} f^2(s)\,ds - E^2 \\ &= \frac{1}{2\pi}\int_{-\pi}^{\pi} f[(G_1\omega_1 s),(G_2\omega_2 s),...,(G_K\omega_K s)]^2 ds - E^2. \end{aligned} \tag{4.13}$$

Fourier series expansion of $f(s)$ in eqn. (4.13) gives,

$$\begin{aligned} V &= \sum_{i=-\infty}^{\infty}(\mathbb{A}_i^2+\mathbb{B}_i^2) - (\mathbb{A}_0^2+\mathbb{B}_0^2) \\ &= 2\sum_{i=1}^{N}(\mathbb{A}_i^2+\mathbb{B}_i^2) \end{aligned} \tag{4.14}$$

where, $\mathbb{A}_i$ and $\mathbb{B}_i$ are Fourier coefficients defined as,

$$\begin{aligned} \mathbb{A}_i &= \frac{1}{2\pi}\int_{-\pi}^{\pi} f(s)cos(is)\,ds \\ \mathbb{B}_i &= \frac{1}{2\pi}\int_{-\pi}^{\pi} f(s)sin(is)\,ds \end{aligned}$$

Conditional variance for parameters x_i to calculate S_i can be calculated as,

$$V_i = 2\sum_{m=1}^{M}(\mathbb{A}_{m\omega_i}^2+\mathbb{B}_{m\omega_i}^2) \tag{4.15}$$

Where, M is the maximum harmonic ($M=6$). Fourier coefficients are numerically evaluated as,

$$\mathbb{A}_i = \begin{cases} \frac{1}{N}(y_0+\sum_{l=1}^{m}(y_l+y_{\sim l})cos(\frac{\pi il}{N})) & \text{if l is even} \\ 0 & \text{otherwise} \end{cases}$$

$$\mathbb{B}_i = \begin{cases} \frac{1}{N}(\sum_{l=1}^{m}(y_l+y_{\sim l})cos(\frac{\pi il}{N})) & \text{if l is odd} \\ 0 & \text{otherwise} \end{cases}$$

where, $q=\frac{N-1}{2}$. Finally the *main effect*, S_i is computed as,

$$S_i = \frac{V_i}{V}. \tag{4.16}$$

For a practical implementation and understanding of the FAST method, the reader is referred to the on-line manual of SimLab, which provides a free development framework for sensitivity and uncertainty analysis [76].

4.2.3 Sparse Grid Stochastic Collocation method (SGSC)

SGSC is a sampled-based variance decomposition method used for uncertainty quantification (UQ) and sensitivity analysis (SA). The method combines the two approaches, stochastic collocation method and sparse grid technique [66–71]. The implementation of the sparse grid (SG) method is similar to the Monte Carlo (MC) method, except the choice of collocation points, which are obtained systematically using polynomial approximation theory (Lagrange interpolation) and the Smolyak algorithm.

4.2.3.1 Tensor product quadrature

Let $\{y_{j=1\ldots mi}^{i=1\ldots K}\}$, prescribe collocation points in a $K-$dimensional hypercube, $[0,1]^K$, where mi and K are the number of collocation points and random dimension respectively. For each random dimension, $i = 1, .., K$, a one-dimensional Lagrange interpolation formula for a smooth function f can be defined as,

$$U^i(f) = \sum_{j=1}^{mi} f(y_j^i) l_j^i(y). \tag{4.17}$$

Here $U^i(f)$ is the i-the dimensional Lagrange interpolation formula and y_j^i are j-th collocation points in the random dimension i. For multivariate, $K > 1$, we define the tensor product of the one-dimensional Lagrange polynomial as,

$$(U^{i_1} \otimes ... \otimes U^{i_K})(f) = \sum_{j_1=1}^{mi_1} ... \sum_{j_K=1}^{mi_K} f(y_{j_1}^{i_1}, ..., y_{j_K}^{i_K})(l_{j_1}^{i_1} \otimes ... \otimes l_{j_K}^{i_K}). \tag{4.18}$$

Eq. (4.18) is known as full tensor product. The problem with the full tensor quadrature is that, the total number of collocation points increases exponentially in high dimensions, e.g. when $K \gg 1$ and N_p is the number of points in each dimension then total number of collocation points in K-dimensional space is $mi = N_p^K$. For example, if we consider level 2 (17 collocation points for each parameter) for carotid bifurcation, where $K = 18$ (R_i, C_i, L_i), the total number of collocation points are 1.4063084×10^{22}, i.e. in a high dimensional space the full tensor product quadrature is computationally too expensive.

4.2.3.2 Sparse grid (sparse tensor product)

For high dimensional problems, $K \gg 1$, the number of collocation points in the tensor product eqn. (4.18) is very large, which makes the tensor product less efficient and computationally expensive. In order to reduce collocation points obtained by the tensor product, while keeping high accuracy in the solution, Smolyak introduced sparse tensor product technique, known as sparse grid technique [72]. In the Smolyak algorithm, the linear combinations of the tensor product formulas are used in such a way that the product with a relatively small number of knots are used and the interpolation property for $K = 1$ is preserved for $K > 1$. Smolyak quadrature formula is written as,

$$\mathfrak{S}(q, K) = \mathfrak{S}_q f(y) = \sum_{q-K+1 \le |i| \le q} (-1)^{q-|i|} \binom{K-1}{q-|i|} (U^{i_1} \otimes ... \otimes U^{i_K}) f(y) \tag{4.19}$$

Where, $|i| = i_1 + ... + i_k$ with multivariate index $i = (i_1, ..., i_k) \in [0,1]^K$ and $q - K$ is the level of interpolation. To compute $\mathfrak{S}_q f(y)$, we need to evaluate the function

on the *sparse grid*. The set of collocation points of the sparse grid is thus collected as,

$$\mathfrak{H}(q,K) = \bigcup_{q-K+1\leq|i|\leq q} (\theta^{i_1} \times ... \times \theta^{i_K}) \tag{4.20}$$

Where, θ^{i_j} are one-dimensional collocation points in dimension j. In the current study, we use the Smolyak algorithm based on Gauss-Hermite abscissas, which obeys the standard normal distribution. For more details readers are referred to [50,73,74]. In figure (4.2) (right), two dimensional (K=2) sparse grid points are shown, with total number of collocation points 5 (level 1) and 17 (level 2).

Finally, the solution can be obtained by solving the cardiovascular model repeatedly on transformed collocation points.

4.2.3.3 Main effect sensitivity

The main effect of each parameter on output uncertainty can be computed as,

$$S_k = \frac{V(E(f|y^k))}{V(f)}, \quad k = 1, ..., K \tag{4.21}$$

where, $V(E(f|y^k))$ is known as conditional variance (keeping y^k fix) and $V(f)$ is the total variance, which is defined as,

$$V(f) = E((f - E(f))^2) \simeq E(\mathfrak{S}_q f^2) - (E(\mathfrak{S}_q f))^2 \tag{4.22}$$

where,

$$E(\mathfrak{S}_q f) = \int_\Gamma \mathfrak{S}_q f(y)\rho(y)dy \tag{4.23}$$

$$= \sum_{q-K+1\leq|i|\leq q} (-1)^{q-|i|} \binom{K-1}{q-|i|} E(U^{i_1} \otimes ... \otimes U^{i_K}) f(y) \tag{4.24}$$

Where, $\Gamma = \Gamma^1 \times \Gamma^2 \times ... \times \Gamma^K$, a K-dimensional domain and

$$E(U^{i_1} \otimes ... \otimes U^{i_K}) f(y)) = \sum_{j_1=1}^{mi_1} ... \sum_{j_K=1}^{mi_K} f(y_{j_1}^{i_1}, ..., y_{j_K}^{i_K})(w_{j_1}^{i_1} \otimes ... \otimes w_{j_K}^{i_K}) \tag{4.25}$$

Where, $w_{j_k}^{i_k}$ are weights, mi, in random dimension i_k (see [50] for more details). Finally the conditional variance is calculated as,

$$V(E(f|y^k)) = \int_{\Gamma^k} \left(\int_{\Gamma_*^k} \mathfrak{S}_q f(y)\rho(y_*^k)dy_*^k \right)^2 \rho(y^k)dy^k - \left(\int_\Gamma \mathfrak{S}_q f(y)\rho(y)dy \right)^2 \tag{4.26}$$

In eqn (4.26), y^k is the k-th parameter, Γ^k is the one-dimensional parameter space for y^k, y_*^k are other parameters than y^k and Γ_*^k is the $K-1$ dimensional parameter spaces other than Γ^k. A simplified scheme for computing *main effect* using sparse grid technique is given in figure (4.4).

4.3 Simulation setup

The in-output quantities of interest (QoI), respective methods and their computational cost are given in appendix A.9. The Chapter mainly concentrates on GSA,

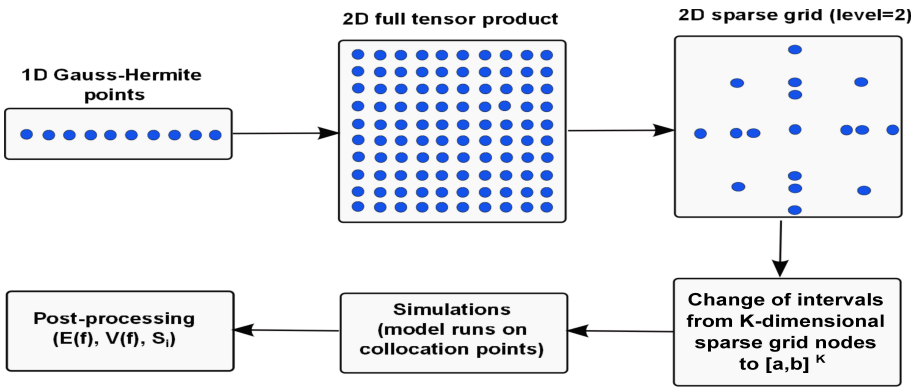

Figure 4.4: A simplified scheme for computing S_i using sparse grid technique.

however, a comparison is made between the results of electrical parameters obtained from LSA and GSA (see section 4.4.1.3).

Variance-based GSA methods are applied to a lumped parameter model of the carotid bifurcation to identify most and least important electrical and structural parameters. At each location, three electrical and four structural parameters are considered for uncertainty and sensitivity analysis with $\pm 10\%$ variation in nominal values.

To overcome the computational cost, network equations are solved by MATLAB built in solver *lsim*, which is fast and efficient solver for the LTI system. In our case, the computational time for one simulation is 0.07s (see appendix A.9 for overall computational cost). Initially the model was run for three heart beats, so that a steady state condition was reached. Then the results from last heart beat were used for sensitivity analysis.

For each electrical and structural parameter there are two sensitivity time series at each node, one for the pressure and one for the flow. For both electrical ($K = 18$) and structural ($K = 24$) parameters, there are, $2 \times N_s \times K$ sensitivity time series. Where N_s is the number of nodes and K is the total number of parameters. To represent and analyze sensitivity time series in a compact form, the mean of absolute values were taken over time with respect to each parameter. The numerical values (%) of time series are given in figure (4.8).

The values of the *main effect*, S_i lies between 0 and 1. Parameters having higher sensitivity values are considered to be most important and vice versa. For purely additive models $\sum_{i=1}^{K} S_i = 1$ and for non-additive models $\sum_{i=1}^{K} S_i < 1$. The latter case indicates interactions between the parameters, which can be explained by the *total effect*, S_{Ti}. The difference $1 - \sum_{i=1}^{K} S_i$ indicates the interactions among the parameters. Generally, the *main effect* is used to identify most important parameters and the *total effect* is considered for factor fixing. In our study, the *main effect* was used for ranking the important parameters as well as factor fixing, as the difference, $1 - \sum_{i=1}^{K} S_i$ is less than 1%. The *main effect* and the *total effect* of electrical parameters in the carotid bifurcation are calculated using Sobol method and displayed in appendices (A.7) and (A.8).

The results of the sensitivity analysis are divided into three parts, which are explained below.

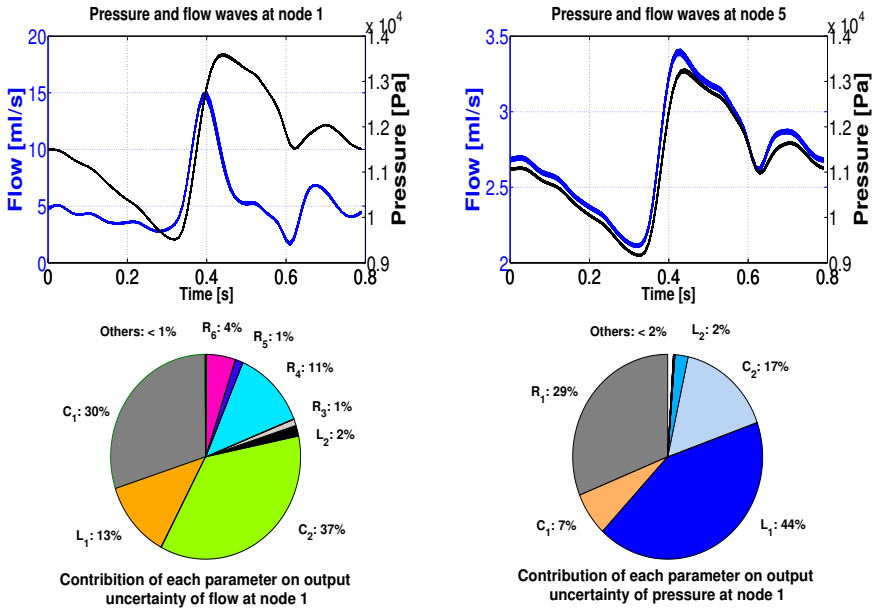

Figure 4.5: 10000 Monte Carlo simulations of pressure and flow at nodes 1 and 5 (top). A large variation can be seen at the diastole and the peak of pressure and flow waves. On the other hand, the output uncertainty of pressure and flow at node 1 is apportioned to input parameters (R_i, C_i, L_i) (bottom).

4.4 Results and discussion

4.4.1 Sensitivity analysis of electrical parameters

In the carotid bifurcation, there are 18-electrical parameters (R_i, C_i, L_i), influencing all state variables. The *main effect*, S_i was computed by averaging time-dependent sensitivity over time for each state variables with respect to each parameter (see figure 4.6).

It is clearly evident, that the flow is sensitive w.r.t. R within RCC, RIC and REC. A large upstream sensitivity can be seen due to the reflections at the terminals nodes (4 and 6) (see figure (4.6, A_1)). In contrast, the flow is sensitive w.r.t. C and L at the first two nodes and has small downstream effect on the following nodes (see figure 4.6, A_3, A_5). On the other hand, the pressure is sensitive w.r.t. R at the node itself. This indicates that most of the uncertainty comes from the node itself or from the adjacent nodes. The fact that R shows higher impact on state variables at the terminal nodes (4 and 6), over 0.88 and 0.70 respectively, suggests the importance of well defined parameters at terminal nodes (see figure (4.6, A_2)). For pressure, C and L are also influential at the first two nodes and have significant downstream influence on pressure at all following nodes (see figure (4.6, A_4, A_6)).

4.4.1.1 Parameter fixing and model simplification

Sensitivity analysis also plays an important role in factor fixing, that leads towards model reduction and simplification. Parameters having negligible impact on state variables can be fixed at their nominal values without any loss of accuracy. This information could benefit during parameter estimation, where important parameters are easy to estimate as compare to less important parameters. In this work, parameters whose *main effect* on all state variables is less than 5%, are fixed at their nominal values. According to this criteria, the values of C and L in the RIC

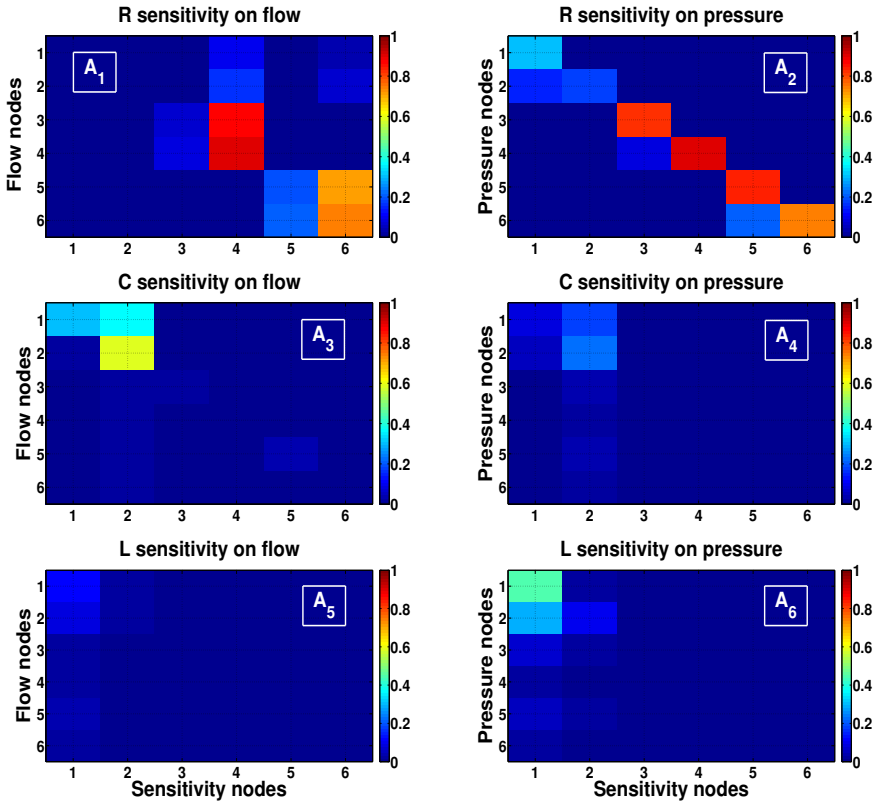

Figure 4.6: Main effect, S_i of electrical parameters (R_i, C_i, L_i) on pressure and flow in the carotid bifurcation. Results reveal that R is most influential within RCC, RIC and REC, particularly at the bifurcation and terminal nodes (A_1, A_2), while C and L show significant effect at the inlet of the carotid bifurcation (A_3, A_4, A_5, A_6).

and REC arteries could be fixed at their base values (see figure (4.8, top)).

4.4.1.2 Ranking of important parameters

In variance-based GSA, the output uncertainty is apportioned into different sources of uncertainty in its inputs, which helps in the ranking of important parameters. In figure (4.8, top), the uncertainty of each state variable is decomposed and assigned to each input parameter (R_i, C_i, L_i). Parameters with large sensitivity values are ranked high and vice versa. We observed, the ranking of key parameters is location dependent and different for each state variable. In figure (4.5), 10000 model runs are plotted at node 1 and 5 to visualize the output uncertainty. Furthermore, pie charts show the ranking of important parameters for pressure and flow at node 1.

For reliable model predictions, the output uncertainty can be reduced by estimation of important parameters. In the parameter estimation process, the *main effect* can be used to identify a subset of important parameters to estimate from a certain set of state variables. For example, if we have in-vitro or in-vivo measurements at nodes 3 or 4, then it is not possible to estimate the parameters at nodes 5 and 6, due to the reason that the parameters at nodes 5 and 6 don't have influence on the pressure and flow at nodes 3 and 4 (figure 4.8, top).

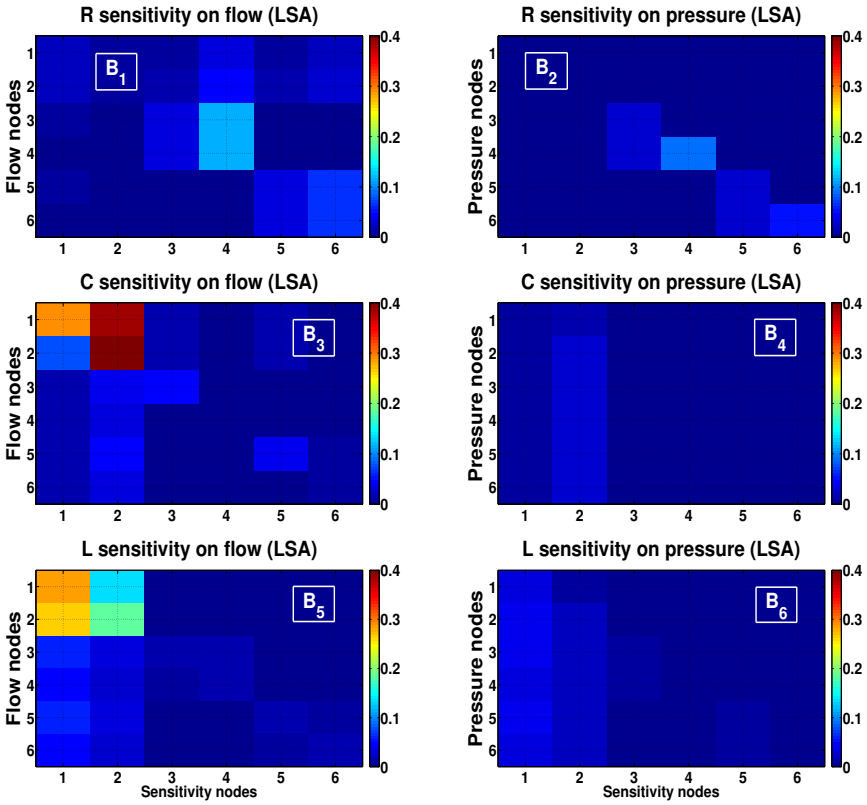

Figure 4.7: Sensitivity coefficients of electrical parameters (R_i, C_i, L_i) on pressure and flow in the carotid bifurcation. Results reveal that R is important within RCC, RIC and REC, particularly at terminal nodes (B_1, B_2), while C and L show impact on pressure and flow at the inlet of the carotid bifurcation (B_3, B_4, B_5, B_6).

4.4.1.3 Results comparison with LSA

A satisfactory agreement can be seen between the results of local and global sensitivity analysis (see figures (4.6), (4.7)). Pressure and flow are sensitive w.r.t. R within RIC and REC, particularly at the terminal nodes. On the other hand, C and L are more influential on the pressure and flow at the inlet nodes (1 and 2). Furthermore, the ranking of important parameters are not the same except at the few locations of the carotid bifurcation.

4.4.2 Sensitivity analysis of structural parameters

In this section, we discuss the sensitivity of state variables w.r.t. structural parameters (E, l, d, h) with ± 10 % variation in their nominal values. Again, the *main effect* was used for parameter ranking and factor fixing, because the interaction effect between structural parameters is less than 2% i.e. $1 - \sum_{i=1}^{K} S_i < 0.02$. It is clearly seen, that d is the most important parameter and hence needs to be estimated correctly to reduce the output uncertainty (see figure (4.8, bottom)) and figure (4.9, C_3, C_4).

Flow is sensitive w.r.t. l and d and strong reflections can be seen from terminal nodes to the RCC artery (figure (4.9, C_1, C_3)), while E and h are less important parameters and could be fixed at their nominal values (figure (4.8, bottom)). Pressure is also sensitive for l and d and most of the uncertainty came from the node itself or nearby nodes (figure (4.9, C_2, C_4)). According to the factor fixing criteria

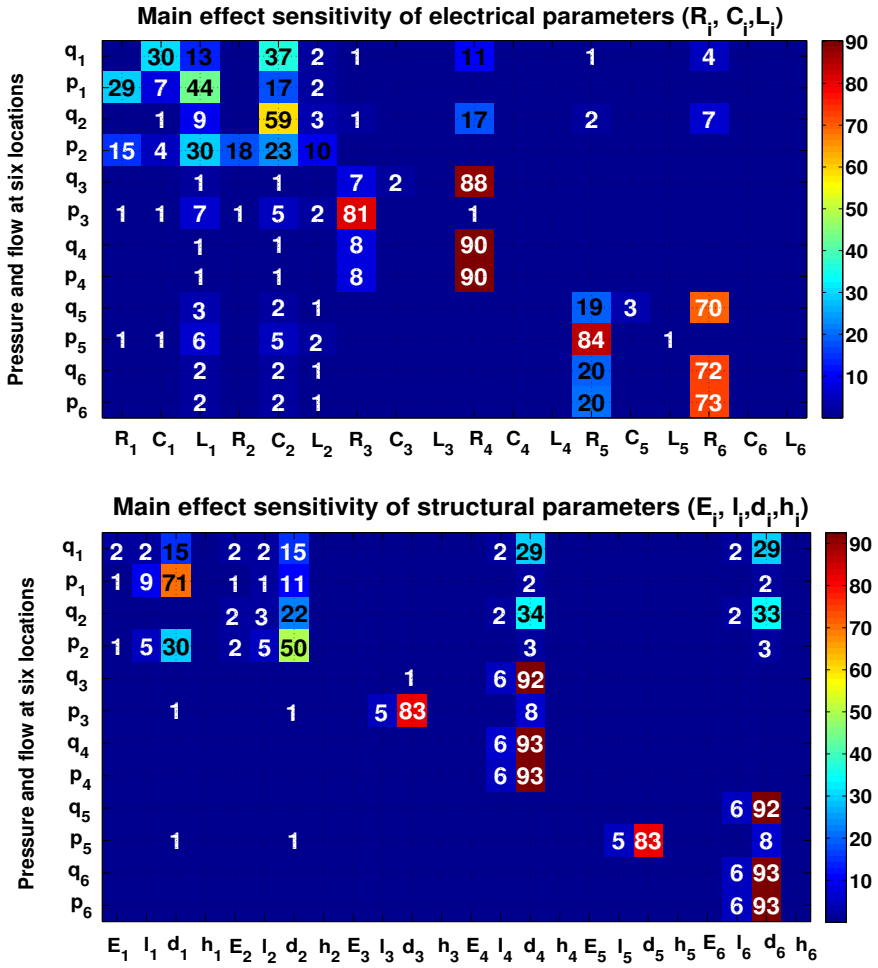

Figure 4.8: Overall *main effect* (%) of electrical and structural parameters on state variables. Main effect less than 1% is considered to 0. Results show that R, d and l are the key parameters which cause most of the uncertainty in the outputs.

described earlier, l (only in RIC and REC arteries), E and h can be fixed at their nominal values. Each row in figure (4.8, bottom), shows the ranking of important structural parameters for each state variable, which further can help to identify the subset of important parameters in the parameter estimation process.

4.4.3 Network location and time dependent sensitivities

The sensitivity of the cardiovascular parameters strongly depends upon the locations within the carotid bifurcation as well as the time regions in the pressure and flow waves. Network location and temporal sensitivities play an important role in finding optimal measurement locations in carotid bifurcation and optimal time regions of state variables with respect to each parameter. These findings can further be used in the parameter estimation process. From network location and temporal sensitivity results, we observed the following findings:

1. Most sensitivity of parameters was found in common time regions i.e. at early systole, peak systole and end diastole (figures (4.10), (4.11)).

2. In time-dependent sensitivity analysis, few parameters show a sensitivity peak

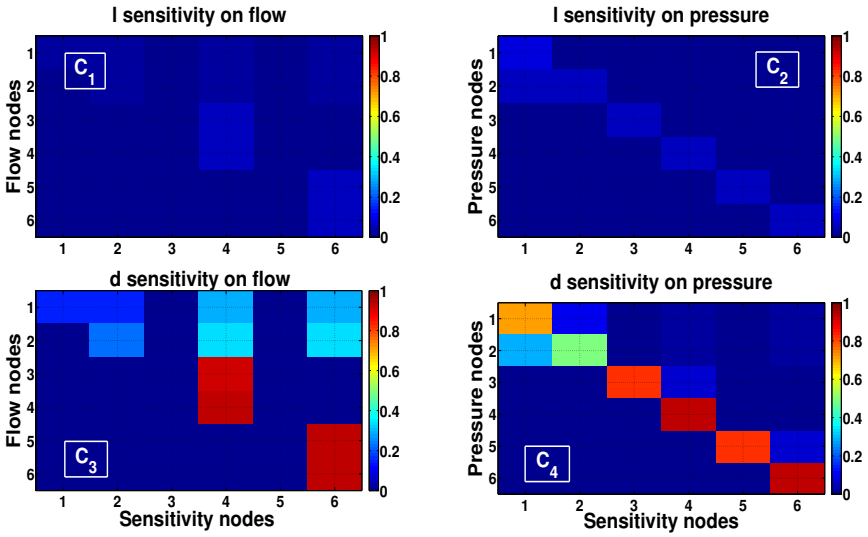

Figure 4.9: The main effect of structural parameters (l_i, d_i) on pressure and flow in the carotid bifurcation. Results indicate that d and l are the key parameters and have a strong upstream influences on state variables from the terminal nodes to the RCC artery.

over a short period of time, which could lead to wrong sensitivity values if the analysis is made over a short period of time (see figure (4.11, E_1, E_2)).

3. At the terminal nodes, the sensitivity values of state variables w.r.t of each parameter are identical, which is in agreement to the boundary conditions chosen (figure (4.10, D_4, D_6)) and figure (4.11, E_4, E_6).

In figures (4.10,4.11), we compare the network location and temporal sensitivities of L_1 on all state variables, calculated by the three GSA methods. As the blood inertia plays a role in acceleration (in systole) and deceleration (in diastole) of the blood, most of the sensitivity was found in early systole, peak systole and end diastole, where the fluid is accelerated and decelerated respectively.

4.5 A general framework for parameter estimation

The sensitivity results obtained in this Chapter provide insights that enable the experimentalists to optimize their experimental setups for estimating the key CV parameters. Which is the first step to build a patient-specific CV model. The *main effect* of parameters and location-dependent sensitivity provides a clear guidance on what to measure (pressure or flow) and where to measure (locations) to estimate key CV parameters. As a complement, time-dependent sensitivity provides optimal time regions in the pressure and flow waves, which makes the estimation process more precise. The framework is divided into two parts:

1. **Factor fixing**

   i Apply global sensitivity analysis on the carotid bifurcation using the scheme given in figure (4.1).

   ii Fix the parameters that have negligible impact on state variables. For example, in case of electrical parameters, the values of C and L can be fixed at RIC and REC. While for structural parameters, the values of l (only in RIC

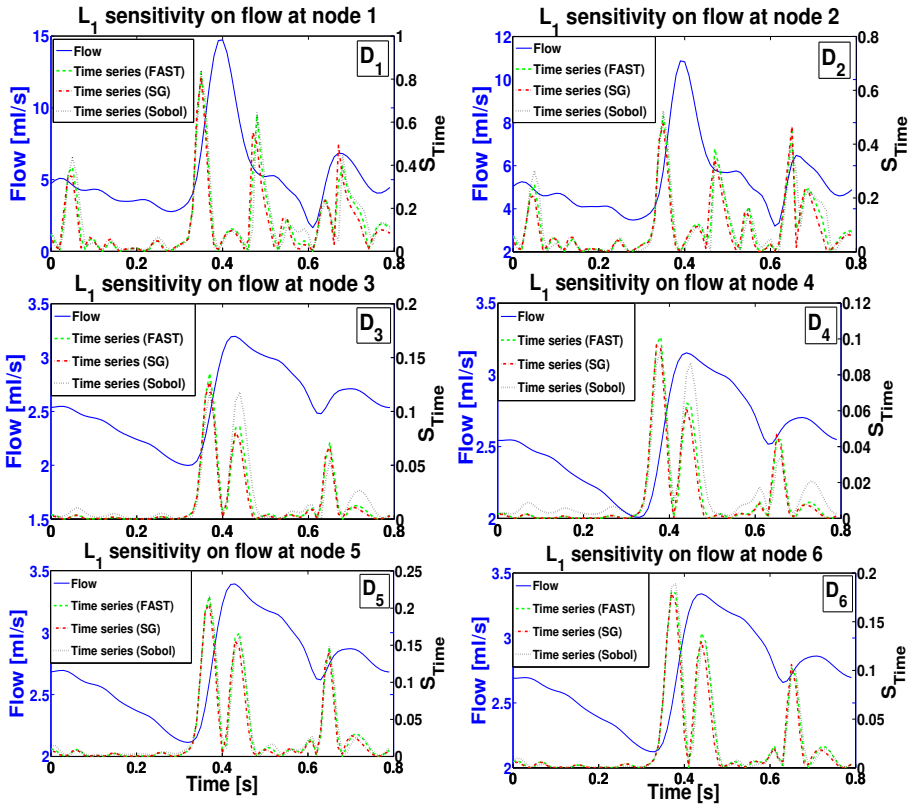

Figure 4.10: Network location and temporal sensitivity of L_1 on flow at all locations in the carotid bifurcation. Sensitivity can be seen in common time regions i.e. at early systole, peak systole and end diastole. The results indicate that, L_1 can be better estimated from flow measurements in the early systole than from other time regions.

and REC arteries), E and h can be fixed at their nominal values. See figure (4.8) for factor fixing.

2. **Estimation of key parameters**

   iii Identify the key parameters, which contribute most on output uncertainty and optimal measurement locations to estimate those important parameters using the sensitivity results given in figure (4.8). For example, to estimate the parameter C_2, it is recommended to take flow measurements at node 1 or 2, or pressure measurements at node 2.

   iv Apply a suitable optimization method to estimate the model parameters using clinically obtained measurements or flow simulator data.

The parameter estimation framework given above is applicable for both a partial and full CVS. For a full CVS, see Chapter 5, where GSA is applied to study some clinically relevant CV parameters.

4.6 Conclusion

In this work, three variance-based GSA methods are applied on a lumped parameter model of the carotid bifurcation. On the basis of computational cost, simplicity

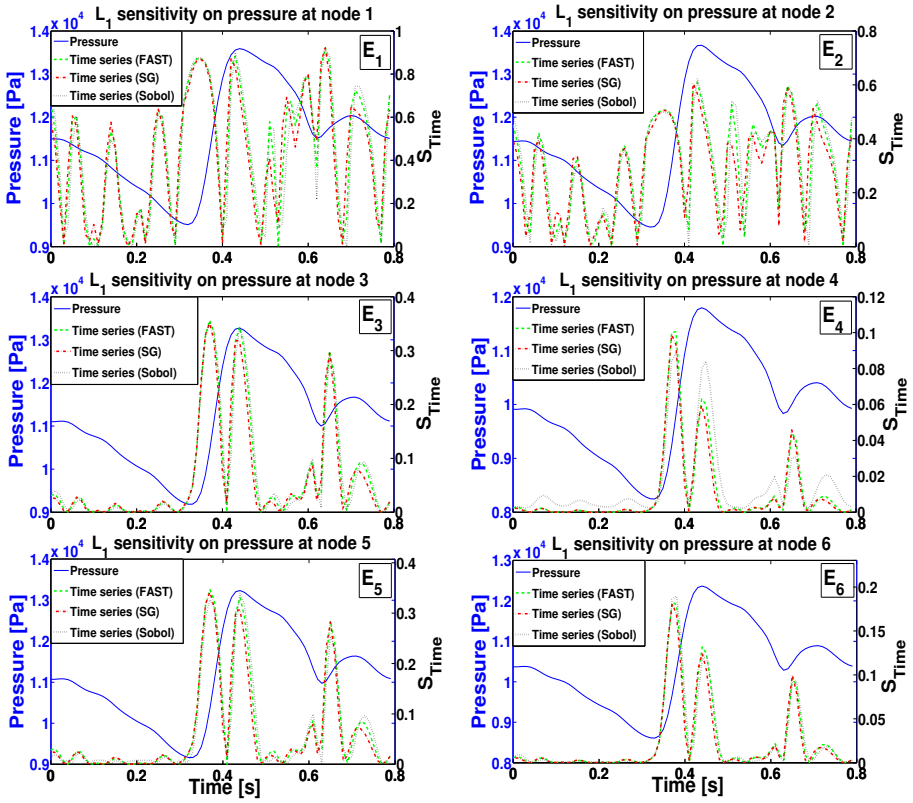

Figure 4.11: Network location and temporal sensitivity of L_1 on pressure in at all locations of the carotid bifurcation. Pressure and flow are sensitive w.r.t L_1 at common time regions i.e. at early systole, peak systole and end diastole. Moreover, at the terminal nodes, the L_1 sensitivity on pressure and flow is identical, due to the constant pressure boundary condition applied (compare E_4 and E_6 to D_4 and D_6 in figure (4.10)).

and straight forward implementation, it is recommended to use Sobol method to calculate sensitivity measures. The methods were used to rank and identify most important parameters as well as to fix less important parameters at their nominal values. For each parameter, we have discussed optimal measurement locations in the carotid bifurcation and optimal time regions in the pressure and flow waves.

The results of the present work are based on the *main effect*, because the interaction effect among the parameters was found to be negligible. The key GSA results of the carotid bifurcation are summarized as:

1. The study identifies a subset of important parameters (electrical and structural), which effect state variables at different locations. The rows in figure (4.8), show the ranking of most important parameters on the state variables.

2. Parameters having a *main effect* sensitivity of less than 5% on each state variable are considered to be less important and are fixed at their nominal values. In general, 8-electrical parameters out of 18 and 16-structural parameters out of 24 could be fixed at their nominal values. More precisely, at each location, the subset selection of important parameters is different for pressure and flow. For a subset selection of important parameters on each state variable, see figure (4.8).

3. Network location and temporal sensitivities identify the important measure-

ment locations in the carotid bifurcation and important time regions in the pressure and flow waves. Generally, time dependent sensitivity was found in common time regions i.e. in early-systole, peak systole and end-diastole.

CHAPTER 5

Sensitivity Analysis of the CVS

5.1 Introduction

In the multi-compartment CV models under consideration, there are plenty of electrical and structural parameters. MACSim has 95 arterial nodes (see section 2.5), while the linear elastic and visco-elastic CV model contains 122 nodes (see section 2.3). At each node, 3-electrical and 4-structural parameters are influencing the state variables. In total, MACSim has 285-electrical and 380-structural parameters with 33 extra boundary resistances, R_b at the boundary nodes. While, the linear elastic and linear visco-elastic CV model contains 366-electrical and 488-structural parameters with 25 boundary resistances, R_b at the boundary nodes. For a patient-specific CV model, it is not practically feasible to estimate all CV parameters accurately from the given measurements.

A possible way out of this situation is to first quantify those parameters which are the key driver of the model outputs and then estimate the key parameters using patient-specific data. In this context, location dependent sensitivity analysis could be used in finding the optimal measurement locations to estimate the key parameters in the arterial network.

In Chapter 3 and 4, LSA and GSA methods are applied to the arm arteries and carotid bifurcation respectively. The results revealed, that the diameter, d and the boundary resistance, R_b are the most important parameters. In this Chapter, sensitivity analysis with respect to d and R_b is applied to the complete CVS. The main objectives of this Chapter are:

1. Quantify the impact of R_b in MACSim for pressure and flow waves at different locations in the arterial network.

2. Study different levels of *stenosis* and *aneurysms* at each location of the visco-elastic CV model by decreasing and increasing the diameter respectively.

3. Finding optimal measurement locations to estimate diameter in the CV models.

5.2 Sensitivity Analysis in MACSim

Currently, MACSim is used for teaching and research purposes like, early detection of *stenosis* and its impact on rest of the cardiovascular system. In MACSim, the *stenosis* in the artificial arteries are created by manually squeezing tube clamps

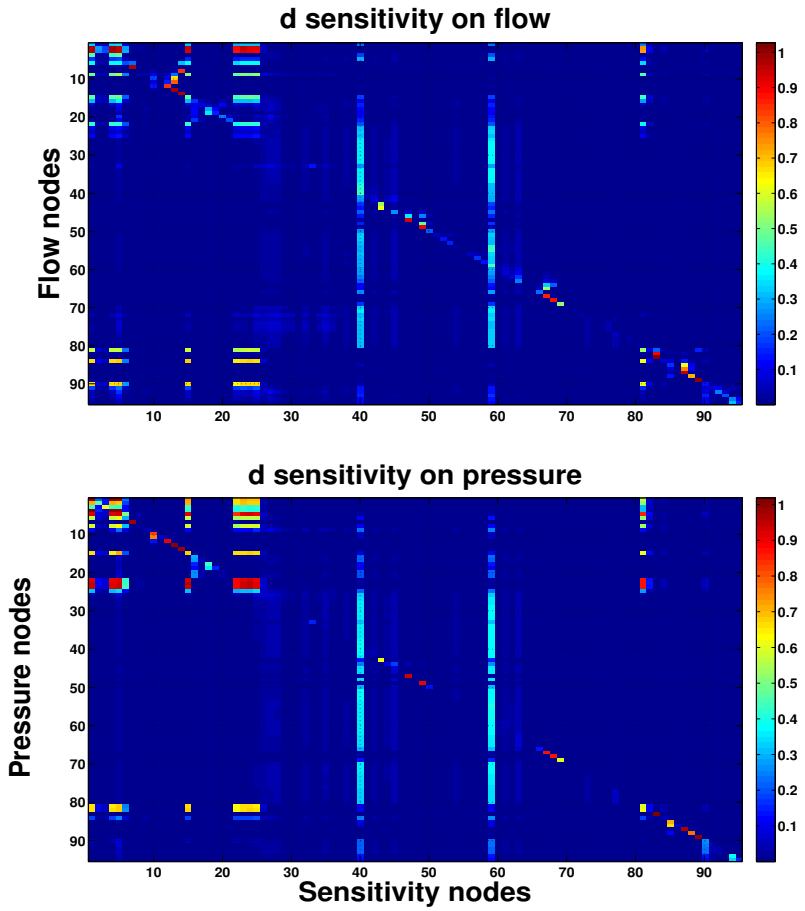

Figure 5.1: Main effect sensitivity of diameter, d in MACSim for flow (top) and pressure (bottom).

at different locations of the systemic circulation [75]. This way of creating and analyzing the *stenosis* is quite time consuming. In this section, a linear elastic model of MACSim is considered and effect of diameter ($\pm 10\%$) is quantified using Sobol method. We also discuss the sensitivity of R_b on state variables and optimal measurement locations of d for parameter estimation. In section 5.3, a detailed study of *stenosis* and *aneurysms* is given.

5.2.1 Sensitivity of the vessel diameter, d

Sobol method ($N = 3000$) is applied on the linear elastic model of MACSim to study the impact of diameter ($\pm 10\%$ variations) on pressure and flow in the CVS. The in-output quantities of interest (QoI) and the computational cost are given in the appendix A.9.

Flow is sensitive w.r.t. the diameter at the location itself, ascending (nodes 1, 4, 5) and descending aorta (nodes 15, 22, 23, 24, 25) and has significant effect on the left/right carotid bifurcations and the left/right arm arteries. Small sensitivity can also be seen on downstream nodes from the descending aorta. A strong downstream and upstream effect from the left/right external iliac arteries (nodes 40, 59) and left/right arm arteries (nodes 6, 81) are observed (see figure (5.1, top)).

Again, pressure is sensitive for the diameter at the location itself, ascending and descending aorta, external iliac arteries and the left/right arm arteries. Also strong

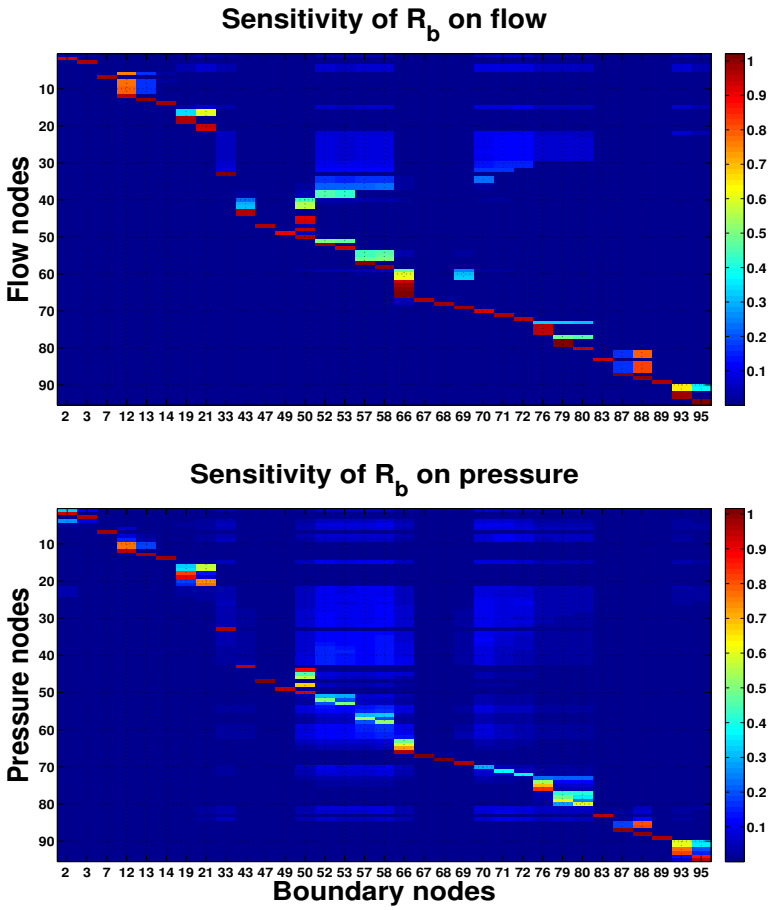

Figure 5.2: Main effect sensitivity of boundary resistance, R_b in MACSim for flow (top) and pressure (bottom).

reflections can be seen from these nodes (see figure (5.1, bottom)).

5.2.2 Sensitivity of the boundary resistance, R_b

In the systemic arterial network, arterioles are the smallest vessels that contain high number of smooth muscles in their *tunica media*. When the smooth muscles relax then the wall of arterioles become wide i.e. the *lumen* diameter of arterioles increases. This increase in the diameter reduces the blood resistance, as a result, blood flow increases. This phenomena is called *vasodilation* and its opposite is known as *vasoconstriction*. *Vasodilation* and *vasoconstriction* plays an important role in controlling the blood flow distribution in the CVS [78].

In this section, R_b is used to study the effect of *vasodilation* and *vasoconstriction* on the CV pressure and flow. The method of Sobol is applied to quantify the impact of R_b on pressure and flow with $N = 3000$, the total number of simulations per parameters. For convergence analysis, see section 4.2.1.3. The feasible region for $R_b(kgs^{-1}m^{-4}) = [min(R)\ ,\ max(R_b)] = [5\times10^7\ ,\ 5\times10^9]$. These values are simply taken from the boundary nodes and natural variation.

For flow, R_b has strong sensitivity at node itself and its adjacent nodes. However, nodes 52 (right iliaca interna), 53 (right iliaca interna), 57 (left iliaca interna), 58 (left iliaca interna), 70 (mesenterica inferior),71 (left renalis),72 (mesenterica superior),76 (right celiaca), 79 (left celiaca) and 80 (left celiaca) have significant

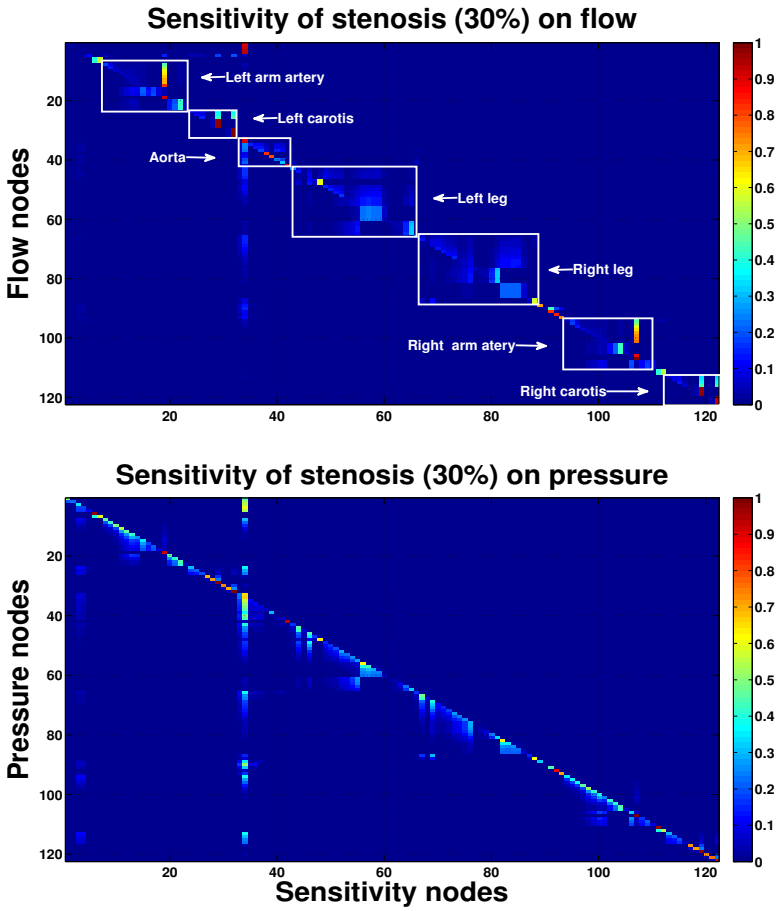

Figure 5.3: Impact of a 30% *stenosis* on the pressure and flow in the visco-elastic CV model.

upstream sensitivities (see figure (5.2, top)).

For pressure, R_b has strong impact on node itself and nearby nodes. Also, R_b is influential for above mentioned nodes, the only difference is, it has upstream as well as downstream effect on pressure in the arterial network (see figure (5.2, bottom)).

5.3 Sensitivity analysis in the visco-elastic CVS

As mentioned in Chapters 3 and 4, the diameter is the key parameter in the CVS. In order to reduce the output uncertainty, the diameter should be estimated accurately through the parameter estimation process. In this section, the variations of the diameter is studied in the context of *stenosis* and *anuerysm* using the Sobol method (N=3000). For in-output quantities of interest and computational cost see appendix A.9.

5.3.1 Stenosis

In this section, different levels of the arterial *stenosis* are created by decreasing the diameter and the impact on the pressure and flow are quantified. The study consists 30%, 60% and 90% arterial *stenosis* at each node of the CVS.

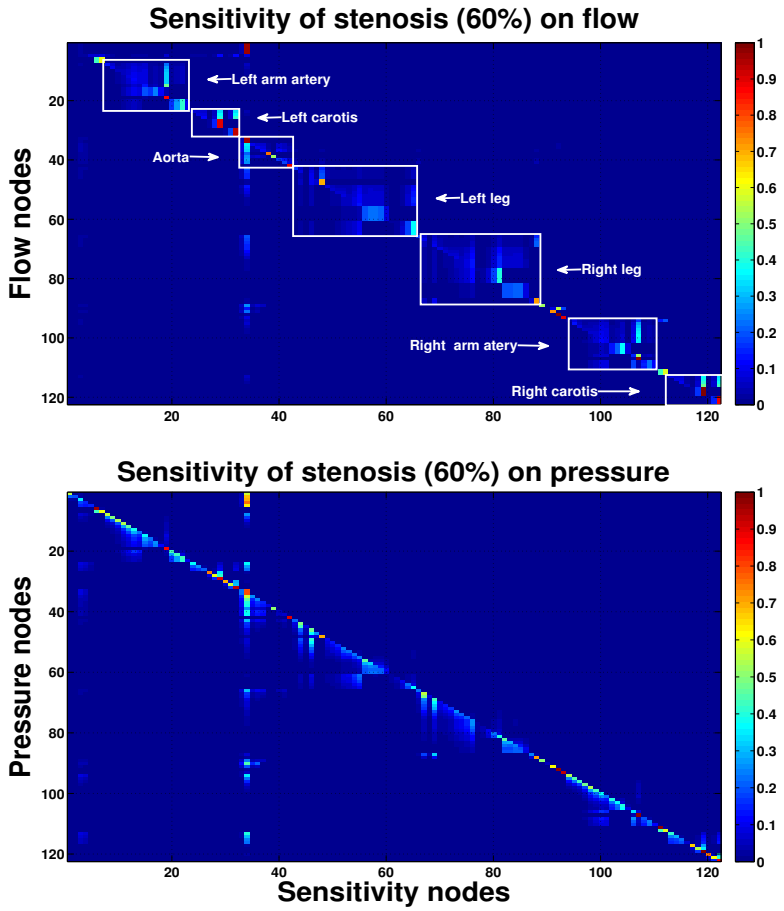

Figure 5.4: Impact of a 60% *stenosis* on the pressure and flow in the visco-elastic CV model.

30% *stenosis*:
In this study, the diameter at each node of the arterial network is decreased by 30% and effect of stenosis is quantified for all state variables. For flow, the sensitivity and reflections can be seen within the individual structures, like left/right carotid bifurcations, left/right legs, aorta and left/right arm arteries. A significant upstream and downstream sensitivity is observed within the aorta (ascending and descending), see figure (5.3, top). For pressure, strong sensitivity is found at node itself and at adjacent nodes. A strong upstream and downstream sensitivity is found at the descending aorta (node 33), see figure (5.3, bottom).

60% *stenosis*:
A significant sensitivity is observed when the level of *stenosis* is increased by 60%. For flow, significant effects and reflections from *stenosis* are seen within the structures. Figure (5.4, top) shows strong reflections in the left/right carotid bifurcations and the descending aorta (node 33). For pressure, strong sensitivity is found at the node itself and nearby nodes. Only downstream sensitivity is observed at each node, except the node 33. At node 33, strong upstream and downstream sensitivity can be seen in figure (5.4, bottom).

90% *stenosis*:
In case of severe *stenosis* (90%), strong sensitivity within each individual structure

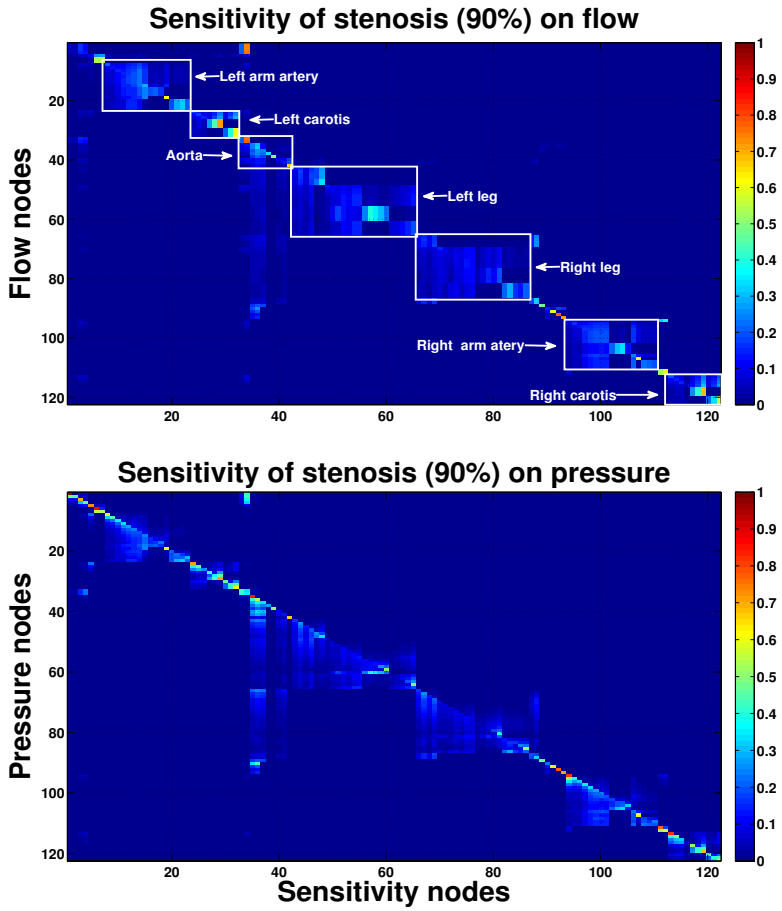

Figure 5.5: Impact of 90% *stenosis* on the pressure and flow in the visco-elastic CV model.

(carotid bifurcations, arms, legs, aorta) can be seen for both pressure and flow. For flow, *stenosis* in the descending aorta has significant downstream and upstream effects. Also, each node has downstream sensitivity as well as reflections within the individual structures (see figure (5.5, top). For pressure, strong downstream and upstream sensitivity at each node, within the arterial structures is observed, see figure (5.5, bottom).

5.3.2 Aneurysm

An *aneurysm* is the abnormal widening or ballooning of the blood vessels due to a weak thin vessel wall. *Aneurysms* can be classified into two categories:

True *aneurysm*: is one that involves all three layers of the vessel wall.
False *aneurysm*: an *aneurysm* that forms outside of an artery wall due to the leaking hole in an artery.

In this section, a true *aneurysm* is created in all segments by increasing the diameter by 200% and 500% . Global sensitivity analysis (Sobol) is used to quantify the impact of *aneurysm* on pressure and flow in the visco-elastic CVS.

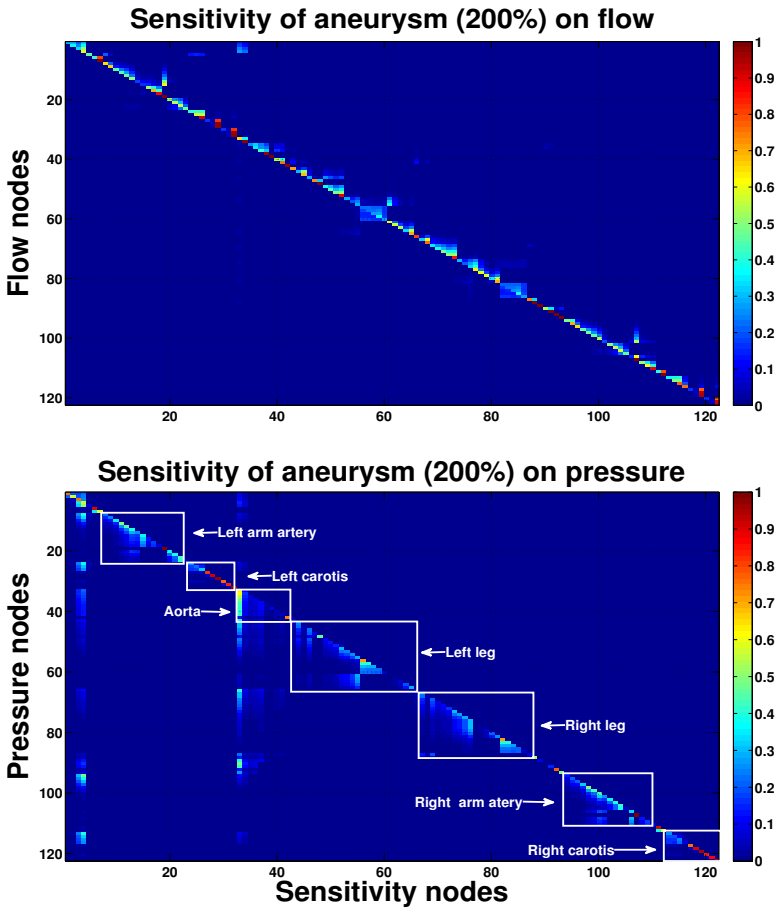

Figure 5.6: Impact of a 200% *aneurysm* on the pressure and flow in the visco-elastic CV model.

200% *aneurysm*:
For flow, the impact of *aneurysm* is strong at the location itself and nearby nodes. Due to the strong sensitivity at the location itself, the identification of pressure and flow sensitivity on other nodes is difficult, see figure (5.6, top). For pressure, the impact of the *aneurysm* is strong within the individual structures (carotid bifurcations, arms, legs, aorta). Most of the sensitivities are seen at the location itself, in internal/external carotid bifurcations and in ascending/descending aorta. Also, the aorta has significant downstream sensitivity on following nodes, see figure (5.6, bottom).

500% *aneurysm*:
In order to study the severe *aneurysm*, 500% variation of the diameter is considered. Flow is most sensitive at the location itself and adjacent nodes. Due to the large sensitivity value at each location, the sensitivity of state variables at other locations cannot be identified (figure (5.7, top)). The sensitivity results of pressure are identical for 200% and 500% *aneurysm* except at the ascending/descending aorta, where high sensitivity values are observed (figure (5.7, bottom)).

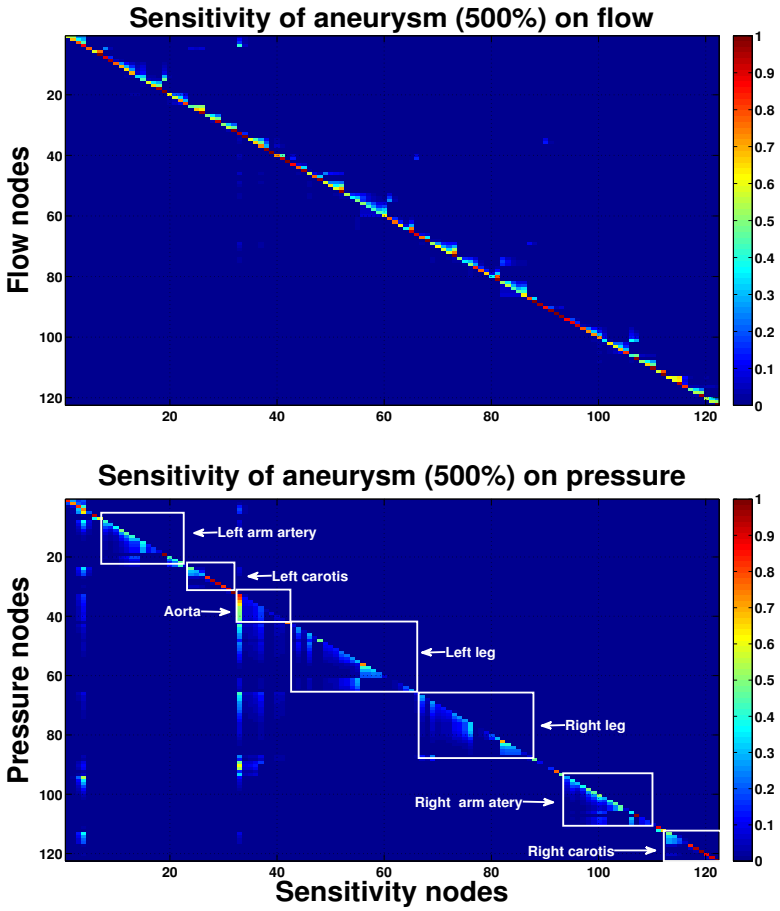

Figure 5.7: Impact of a 500% *aneurysm* on the pressure and flow in the visco-elastic CV model.

5.4 Optimal measurement locations to detect an abdominal aortic aneurysm

An abdominal aortic aneurysm (AAA) is an abnormal widening in the lower part of the aorta, see figure (2.3) nodes 37, 40 and 41. Sensitivity analysis of a large AAA guides the experimentalists what to measure (pressure and flow), where to measure (optimal measurement locations) and which parts of the measurement should be considered (optimal time regions) to detect an aneurysm. By considering the flow measurements, the AAA can be detected at the location itself, node 36 (aorta thoracalis) and 35 (aorta thoracalis), see figure (5.8, top). On the other hand, if the pressure measurements are being considered then the aneurysm can be detected at the location itself, nodes 38 to 52, 66 to 73 and 87 to 89, see figure (5.8, bottom). The optimal time regions for pressure and flow waves are early systole, end systole and early diastole (see figure (5.8)).

5.5 Potential applications

The study has two major potential applications and can be used in teaching and research areas.

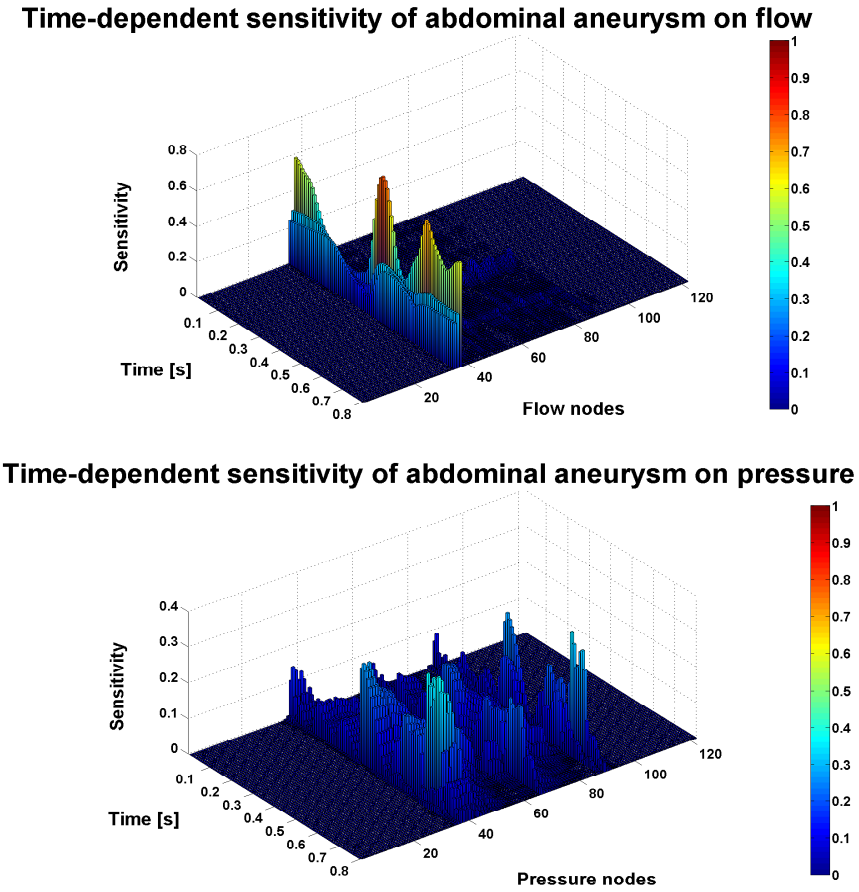

Figure 5.8: Optimal measurement locations to detect the abdominal *aneurysm* (500%) created at node 37 in the CVS (figure (2.3)).

5.5.1 Education

Sensitivity analysis can be used for teaching purposes, like, early detection of vessel abnormalities (*stenosis*, *aneurysms*) and their impact on the rest of the cardiovascular system. These abnormalities are being created by decreasing (*stenosis*) and increasing (*aneurysm*) the diameter of the vessel up to the different levels. Also, it helps medical teachers and students to observe the hemodynamical changes at each node of the arterial network, while changing the diameter. With sensitivity analysis medical students can perturb the diameter in order to replicate the hemodynamics they observe in patients [77]. In this way, medical students can enhance their understanding of hemodynamics.

5.5.2 Research

The results of sensitivity analysis can be used in model design and system identification, i.e. to help experimentalists what to measure (pressure and flow) and where to measure (optimal locations) to estimate the important parameters. As a complement to the parameter estimation process, time-dependent sensitivity provides the optimal time regions in the pressure and flow waves.

CHAPTER 6

Concluding Remarks and Future Directions

The thesis has successfully concluded the aims set out in section (1.7). One of the main aims of this thesis was to built a multi-compartment lumped-parameter model of CVS and apply sensitivity analysis (local and global) to quantify the impact of input parameter to output variables. Prior to sensitivity analysis it is important to know the in- and output quantities of interest (QoI). Within this work, the input quantities of interest were electrical ($R_i,\ C_i,\ L_i,\ R_b$) and structural parameters ($E_i,\ l_i,\ d_i,\ h_i$), while pressure and flow at each location of the CVS were the output quantities of interest. The ultimate goal was to provide a parameter estimation framework on the basis of SA to built a patient-specific CV model. In this Chapter major results are summarized in section (6.1) and potential future directions of this research work are given in section (6.2).

6.1 Conclusion of the thesis

In Chapter 2, multi-compartment lumped-parameter model of human systemic circulation was developed. The model has included the elastic and visco-elastic vessel walls behavior. In multi-compartment CV model, the major arteries of the systemic circulation were divided into 122 vessel segments (nodes or compartments) including one heart node for input pressure boundary condition. Each non-terminal and terminal node was represented by its corresponding non-terminal and terminal electric circuits (elastic and visco-elastic).

At each node, there were 3-electrical and 4-structural parameters influencing the state variables (pressure and flow). That means, the complete CV model had 366-electrical or 488-structure parameters. For a patient-specific CV model, it is not practically feasible to estimate a large number of CV parameters from patient-specific data (measurements). In order to tackle this situation, sensitivity analysis was used to quantify and rank the key parameters (estimands) and fix less sensitive parameters at their nominal values.

In Chapter 3, two local sensitivity analysis methods (normalized partial derivative and norm sensitivity) were applied on a linear elastic model of the arm artery (with and without anastomosis). Sensitivity analysis was carried out for electrical and structure parameters. It was found that R, R_b and d were the most important parameters. In the arm artery anastomosis, R was the most important parameter in the brachial artery and its counterpart SUC-PUR anastomosis.

In order to overcome the limitations of LSA, GSA was examined in Chapter 4. Three variance-based GSA methods were applied on the visco-elastic model of the

carotid bifurcation. As the model under consideration is linear but non-linear in parameters, we expect some interactions effects among the parameters. Later on, the results of GSA methods revealed the negligible interactions effects between the parameters ($< 2\%$). Therefore, we used the *main effect* to quantify and rank the key parameters and for factor fixing. Pressure and flow were most sensitive w.r.t RCL at the right common carotid (RCC) artery. Strong reflections were observed at bifurcations and terminal nodes. Due to the large sensitivity values of pressure and flow w.r.t R and d at the terminal nodes, the sensitivity of state variables w.r.t. other parameters was not identifiable. These results suggest a better remodeling of the terminal nodes. In general 8-electrical out of 18 and 16-structural parameters out of 24 were fixed at their nominal values. In the context of time-dependent sensitivity analysis, most of the sensitivity was found in common time regions i.e. early systole, peak systole and end diastole.

The computational cost is the main issue in GSA. In Chapter 4, the computational cost of three GSA methods was compared. On the basis of less computational cost, simplicity and straightforward implementation, Sobol method was recommended with minimum number of simulations was 3000.

In Chapter 5, the method of Sobol was applied on the linear elastic model of MACSim (Major Arterial Cardiovascular Simulator). The sensitivity analysis of state variables was carried out w.r.t. d and R_b. Pressure and flow were sensitive w.r.t. d at the location itself, ascending (nodes 1, 4, 5) and descending aorta (nodes 15, 22, 23, 24, 25) and has significant effect on left/right carotid bifurcations and left/right arm arteries. A strong downstream and upstream effects from left/right external iliac arteries (nodes 40, 59) and left/right arm arteries (nodes 6, 81) were observed. These are the best measurement access points to estimate the diameter, d.

R_b showed strong effect on the pressure and flow at the node itself and its adjacent nodes. However, significant upstream sensitivities were found at nodes 52 (right iliaca interna), 53 (right iliaca interna), 57 (left iliaca interna), 58 (left iliaca interna), 70 (mesenterica inferior), 71 (left renalis), 72 (mesenterica superior), 76 (right celiaca), 79 (left celiaca) and 80 (left celiaca).

One of the main aims of this thesis was to study different levels of *stenosis* and *aneurysms* at each location of the CVS. Different levels of *stenosis* and *aneurysms* were being created by decreasing (30%, 60%, 90%) and increasing (200%, 500%) the diameter respectively at each location of visco-elastic lumped-parameter model of the CVS. Furthermore, Sobol method was used to study the impact of *stenosis* and *aneurysms* on each state variable. According to our analysis, when the level of *stenosis* is increased by 60% then strong sensitivity was found within the individual structure (arms, carotid bifurcations, legs, aorta). On the other hand, *aneurysms* had strong impact on the pressure within the individual structure (carotid bifurcations, arms, legs, aorta). Most of the sensitivity was observed at the location itself, in internal/external carotid bifurcations and in the ascending/descending aorta.

Sensitivity analysis guides experimentalists what to measure (pressure and flow) where to measure (locations) to estimate the key CV parameters. As a complement to the parameter estimation, patient-specific data (if available) or MACSim measurements can be used to build a patient-specific CV model. Sensitivity analysis also allows medical students to improve their understanding of the normal physiology and pathology of the CVS. In Chapter 5, sensitivity w.r.t. d was studied in detail, which could be used in the field of education and research. Doctors and medical students can study the impact of *stenosis* and *aneurysms* on state variables in the CVS. With the help of sensitivity analysis students can perturb the diameter in order to replicate the hemodynamics they observe in patients. On the other hand, researchers can get optimal measurement locations (access points) to estimate the diameter, which is according to our analysis, one of the major cause

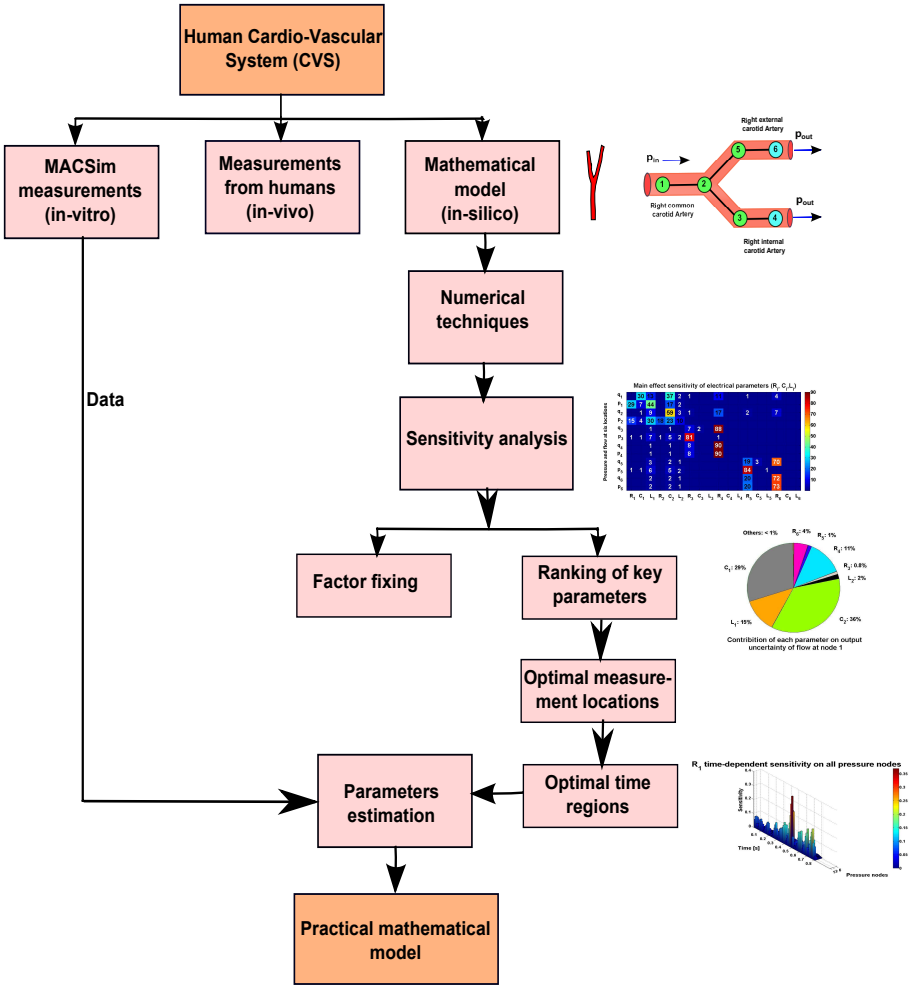

Figure 6.1: A general framework for parameter estimation using sensitivity analysis.

of uncertainty in the CVS. In section 4.5 and figure (6.1), a parameter estimation framework through sensitivity analysis is given, which was the main theme of this thesis.

6.2 Future directions

As mentioned earlier, the main theme of this work was to develop a framework to estimate important parameters, based on SA (figure (6.1)). In the first instance, important (key, influential) parameters in the carotid bifurcation will be estimated using measurements from a fluid dynamical cardiovascular simulator (MACSim). Other possible model improvements are:

1. Formulation of the closed loop CV model with the inclusion of a heart and venous system. This will reduce the uncertainty that comes from the in-output boundary conditions.

2. Include pressure-dependent compliance in the modeling framework, that better explains the non-linear visco-elastic behavior of the vessel walls.

3. Lumped-parameter model of CVS has few limitations, like, incapability to study the wave transmission phenomena, the effect of local vessel changes and

the changes in the blood flow distributions. To overcome these limitations, 1D and 3D model will be used in the future [10].

4. Couple 1D models of desired vascular structures [79] with complete lumped-parameter model of the CVS, developed in this thesis.

BIBLIOGRAPHY

[1] Mazumdar, J. N., Bio-fluid mechanics. 3rd ed. Singapore. World Scientific Publishing Co. Pvt. Ltd., 17-29 (2004).

[2] Klabunde, R. E., Cardiovascular physiology concepts. 2nd ed. Baltimore. Lippincott Williams and Wilkins (2004).

[3] World Health Organization 2015, Cardiovascular diseases (CVDs), The United Nations, accessed 11 May 2015. <http://www.who.int/mediacentre/factsheets/fs317/en/>.

[4] World Heart Federation 2015, Cardiovascular disease risk factors, accessed 11 May 2015. <http://www.world-heart-federation.org/cardiovascular-health/cardiovascular-disease-risk-factors/>.

[5] World Heart Federation 2015, Quick facts on hypertension and high blood pressure accessed 11 May 2015. < http://www.world-heart-federation.org/press/fact-sheets/cardiovascular-disease-risk-factors/quick-facts-on-hypertension-high-blood-pressure/>.

[6] John B. W., Ibn al-Nafis, the pulmonary circulation and the Islamic Golden Age. Journal of Applied Physiology. 105(6), 1877-1880 (2008).

[7] Euler, L., Principia pro motu sanguinis per artrias determinando. Opera posthuma mathematica et physica anno 1844 detecta, 2, 1814-1823 (1775).

[8] Paeme, S. et al., Mathematical multi-scale model of the cardiovascular system including mitral valve dynamics. Application to ischemic mitral insufficiency. BioMedical Engineering OnLine, 10:86 (2011).

[9] Liang F.Y., Takagi S., Himeno R., Liu H., Biomechanical characterization of ventricular-arterial coupling during aging: a multi-scale model study. Journal of Biomechanics, 42, 692-704, (2009).

[10] Formaggia, L., Nobile, F., Quarteroni, A., Veneziani, A., Multiscale modeling of the circulatory system: a preliminary analysis. Computing and Visualization in Science, 2, 75-83 (1999).

[11] Formaggia, L., Veneziani, A., Reduced and multiscale models for the human cardiovascular system. Lecture notes VKI, Lecture Series 07, Brussels (2003).

[12] Lagana, K., Balossinoa, R., Migliavaccaa, F., Pennatia, G., Boveb, E. L. de Levalc, M., R., Dubinid, G., Multiscale modeling of the cardiovascular system: application to the study of pulmonary and coronary perfusions in the univentricular circulation. Journal of Biomechanics, 38, 1129-1141 (2005).

[13] Burattini, R. and Natalucci, S., Complex and frequency-dependent compliance of viscoelastic windkessel resolves contradictions in elastic windkessel. Medical Engineering and Physics, 20, 502-514 (1998).

[14] Avolio, A. P., Multi-branched model of the human arterial system. Medical and Biological Engineering and Computing, 18, 709-718 (1980).

[15] Watrous, R. L., A computational model of cardiovascular physiology and heart sound generation. Conference Proceedings IEEE Engineering in Medicine and Biology Society, 3105-3110 (2009).

[16] Westerhof N, Elzinga G, Sipkema P., An artificial arterial system for pumping hearts. Journal of Applied Physiology, 31, 776-781 (1971).

[17] Womersley J. R., Method for the calculation of velocity, rate of flow and viscous drag in arteries when the pressure gradient is known. Journal of Physilogy, 127, 553-563 (1955).

[18] Hamby, D. M., A review of techniques of parameter sensitivity analysis of environmental models. Journal of Environmental Monitoring and Assessment, 2, 135-154 (1994).

[19] Saltelli, A., Chan, k., Scott, E. M., Sensitivity Analysis Wiley Series in Probability and Statistics England, John Wiley and Sons Ltd, (2000).

[20] Quarteroni, A., Ragni, S. and Veneziani, A., Coupling between lumped and distributed models for blood flow problems. Computing and Visualization in Science, 4, 111-124 (2001).

[21] Milisic, V. and Quarteroni, A., Analysis of lumped parameter models for blood flow simulations and their relation with 1D models. Mathematical Modeling and Numerical Analysis, 38, 613-632 (2004).

[22] Westerhof, N., Bosman, F., De Vries, C.J. and Noordergraaf, A., Analog studies of the human systemic arterial tree. Journal of Biomechanics, 2, 121-143 (1969).

[23] Noordergraaf, A., Verdouw, P.D. and Boom, H.B.K., The use of an analog computer in a circulation model. Progress in Cardiovascular Diseases, 5, 419-439 (1963).

[24] Christopher D. Prevel, MD, Hani S. et. al., The extrinsic blood supply of the ulnar nerve at the elbow: An anatomic study. The Journal of Hand Surgery, 18A, 433-438 (1993).

[25] Phillips, C., A simple lumped parameter model of the cardiovascular system. PhD thesis, Colorado State University Fort Collins, Colorado (2011).

[26] Shim, E. B., Sah, J. Y. and Youn, C. H., Mathematical modeling of cardiovascular system dynamics using a lumped parameter method. Japanese Journal of Physiology, 54, 545-553 (2004).

[27] Yobing, S., Lumped parameter modeling of cardiovascular system dynamics under different healthy and diseased conditions. PhD thesis, University of Sheffield (2013).

[28] Sherwin, S. J., Franke, V., Peiro, V., and Parker, K., One dimensional modeling of a vascular network in space time variables. Kluwer Academic Publishers, 47, 217-250 (2003).

[29] Phillips, C., A simple lumped-parameter model of the cardiovascular system. PhD thesis, Colorado State University, Fort Collins, Colorado (2011).

[30] Ghasemalizadeh, O., Mirzaee, M. R., Firoozabadi, B., Hassani, K., Exact modeling of cardiovascular system using exact method. International Conference on Bioinformatics and Computational Biology, BIOCOMP. July 14-17, Las Vegas Nevada, USA, 2 (2008).

[31] Rideout V. C., Mathematical and computer modeling of physiological systems. New York: Prentice Hall, (1991).

[32] Epstein, S., Willemet, M., Chowienczyk, P. and Alastruey, J., Reducing the number of parameters in 1D arterial blood flow modelling: Less is more for patient-specific simulations. American Journal of Physiology - Heart and Circulatory Physiology, DOI: 10.1152/ajpheart.00857.2014 (2015).

[33] Shi, Y., Lawford, P., Hose, R., Review of zero-D and 1-D models of blood flow in the cardiovascular system. BioMedical Engineering Online, 10, 33 (2011).

[34] Quarteroni, A. and Valli, A., Domain decomposition methods for partial differential equations. Numerical Mathematics and Scientific Computation. The Clarendon Press and Oxford University Press, Oxford, Oxford Science Publications (1999).

[35] Kappel, F. and Batzel, J., Sensitivity analysis of a model of the cardiovascular system. IEEE, Engineering and Medicine and Biology Society (conference proceedings), Aug. 30-Sept. 3, 359-362 (2006).

[36] Samira, J. et. al., Parameter sensitivity analysis of a lumped-parameter model of a chain of lymphangions in series. American Journal of Physioligy, Heart and Circulatory Physiology. DOI: 10.1152/ajpheart.00403.2013 (2013).

[37] Ataee, P. et. al., Identification of cardiovascular baroreflex for probing homeostatic stability. Computing in Cardiology (conference proceedings), Sept. 26-19, 141-144 (2010).

[38] Sumner, T., Sensitivity analysis in system biology modeling and its application to a multi-scale model of the blood glucose homeostatis. PhD thesis, University College London, UK (2010).

[39] Harvey, W., Exercitatio anatomica de motu cordis et sanguinis in animalibus, Frankford, chapter 14 (1628).

[40] Weber, EH., De pulsu, resorptione, auditu et tactu. Annotationes Anatomicae et Physiologicae, Lipsiae, (1834).

[41] Liebau, G., Die Bedeutung der Trägheitskräfte für die Dynamik des Blutkreislaufs. Zs Kreislaufforschung, 4, 428-438 (1957).

[42] Maximilian, M., Johnnie, W. H., Graham, S. S., Thomas, K., Noordergraaf, A.,Impedance defined flow: Generalization of William Harvey's concept of the circulation-370 year later. International Journal of Cardiovascular Medicine and science, 1, 205-2011 (1998).

[43] Bernhard, S., Al Zoukra, K. and Schütte, C., Statistical parameter estimation and signal classification in cardiovascular diagnosis. Environmental Health and Biomedicine, 15, 458-469 (2011).

[44] Zi, Z., Sensitivity analysis approaches applied to systems biology models. IET system biology, 5, issue 6, 336-346 (2011).

[45] Saltelli, A., Ratto, M., Andres, T., Campolongo, F., Cariboni, J., Gatelli, D. Saisana, M., and Tarantola, S., Global Sensitivity Analysis. The Primer, John Wiley Sons (2008).

[46] Saltelli, A., Tarantola, S. and Chan, K. P. S., A quantitative model independent method for global sensitivity analysis of model output. Technometrics, 41(1), 39-56 (1999).

[47] Morris, M. D., Factorial sampling plans for preliminary computational experiments. Technometrics, 33, 161-174 (1991).

[48] Sobol, I., Sensitivity estimates for nonlinear mathematical models. Matematicheskoe Modelirovanie 2, 112-118. In Russian, translated in English (1990).

[49] Homma, T., Saltelli, A., Importance measures in global sensitivity analysis of nonlinear models. Reliability Engineering and System Safety, 52, 117 (1996).

[50] Chen, P., Quarteroni, A. and Rozza, G., Simulation-based uncertainty quantification of human arterial network hemodynamics. International Journal for Numerical Methods in Biomedical Engineering 00, 1-24 (2013).

[51] Cukier, R. I., Fortuin, C.M., Shuler, K.E., Petschek, A.G., and Schaibly, J.H., Study of the sensitivity of coupled reaction systems to uncertainties in rate coefficients. I Theory. Journal of Chemical Physics, 59, 3873-3878 (1973).

[52] Leguy, C. A. D., On the clinical estimation of the hemodynamical and mechanical properties of the arterial tree. PhD Thesis, TU Eindhoven, Netherlands (2010).

[53] Gul, R. and Bernhard, S., Mathematical modeling and sensitivity analysis of arterial anastomosis in arm arteries. Applied Mathematical Modeling (submitted) (2015).

[54] Sato, T., Yamashiro, S.M., Vega, D. and Grodins, F.S., Parameter sensitivity analysis of a network model of systemic circulatory mechanics. Annals of Biomedical Engineering, 2, 289-306 (1974).

[55] Yu, Y. C., Boston, J. R., Simaan, M. A. and Antaki, J. F., Sensitivity analysis of cardiovascular models for minimally invasive estimation of systemic vascular parameters. Proceedings of American Control Conference, San Diago, California (1999).

[56] Westerhof, N. and Noordergraaf, A., Arterial viscoelasticity: A generalized model, effect of input impedance and wave travel in the systemic tree. Journal of Biomechanics, 3, 357-379 (1970).

[57] Karel, H. W., Weber, H. and Ben de Wit, Estimated five component viscoelastic model parameters for human arterial wall. Journal of Biomechanics, 6, 13-24 (1973).

[58] McKay, M. D., Beckman, R. J., Conover, W. J., A comparison of three methods for selecting values of input variables in the analysis of output from a computer code. Technometrics (American Statistical Association), 21, 239-245 (1979).

[59] Jansen, M. J. W., Analysis of variance designs for model output. Computer Physics Communications, 117, 35-43 (1999).

[60] Jansen, M. J. W., Rossing, W. A. H. and Daamen, R.A., Monte Carlo estimation of uncertainty contributions from several independent multivariate sources. Predictability and Nonlinear Modeling in Natural Sciences and Economics, Kluwer Academic Publishers, Dordrecht, 334-343 (1994).

[61] Yang, J., Convergence and uncertainty analyses in Monte-Carlo based sensitivity analysis. Environmental Modeling and Software, 26, 444-457 (2011).

[62] Maria, R. F., Banga, J. R., Doyle, F. J., Novel global sensitivity analysis methodology accounting for the crucial role of distribution of input parameters: application to system biology models. International Journal of Robust and Nonlinear Control, 00, 1-18 (2011).

[63] Hubert, W. et al., A sensitivity analysis of personalized pulse wave propagation model for arteriovenous fistula surgery. Part A: Identification of most influential model parameters. Medical Engineering and Physics, 35, 810-826 (2013).

[64] Archer, G. E. B., Saltelli, A., Sobol, I. M., Sensitivity measures, ANOVA-like techniques and the use of bootstrap. Journal of Statistical Computation and Simulation, 58(2), 99-120 (1997).

[65] Weyl, H., Mean motion. American Journal of Mathematics, 60, 889-896 (1938).

[66] Xiu, D., and Jan, S. H., High-order collocation methods for differential equations with random inputs. SIAM Journal of Scientific Computing, 27(3), 1118-1139 (2005).

[67] Xiu, D., Sherwin, S. J., Parametric uncertainty analysis of pulse wave propagation in a model of human arterial network. Journal of Computational Physics, 226, 1385-1407 (2007).

[68] Skrainka, B. S., Judd, K. L., High performance quadrature rules: how numerical integration affects a popular model of product. Advanced computational methods for estimation and policy analysis in economics differentiation, London (conference paper) (2010).

[69] Tang, G., Iaccarino, G., Global sensitivity analysis for stochastic collocation. 51st AIAA/ASME/ASCE/AHS/ASC Structures, Structural Dynamics and Materials Conference, Orlando, Florida (2010).

[70] Eldred, M. S., Swiler, L. P., Towards goal-oriented stochastic design employing adaptive collocation methods. 13th AIAA/ISSMO Multidisciplinary Analysis Optimization Conference, Fort Worth, Texas (2010).

[71] Nobile, F., Tempone, R., Webster, C. G., An anisotropic sparse grid stochastic collocation method for partial differential equations with random input data. SIAM Journal of Numerical Analysis, 46(5), 2411-2442 (2008).

[72] Smolyak, S. A., Quadrature and interpolation formulas for tensor products of certain classes of functions. Soviet Mathematics Doklady, 4, 240-243 (1963).

[73] Azevedo1, J. D. S., Oliveira, S. P., A numerical comparison between quasi-Monte Carlo and sparse grid stochastic collocation methods. Computer Physics Communications, 10, 1-19 (2011).

[74] Lin, G., Karniadakis, G. E., Sensitivity analysis and stochastic simulations of non-equilibrium plasma flow. International Journal for Numerical Methods in Engineering, 80, 738-766 (2009).

[75] Schlett, P. and Brensing, A. and Bernhard S., Development of a major arterial cardiovascular simulator MACSim for the investigation of parametric uncertainties in the cardiovascular system. (submitted).

[76] SIMLAB. Ver 2.2. http://ipsc.jrc.ec.europa.eu/?id=756, European Commission, Joint Research Centre, Ispra (2007)

[77] Heldt, T., Mukkamala, R., Moody, G. B., Mark, R. G., CVSim: An open-source cardiovascular simulator for teaching and research. The Open Pacing, Electrophysiology and Therapy Journal. 3, 45-54 (2010).

[78] Siddiqui, A., Effects of vasodilation and arterial resistance on cardiac output.Journal of Clinical and Experimental Cardiology, 2:170, doi:10.4172/2155-9880.1000170 (2011).

[79] Arimon, J. A., Numerical modeling of pulse wave propagation in the cardiovascular system: development, validation and clinical applications. PhD thesis, Department of Aeronautics and Bioengineering, Imperial college London, UK (2006).

APPENDIX A

Appendices

A.1 State representation matrices of the linear elastic vessel segment

For non-terminal segment

$$A = \begin{pmatrix} -\frac{R}{L} & -\frac{1}{L} \\ \frac{1}{C} & 0 \end{pmatrix} \qquad B = \begin{pmatrix} \frac{p_{in}}{L} \\ -\frac{q_{out}}{C} \end{pmatrix}$$

$$C = \begin{pmatrix} 1 & 0 \\ 0 & 1 \end{pmatrix} \qquad D = \begin{pmatrix} 0 & 0 \\ 0 & 0 \end{pmatrix}$$

For terminal segment

$$A = \begin{pmatrix} -\frac{2R}{L} & -\frac{2}{L} & 0 \\ \frac{1}{C} & 0 & -\frac{1}{C} \\ 0 & \frac{2}{L} & -\frac{2R_b}{L} \end{pmatrix} \qquad B = \begin{pmatrix} \frac{2p_{in}}{L} \\ 0 \\ -\frac{2p_{out}}{L} \end{pmatrix}$$

$$C = \begin{pmatrix} 1 & 0 & 0 \\ 0 & 1 & 0 \\ 0 & 0 & 1 \end{pmatrix} \qquad D = \begin{pmatrix} 0 & 0 & 0 \\ 0 & 0 & 0 \\ 0 & 0 & 0 \end{pmatrix}$$

A.2 State representation matrices of the linear visco-elastic vessel segment

For non-terminal segment

$$A = \begin{pmatrix} \frac{-R}{L} & \frac{-1}{L} \\ \frac{1}{C} - \frac{R_{dR}}{L} & -\frac{R_d}{L} \end{pmatrix} \qquad B = \begin{pmatrix} \frac{p_{in}}{L} \\ \frac{R_d p_{in}}{L} - \frac{q_{out}}{C} \end{pmatrix}$$

$$C = \begin{pmatrix} 1 & 0 \\ 0 & 1 \end{pmatrix} \qquad D = \begin{pmatrix} 0 & 0 \\ 0 & 0 \end{pmatrix}$$

For terminal segment

$$A = \begin{pmatrix} -\frac{2R}{L} & \frac{-2}{L} & 0 \\ \frac{1}{C} - \frac{2R_d R}{L} & -\frac{4R_d}{L} & -\frac{1}{C} + \frac{2R_d R_b}{L} \\ 0 & \frac{2}{L} & -\frac{-2R_b}{L} \end{pmatrix} \qquad B = \begin{pmatrix} \frac{2p_{in}}{L} \\ \frac{2R_d p_{in}}{L} + \frac{2R_d p_{out}}{L} \\ -\frac{2p_{in}}{L} \end{pmatrix}$$

$$C = \begin{pmatrix} 1 & 0 & 0 \\ 0 & 1 & 0 \\ 0 & 0 & 1 \end{pmatrix} \qquad D = \begin{pmatrix} 0 & 0 & 0 \\ 0 & 0 & 0 \\ 0 & 0 & 0 \end{pmatrix}$$

A.3 State representation matrices of the carotid bifurcation

$$A = \begin{bmatrix}
\frac{-R_1}{L_1} & \frac{-1}{L_1} & 0 & 0 & 0 & 0 & 0 & 0 & 0 & 0 & 0 & 0 & 0 & 0 \\
a^* & \frac{-R_{d_1}}{L_1} & \frac{-1}{C_1} & 0 & 0 & 0 & 0 & 0 & 0 & 0 & 0 & 0 & 0 & 0 \\
0 & \frac{1}{L_2} & \frac{-R_2}{L_2} & \frac{-1}{L_2} & 0 & 0 & 0 & 0 & 0 & 0 & 0 & 0 & 0 & 0 \\
0 & \frac{R_{d_2}}{L_2} & b^* & \frac{-R_{d_2}}{L_2} & \frac{-1}{C_2} & 0 & 0 & 0 & 0 & \frac{-1}{C_2} & 0 & 0 & 0 & 0 \\
0 & 0 & 0 & \frac{1}{L_3} & \frac{-R_3}{L_3} & \frac{-1}{L_3} & 0 & 0 & 0 & 0 & 0 & 0 & 0 & 0 \\
0 & 0 & 0 & \frac{R_{d_3}}{L_3} & c^* & \frac{-R_{d_3}}{L_3} & \frac{-1}{C_3} & 0 & 0 & 0 & 0 & 0 & 0 & 0 \\
0 & 0 & 0 & 0 & 0 & \frac{2}{L_4} & \frac{-2}{R_4 L_4} & \frac{-2}{L_4} & 0 & 0 & 0 & 0 & 0 & 0 \\
0 & 0 & 0 & 0 & 0 & \frac{2R_{d_4}}{L_4} & \frac{1}{C_4} - \frac{2R_{d_4} R_4}{L_4} & \frac{-4R_{d_4}}{L_4} & \frac{2R_{d_4} R_{b_4}}{L_4} - \frac{1}{C_4} & 0 & 0 & 0 & 0 & 0 \\
0 & 0 & 0 & 0 & 0 & 0 & 0 & \frac{2}{L_4} & \frac{-2R_{b_4}}{L_4} & 0 & 0 & 0 & 0 & 0 \\
0 & 0 & 0 & \frac{1}{L_5} & 0 & 0 & 0 & 0 & 0 & \frac{-R_4}{L_5} & \frac{-1}{L_5} & 0 & 0 & 0 \\
0 & 0 & 0 & \frac{R_{d_5}}{L_5} & 0 & 0 & 0 & 0 & 0 & d^* & \frac{-R_{d_5}}{L_5} & \frac{-1}{C_5} & 0 & 0 \\
0 & 0 & 0 & 0 & 0 & 0 & 0 & 0 & 0 & 0 & \frac{2}{L_6} & \frac{-2}{R_6 L_6} & \frac{-2}{L_6} & 0 \\
0 & 0 & 0 & 0 & 0 & 0 & 0 & 0 & 0 & 0 & \frac{2R_{d_6}}{L_6} & \frac{1}{C_6} - \frac{2R_{d_6} R_6}{L_6} & \frac{-4R_{d_6}}{L_6} & \frac{2R_{d_6} R_{b_6}}{L_6} - \frac{1}{C_6} \\
0 & 0 & 0 & 0 & 0 & 0 & 0 & 0 & 0 & 0 & 0 & 0 & \frac{2}{L_6} & \frac{2R_{b_6}}{L_6}
\end{bmatrix}$$

$$B = \begin{bmatrix}
\frac{1}{L_1} & 0 & 0 \\
\frac{R_{d_1}}{L_1} & 0 & 0 \\
0 & 0 & 0 \\
0 & 0 & 0 \\
0 & 0 & 0 \\
0 & 0 & 0 \\
0 & 0 & 0 \\
0 & \frac{2R_{d_4}}{L_4} & 0 \\
0 & \frac{-2}{L_4} & 0 \\
0 & 0 & 0 \\
0 & 0 & 0 \\
0 & 0 & 0 \\
0 & 0 & \frac{2R_{d_6}}{L_6} \\
0 & 0 & \frac{-2}{L_6}
\end{bmatrix}, \quad C = \begin{bmatrix}
1 & 0 & 0 & 0 & 0 & 0 & 0 & 0 & 0 & 0 & 0 & 0 & 0 & 0 \\
0 & 1 & 0 & 0 & 0 & 0 & 0 & 0 & 0 & 0 & 0 & 0 & 0 & 0 \\
0 & 0 & 1 & 0 & 0 & 0 & 0 & 0 & 0 & 0 & 0 & 0 & 0 & 0 \\
0 & 0 & 0 & 1 & 0 & 0 & 0 & 0 & 0 & 0 & 0 & 0 & 0 & 0 \\
0 & 0 & 0 & 0 & 1 & 0 & 0 & 0 & 0 & 0 & 0 & 0 & 0 & 0 \\
0 & 0 & 0 & 0 & 0 & 1 & 0 & 0 & 0 & 0 & 0 & 0 & 0 & 0 \\
0 & 0 & 0 & 0 & 0 & 0 & 1 & 0 & 0 & 0 & 0 & 0 & 0 & 0 \\
0 & 0 & 0 & 0 & 0 & 0 & 0 & 1 & 0 & 0 & 0 & 0 & 0 & 0 \\
0 & 0 & 0 & 0 & 0 & 0 & 0 & 0 & 1 & 0 & 0 & 0 & 0 & 0 \\
0 & 0 & 0 & 0 & 0 & 0 & 0 & 0 & 0 & 1 & 0 & 0 & 0 & 0 \\
0 & 0 & 0 & 0 & 0 & 0 & 0 & 0 & 0 & 0 & 1 & 0 & 0 & 0 \\
0 & 0 & 0 & 0 & 0 & 0 & 0 & 0 & 0 & 0 & 0 & 1 & 0 & 0 \\
0 & 0 & 0 & 0 & 0 & 0 & 0 & 0 & 0 & 0 & 0 & 0 & 1 & 0
\end{bmatrix} \quad \text{and} \quad D=0$$

$$a^* = \frac{1}{C_1} - \frac{R_{d_1} R_1}{L_1} \quad b^* = \frac{1}{C_2} - \frac{R_{d_2} R_2}{L_2}$$
$$c^* = \frac{1}{C_3} - \frac{R_{d_3} R_3}{L_3} \quad d^* = \frac{1}{C_5} - \frac{R_{d_5} R_5}{L_5}$$

A.4 Direct Differential Method (DDM)

In this approach, the sensitivity coefficients are derived by differentiating eqn. (2.33) with respect to the model parameters, θ as

$$\frac{\partial}{\partial\theta}\Big(\dot{x}_i\Big) = \frac{\partial}{\partial\theta}\Big(Ax_i + Bu\Big) = \frac{\partial f_i(x,\theta,t)}{\partial\theta}$$

applying the chain rule and Clairaut's theorem, gives

$$\begin{aligned}
\frac{\partial}{\partial t}\Big(\frac{\partial x_i}{\partial\theta}\Big) &= A'(\theta)x_i + A(\theta)\frac{\partial x_i}{\partial\theta} + B'(\theta)u \\
\frac{\partial}{\partial t}\Big(S_i\Big) &= \underbrace{A'(\theta)x_i + B'(\theta)u}_{f_\theta} + \underbrace{A(\theta)}_{\mathrm{J}}\underbrace{\frac{\partial x_i}{\partial\theta}}_{\mathrm{S}} \\
\dot{S} &= f_\theta + J \times S
\end{aligned}$$

Where, J is $n \times n$, Jacobian matrix, f is right hand side function in eqn. (2.33), $f_\theta = \frac{\partial f_i}{\partial\theta}$ and $S = \frac{\partial x_i}{\partial\theta}$.

A.5 Parameter values for the SUC-PUR anastomosis

Nodes	E	l	d	h	R	C	L
units	$kgm^{-2}s^{-2}$ $*10^5$	m $*10^{-2}$	m $*10^{-3}$	m $*10^{-4}$	$kgs^{-1}m^{-4}$ $*10^6$	$m^4s^2kg^{-1}$ $*10^{-11}$	kgm^{-4} $*10^6$
16	8	6	2.3	1.95	349	0.366	15.16
17	8	6	2	1.7	611	0.277	20
18	16	6	1.8	1.53	931	0.112	24.75

A.6 Parameter values for the arterial network

#	Name of artery	Young's modulus E $(kgm^{-2}s^2)$ $*10^5$	Length l (m) $*10^{-2}$	Diameter d (m) $*10^{-3}$	Wall thickness h (m) $*10^{-4}$	Blood resistance R $(kgs^{-1}m^{-4})$ $*10^8$	Compliance C $(kg^{-1}s^2m^4)$ $*10^{-10}$	Blood inertia L (kgm^{-4}) $*10^7$	Wall resistance R_d	Boundary resistance R_b
1	Aorta ascendens	4	1	29.4	16.4	2.18×10^{3}	3.04×10^{-10}	1.55×10^{4}	3.29×10^{7}	—
2	Aorta ascendens	4	1	29.4	16.4	2.17×10^{3}	3.05×10^{-10}	1.54×10^{4}	3.28×10^{7}	—
3	Arcus aorta	4	3.98	28.8	16.1	9.42×10^{3}	1.15×10^{-9}	6.42×10^{4}	8.60×10^{6}	—
4	Arcus aorta	4	2	22.4	13.2	1.29×10^{4}	3.34×10^{-10}	5.33×10^{4}	2.99×10^{7}	—
5	A.subclavia	4	3.4	12.4	8.6	2.34×10^{5}	1.48×10^{-10}	2.95×10^{5}	6.76×10^{7}	—
6	A.vertebralis	8	7.1	3.76	4.6	5.78×10^{7}	8.05×10^{-12}	6.71×10^{6}	1.24×10^{9}	—
7	A.vertebralis	8	7.7	3.66	4.5	6.99×10^{7}	8.05×10^{-12}	7.68×10^{6}	1.21×10^{9}	2.59×10^{9}
8	A.subclavia	4	6.8	8.06	6.6	2.62×10^{6}	1.06×10^{-10}	1.39×10^{6}	9.44×10^{7}	—
9	A.axillaris	4	6.1	7.28	6.2	3.53×10^{6}	7.45×10^{-11}	1.53×10^{6}	1.34×10^{8}	—
10	Aaxillaris	4	5.6	6.28	5.7	5.86×10^{6}	4.77×10^{-11}	1.89×10^{6}	2.09×10^{8}	—
11	A.brachialis	4	6.3	5.64	5.5	1.01×10^{7}	4.03×10^{-11}	2.64×10^{6}	2.48×10^{8}	—
12	A.brachialis	4	6.3	5.32	5.3	1.28×10^{7}	3.51×10^{-11}	2.97×10^{6}	2.85×10^{8}	—
13	A.brachialis	4	6.3	5	5.2	1.64×10^{7}	2.97×10^{-11}	3.36×10^{6}	3.36×10^{8}	—
14	A.brachialis	4	4.6	4.72	5	1.51×10^{7}	1.90×10^{-11}	2.76×10^{6}	5.26×10^{8}	—
15	A.ulnaris	8	6.7	4.3	4.9	3.19×10^{7}	1.06×10^{-11}	4.84×10^{6}	9.37×10^{8}	—
16	A.ulnaris	8	6.7	4.06	4.7	4.02×10^{7}	9.37×10^{-12}	5.43×10^{6}	1.06×10^{9}	—
17	A.ulnaris	8	6.7	3.84	4.6	5.02×10^{7}	8.10×10^{-12}	6.07×10^{6}	1.23×10^{9}	—
18	A.ulnaris	8	3.7	3.66	4.5	3.36×10^{7}	3.96×10^{-12}	3.69×10^{6}	2.52×10^{9}	3.24×10^{9}
19	Ainterossea volaris	16	7.9	1.82	2.8	1.17×10^{9}	8.30×10^{-13}	3.18×10^{7}	1.19×10^{10}	3.24×10^{9}
20	A.radialis	8	7.1	3.48	4.4	7.89×10^{7}	6.68×10^{-12}	7.83×10^{6}	1.49×10^{9}	—
21	A.radialis	8	7.1	3.24	4.3	1.05×10^{8}	5.51×10^{-12}	9.04×10^{6}	1.81×10^{9}	—
22	A.radialis	8	7.1	3	4.2	1.42×10^{8}	4.48×10^{-12}	1.05×10^{7}	2.23×10^{9}	—
23	A.radialis	8	2.2	2.84	4.1	5.51×10^{7}	1.21×10^{-12}	3.64×10^{6}	8.28×10^{9}	3.92×10^{9}
24	A. carotis corn. sin.	4	5.9	7.4	6.3	3.20×10^{6}	7.45×10^{-11}	1.44×10^{6}	1.34×10^{8}	—
25	A. carotis corn. sin.	4	5.9	7.4	6.3	3.20×10^{6}	7.45×10^{-11}	1.44×10^{6}	1.34×10^{8}	—
26	A. carotis corn. sin.	4	5.9	7.4	6.3	3.20×10^{6}	7.45×10^{-11}	1.44×10^{6}	1.34×10^{8}	—

27	A.car.ext.sin.	8	5.9	3.54	4.5	6.12×10^{7}	5.71×10^{-12}	6.29×10^{6}	1.75×10^{9}	—
28	A.car.ext.sin.	8	5.9	2.58	3.9	2.17×10^{8}	2.55×10^{-12}	1.18×10^{7}	3.92×10^{9}	—
29	A.car.ext.sin.	16	5.9	1.66	2.6	1.26×10^{9}	5.10×10^{-13}	2.86×10^{7}	1.96×10^{10}	3.11×10^{9}
30	A.car.int.sin.	8	5.9	3.54	4.5	6.12×10^{7}	5.71×10^{-12}	6.29×10^{6}	1.75×10^{9}	—
31	A.car.int.sin.	8	5.9	2.58	3.9	2.17×10^{8}	2.55×10^{-12}	1.18×10^{7}	3.92×10^{9}	—
32	A.cerebri anterior sin	16	5.9	1.66	2.6	1.26×10^{9}	5.09×10^{-13}	2.86×10^{7}	1.96×10^{10}	3.11×10^{9}
33	Arcus aorta	4	3.9	21.4	12.7	3.03×10^{4}	5.90×10^{-10}	1.14×10^{5}	1.69×10^{7}	—
34	Aorta thoracalis	2	5.2	50	12	1.40×10^{3}	$2.12 \times 10^{-9}0$	2.80×10^{4}	4.70×10^{6}	—
35	Aorta thoracalis	4	5.2	13.5	9	2.55×10^{5}	2.79×10^{-10}	3.81×10^{5}	3.58×10^{7}	—
36	Aorta thoracalis	4	5.2	12.9	8.7	3.06×10^{5}	2.52×10^{-10}	4.18×10^{5}	3.96×10^{7}	—
37	Aorta abdominalis	4	5.3	12.2	8.4	3.89×10^{5}	2.25×10^{-10}	4.76×10^{5}	4.44×10^{7}	—
38	A.renalis	4	5.9	8.7	6.9	1.67×10^{6}	1.11×10^{-10}	1.04×10^{6}	9.04×10^{7}	3.45×10^{9}
39	Amesenterica sup.	4	3.2	5.2	5.2	7.13×10^{6}	1.69×10^{-11}	1.58×10^{6}	5.88×10^{8}	3.75×10^{9}
40	Aorta abdominalis	4	5.3	11.6	8.2	4.77×10^{5}	1.98×10^{-10}	5.27×10^{5}	5.04×10^{7}	—
41	Aorta abdominalis	4	5.3	10.96	7.8	5.99×10^{5}	1.75×10^{-10}	5.89×10^{5}	5.69×10^{7}	—
42	A.mesenterica inf	4	5	3.2	4.3	7.77×10^{7}	7.48×10^{-12}	6.52×10^{6}	1.33×10^{9}	3.75×10^{9}
43	A.iliaca communis	4	5.8	7.36	6.3	3.22×10^{6}	7.21×10^{-11}	1.43×10^{6}	1.38×10^{8}	—
44	A.iliaca extema	4	5.8	5.8	5.5	8.35×10^{6}	4.04×10^{-11}	2.30×10^{6}	2.47×10^{8}	—
45	A.iliaca extema	4	2.5	5.8	5.5	3.60×10^{6}	1.74×10^{-11}	9.93×10^{5}	5.74×10^{8}	—
46	A.femoralis	4	6.1	5.4	5.3	1.16×10^{7}	3.56×10^{-11}	2.79×10^{6}	2.81×10^{8}	—
47	A.profundus	16	6.3	5.1	5.2	1.51×10^{7}	7.88×10^{-12}	3.23×10^{6}	1.26×10^{9}	—
48	A.profundus femor	16	6.3	3.72	4.6	5.36×10^{7}	3.46×10^{-12}	6.08×10^{6}	2.88×10^{9}	4×10^{9}
49	A.femoralis	4	6.1	5.18	5.2	1.38×10^{7}	3.20×10^{-11}	3.03×10^{6}	3.12×10^{8}	—
50	A.femoralis	4	6.1	4.98	5.1	1.61×10^{7}	2.90×10^{-11}	3.28×10^{6}	3.44×10^{8}	—
51	A.femoralis	4	6.1	4.76	5	1.93×10^{7}	2.58×10^{-11}	3.59×10^{6}	3.87×10^{8}	—
52	A.femoralis	4	7.1	4.5	4.9	2.82×10^{7}	2.59×10^{-11}	4.68×10^{6}	3.86×10^{8}	—
53	A.poplitea	8	6.3	4.26	4.8	3.11×10^{7}	9.96×10^{-12}	4.64×10^{6}	1×10^{9}	—
54	A.poplitea	8	6.3	4.04	4.7	3.85×10^{7}	8.68×10^{-12}	5.16×10^{6}	1.15×10^{9}	—
55	A.poplitea	8	6.3	3.8	4.6	4.92×10^{7}	7.38×10^{-12}	5.83×10^{6}	1.35×10^{9}	—
56	A.tibialis anterior	16	7.5	2.6	3.9	2.67×10^{8}	1.66×10^{-12}	1.48×10^{7}	6.02×10^{9}	—
57	A.tibialis anterior	16	7.5	2.6	3.9	2.67×10^{8}	1.66×10^{-12}	1.48×10^{7}	6.02×10^{9}	—
58	A.tibialis anterior	16	7.5	2.6	3.9	2.67×10^{8}	1.66×10^{-12}	1.48×10^{7}	6.02×10^{9}	—

59	A.tibialis anterior	16	7.5	2.6	3.9	2.67×10^{8}	1.66×10^{-12}	1.48×10^{7}	6.02×10^{9}	—
60	A.tibialis anterior	16	4.3	2.6	3.9	1.53×10^{8}	9.51×10^{-13}	8.50×10^{6}	1.05×10^{10}	5.16×10^{9}
61	A.tibialis posterior	16	6.7	4.94	5.1	1.83×10^{7}	7.77×10^{-12}	3.67×10^{6}	1.28×10^{9}	—
62	A.tibialis posterior	16	6.7	4.38	4.9	2.96×10^{7}	5.64×10^{-12}	4.66×10^{6}	1.77×10^{9}	—
63	A.tibialis posterior	16	6.7	3.84	4.6	5.02×10^{7}	4.05×10^{-12}	6.07×10^{6}	2.47×10^{9}	—
64	A.tibialis posterior	16	6.7	3.3	4.4	9.20×10^{7}	2.69×10^{-12}	8.22×10^{6}	3.72×10^{9}	—
65	A.tibialis posterior	16	5.3	2.82	4.1	1.36×10^{8}	1.42×10^{-12}	8.91×10^{6}	7.02×10^{9}	5.65×10^{9}
66	A.iliaca communis	4	5.8	7.36	6.3	3.22×10^{6}	7.20×10^{-11}	1.43×10^{6}	1.38×10^{8}	—
67	A.iliaca extema	4	5.8	5.8	5.5	8.35×10^{6}	4.04×10^{-11}	2.30×10^{6}	2.47×10^{8}	—
68	A.iliaca extema	4	2.5	5.8	5.5	3.60×10^{6}	1.74×10^{-11}	9.93×10^{5}	5.74×10^{8}	—
69	A.femoralis	4	6.1	5.4	5.3	1.16×10^{7}	3.55×10^{-11}	2.79×10^{6}	2.81×10^{8}	—
70	A.femoralis	4	6.1	5.18	5.2	1.38×10^{7}	3.20×10^{-11}	3.03×10^{6}	3.12×10^{8}	—
71	A.femoralis	4	6.1	4.98	5.1	1.61×10^{7}	2.90×10^{-11}	3.28×10^{6}	3.44×10^{8}	—
72	A.femoralis	4	6.1	4.76	5	1.93×10^{7}	2.58×10^{-11}	3.59×10^{6}	3.87×10^{8}	—
73	A.femoralis	4	7.1	4.5	4.9	2.82×10^{7}	2.59×10^{-11}	4.68×10^{6}	3.85×10^{8}	—
74	A.poplitea	8	6.3	4.26	4.8	3.11×10^{7}	9.96×10^{-12}	4.64×10^{6}	1×10^{9}	—
75	A.poplitea	8	6.3	4.04	4.7	3.85×10^{7}	8.68×10^{-12}	5.16×10^{6}	1.15×10^{9}	—
76	A.poplitea	8	6.3	3.8	4.6	4.92×10^{7}	7.38×10^{-12}	5.83×10^{6}	1.35×10^{9}	—
77	A.tibialis posterior	16	6.7	4.94	5.1	1.83×10^{7}	7.77×10^{-12}	3.67×10^{6}	1.28×10^{9}	—
78	A.tibialis posterior	16	6.7	4.38	4.9	2.96×10^{7}	5.64×10^{-12}	4.66×10^{6}	1.77×10^{9}	—
79	A.tibialis posterior	16	6.7	3.84	4.6	5.02×10^{7}	4.05×10^{-12}	6.07×10^{6}	2.47×10^{9}	—
80	A.tibialis posterio	16	6.7	3.3	4.4	9.20×10^{7}	2.69×10^{-12}	8.22×10^{6}	3.72×10^{9}	—
81	Atibialis posterior	16	5.3	2.82	4.1	1.36×10^{8}	1.42×10^{-12}	8.91×10^{6}	7.02×10^{9}	5.65×10^{9}
82	Atibialis anterior	16	7.5	2.6	3.9	2.67×10^{8}	1.66×10^{-12}	1.48×10^{7}	6.02×10^{9}	—
83	Atibialis anterior	16	7.5	2.6	3.9	2.67×10^{8}	1.66×10^{-12}	1.48×10^{7}	6.02×10^{0}	—
84	Atibialis anterior	16	7.5	2.6	3.9	2.67×10^{8}	1.66×10^{-12}	1.48×10^{7}	6.02×10^{9}	—
85	Atibialis anterior	16	7.5	2.6	3.9	2.67×10^{8}	1.66×10^{-12}	1.48×10^{7}	6.02×10^{9}	—
86	Atibialis anterior	16	4.3	2.6	3.9	1.53×10^{8}	9.51×10^{-13}	8.50×10^{6}	1.05×10^{10}	5.16×10^{9}
87	A.profundus	16	6.3	5.1	5.2	1.51×10^{7}	7.89×10^{-12}	3.23×10^{6}	1.26×10^{9}	—
88	A.profundus femoris	16	6.3	3.72	4.6	5.36×10^{7}	3.46×10^{-12}	6.08×10^{6}	2.88×10^{9}	4×10^{9}
89	A.renalis	4	3.2	5.2	5.2	7.13×10^{6}	1.69×10^{-11}	1.58×10^{6}	5.89×10^{8}	3.45×10^{9}
90	A.coelica	4	1	7.8	6.4	4.40×10^{5}	1.45×10^{-11}	2.20×10^{5}	6.87×10^{8}	—

91	A.gastrica sin.	4	6.3	5.46	5.4	1.15×10^{7}	3.73×10^{-11}	2.82×10^{6}	2.68×10^{8}	4.24×10^{9}
92	A.lienalis	4	7.1	3.6	4.5	6.88×10^{7}	1.45×10^{-11}	7.32×10^{6}	6.91×10^{8}	3.75×10^{9}
93	A.hepatica	4	6.6	4.4	4.9	2.86×10^{7}	2.25×10^{-11}	4.55×10^{6}	4.43×10^{8}	3.54×10^{9}
94	A.anonyma	4	3.4	8.46	6.7	1.08×10^{6}	6.03×10^{-11}	6.35×10^{5}	1.65×10^{8}	—
95	A.subclavia	4	6.8	8.06	6.6	2.62×10^{6}	1.05×10^{-10}	1.39×10^{6}	9.44×10^{7}	—
96	A.axillaris	4	6.1	7.28	6.2	3.53×10^{6}	7.45×10^{-11}	1.53×10^{6}	1.34×10^{8}	—
97	A.axillaris	4	5.6	6.28	5.7	5.86×10^{6}	4.78×10^{-11}	1.89×10^{6}	2.09×10^{8}	—
98	A.brachialis	4	6.3	5.64	5.5	1.01×10^{7}	4.04×10^{-11}	2.64×10^{6}	2.47×10^{8}	—
99	A.brachialis	4	6.3	5.32	5.3	1.28×10^{7}	3.51×10^{-11}	2.97×10^{6}	2.84×10^{8}	—
100	A.brachialis	4	6.3	5	5.2	1.64×10^{7}	2.95×10^{-11}	3.36×10^{6}	3.36×10^{8}	—
101	A.brachialis	4	4.6	4.72	5	1.51×10^{7}	1.90×10^{-11}	2.76×10^{6}	5.26×10^{8}	—
102	A.radialis	8	7.1	3.48	4.4	7.89×10^{7}	6.68×10^{-12}	7.83×10^{6}	1.49×10^{9}	—
103	A.radialis	8	7.1	3.24	4.3	1.05×10^{8}	5.51×10^{-12}	9.04×10^{6}	1.81×10^{9}	—
104	A.radialis	8	7.1	3	4.2	1.42×10^{8}	4.48×10^{-12}	1.05×10^{7}	2.23×10^{9}	—
105	A.radialis	8	2.2	2.84	4.1	5.51×10^{7}	1.21×10^{-12}	3.64×10^{6}	8.28×10^{9}	3.92×10^{9}
106	A.ulnaris	8	6.7	4.3	4.9	3.19×10^{7}	1.06×10^{-11}	4.84×10^{6}	9.37×10^{8}	—
107	Ainterossea volaris	16	7.9	1.82	2.8	1.17×10^{9}	8.34×10^{-13}	3.18×10^{7}	1.19×10^{10}	3.24×10^{9}
108	A.ulnaris	8	6.7	4.06	4.7	4.02×10^{7}	9.37×10^{-12}	5.43×10^{6}	1.06×10^{9}	—
109	A.ulnaris	8	6.7	3.84	4.6	5.02×10^{7}	8.10×10^{-12}	6.07×10^{6}	1.23×10^{9}	—
110	A.ulnaris	8	3.7	3.66	4.5	3.36×10^{7}	3.96×10^{-12}	3.69×10^{6}	2.52×10^{9}	3.24×10^{9}
111	A.vertebralis	8	7.1	3.76	4.6	5.79×10^{7}	8.05×10^{-12}	6.71×10^{6}	1.24×10^{9}	—
112	A.vertebralis	8	7.7	3.66	4.5	6.99×10^{7}	8.24×10^{-12}	7.68×10^{6}	1.21×10^{9}	2.59×10^{9}
113	A.anonyma	4	5.9	7.4	6.3	3.20×10^{6}	7.45×10^{-11}	1.44×10^{6}	1.34×10^{8}	—
114	A.car.com.dextra	4	5.9	7.4	6.3	3.20×10^{6}	7.45×10^{-11}	1.44×10^{6}	1.34×10^{8}	—
115	A.car.com.dextra	4	5.9	7.4	6.3	3.20×10^{6}	7.45×10^{-11}	1.44×10^{6}	1.34×10^{8}	—
116	A.car.com.dextra	4	3.1	7.4	6.3	1.68×10^{6}	3.91×10^{-11}	7.57×10^{5}	2.55×10^{8}	—
117	A.car.int.dextm	8	5.9	3.54	4.5	6.12×10^{7}	5.71×10^{-12}	6.29×10^{6}	1.75×10^{9}	—
118	A.car.int.dextm	8	5.9	2.58	3.9	2.17×10^{8}	2.55×10^{-12}	1.18×10^{7}	3.92×10^{9}	—
119	A.car.int.dextm	16	5.9	1.66	2.6	1.26×10^{9}	5.09×10^{-13}	2.86×10^{7}	1.96×10^{10}	3.11×10^{9}
120	A.car.ext.dextra	8	5.9	3.54	4.5	6.12×10^{7}	5.71×10^{-12}	6.29×10^{6}	1.75×10^{9}	—
121	A.car.ext.dextra	8	5.9	2.58	3.9	2.17×10^{8}	2.55×10^{-12}	1.18×10^{7}	3.92×10^{9}	—
122	A.car.ext.dextra	16	5.9	1.66	2.6	1.26×10^{9}	5.09×10^{-13}	2.86×10^{7}	1.96×10^{10}	3.11×10^{9}

A.7 Main and total effect of electrical parameters for flow in the carotid bifurcation

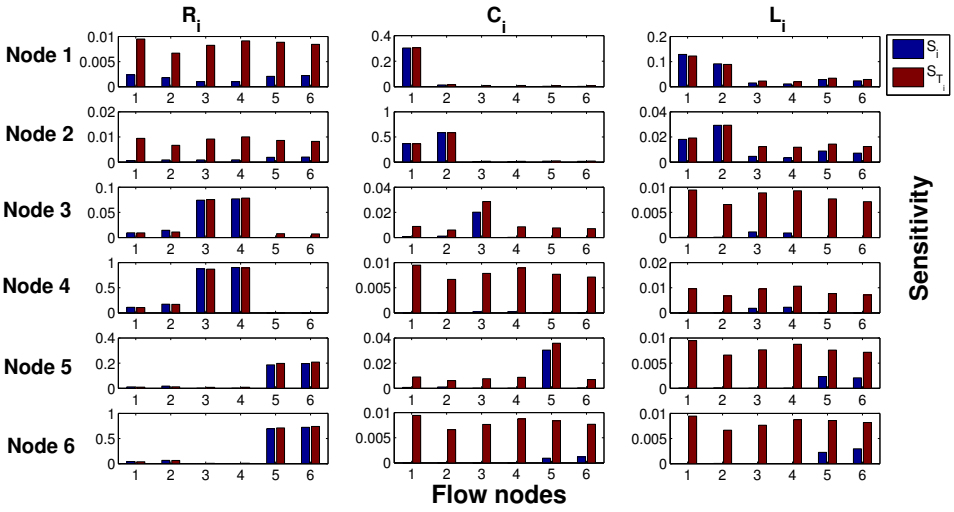

A.8 Main and total effect of electrical parameters for pressure in the carotid bifurcation

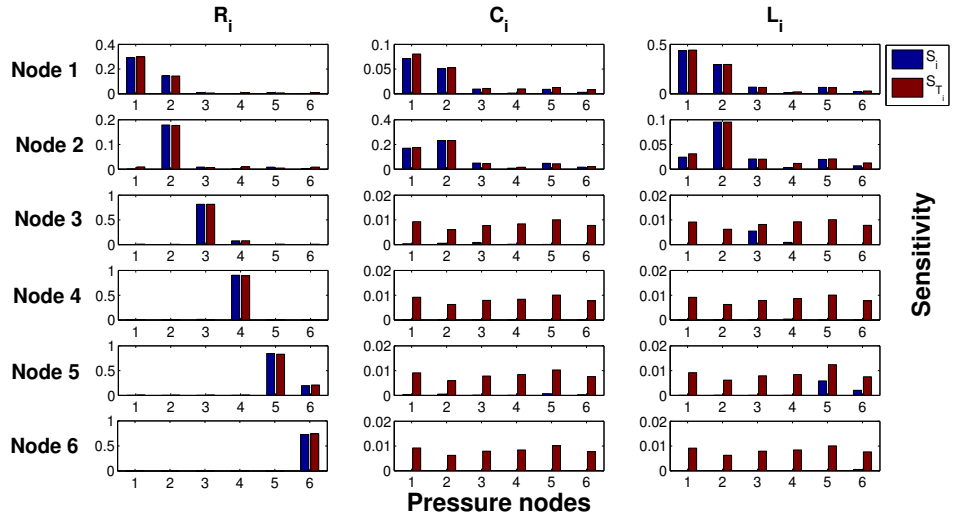

A.9 Computational cost of sensitivity analysis methods

Input QoI	Output QoI	Model geometry	Methods of SA	Computational cost
$Eldh$	(q,p)	Arm artery	Normalized partial derivative (LSA)	5 sec
$Eldh$	(q,p)	Arm artery	Norms (LSA)	5 sec
RCL	(q,p)	Arm artery	Normalized partial derivative (LSA)	5 sec
R, R_b	(q,p)	Arm artery anastomosis	Normalized partial derivative (LSA)	7 sec
RCL	(q,p)	Carotid bifurcation	Sobol (GSA) ($N = 10,000$)	79 min
$Eldh$	(q,p)	Carotid bifurcation	Sobol (GSA) ($N = 10,000$)	113 min
RCL	(q,p)	Carotid bifurcation	FAST (GSA) ($M = 6,\ N = 10,000$)	115 min
RCL	(q,p)	Carotid bifurcation	SGSC (GSA) (level 1)	1920 min
RCL	(q,p)	Carotid bifurcation	Norms (LSA)	4 sec
d, R_b	(q,p)	MACSim	Sobol (GSA) ($N = 3000$)	720 min
d	(q,p)	Visco-elastic CV model	Sobol (GSA) (N=3000)	1410 min